Found 42 Records

SESSION TITLE: Late Breaking Session 03: Preclinical, Probe Concepts & New Biology (all categories)
CONTROL ID: 2805333
TITLE: Development of theranostic nanoemulsions with NIR, ^{19}F MR, and PET imaging capabilities for the treatment of chronic inflammatory diseases
PRESENTER: Michele Herneisey
AUTHORS (FIRST NAME, LAST NAME): Michele Herneisey[2], Marie-Caline Abadjian[1], Carolyn J. Anderson[1], Jelena M. Janjic[2]
INSTITUTIONS (ALL):
1. Radiology, University of Pittsburgh, Pittsburgh, PA, United States.
2. Pharmaceutics, Duquesne University, Pittsburgh, PA, United States.
ABSTRACT BODY:
Abstract Body: Theranostic nanomedicines allow for simultaneous delivery of a therapeutic drug and imaging drug targeting and effectiveness in living subjects in real time. Theranostic dosage and frequency of administration can therefore be adjusted based on an individual patient's needs and outcome, providing truly personalized medicine. Nanoemulsions are a promising approach for the development of theranostic platforms because they are produced with generally regarded as safe materials for human use and they can be produced on large scale, leading to faster clinical translation. Most reported nanoemulsions in literature are biphasic oil in water nanoemulsion systems. However, triphasic (perfluorocarbon/oil/water) theranostic nanoemulsion systems have also been developed in recent years (Patel, Zhang et al. 2013, Janjic, Shao et al. 2014, Mountain, Jelier et al. 2014, Liu, Bagia et al. 2015, Patel, Beaino et al. 2015, Herneisey, Williams et al. 2016). These triphasic nanoemulsions consist of a perfluorocarbon core that can be imaged with ^{19}F MRI and serve as a carrier of other imaging moieties via conjugation. Here, triphasic theranostic nanoemulsions were developed for the targeted delivery of resveratrol, a natural anti-inflammatory compound, to macrophages, immune cells that are crucial in the pathogenesis of cancer and many chronic inflammatory diseases (Herneisey, Williams et al. 2016). The developed nanoemulsions contain the fluorescent dye DiR for NIRF imaging and the perfluorocarbon perfluoropolyether (PFPE) for ^{19}F MRI. Nanoemulsions maintain colloidal stability for 350 days, incorporate resveratrol at concentrations of 2.8mM, provide extended release of resveratrol for a period of 285h, and are readily internalized by RAW 264.7 macrophages, as determined with fluorescence microscopy. Further, resveratrol nanoemulsions are shown to be more effective at reducing tumor necrosis factor-α production than a solution of resveratrol in dimethyl sulfoxide. Importantly, the presence of PFPE did not impact nanoemulsion colloidal stability, drug loading, drug release, or pharmacological efficacy, demonstrating that the diagnostic component of the theranostic resveratrol nanoemulsion does not affect its therapeutic properties. To improve the imaging sensitivity and clinical translatability of the resveratrol theranostic nanoemulsion platform, novel nanoemulsions were developed that incorporate PET imaging moieties in addition to NIRF and ^{19}F MRI moieties. The PET moiety was incorporated into the nanoemulsion via direct conjugation to PFPE. Nanoemulsion radiolabeling conditions were then optimized to maximize specific activity and minimize nonspecific binding through design of experiments. To the best of our knowledge, post-emulsification nanoemulsion labeling with a radioactive ligand has not been reported. Further, this is the first report of applying mathematical modeling to development of multimodal imaging agents and theranostic nanomedicines with three imaging modalities. We believe that the presented approach to rational nanomedicine is of high impact as it can be adapted to therapeutic and imaging nanosystems in applications beyond nanomedicine.

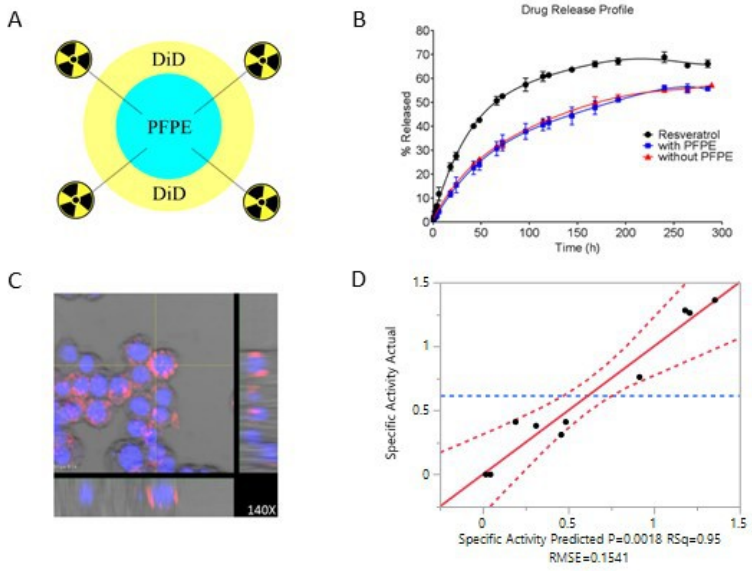

(A) Proposed structure of a theranostic (therapeutic and diagnostic) nanoemulsion containing near infrared (NIR), 19F magnetic resonance (MR) and positron emission tomography (PET) imaging capabilities. Theranostic nanoemulsions are designed to provide image guided resveratrol delivery to macrophages as a treatment for inflammatory diseases; (B) The drug release profile of resveratrol loaded theranostic nanoemulsions with and without the 19F MRI agent perfluoropolyether PFPE demonstrates that incorporation of the MRI agent does not impact nanoemulsion drug release properties; (C) Composite z-stack fluorescent and DIC image of RAW 264.7 macrophages (blue) after 24h exposure to fluorescently labeled resveratrol loaded theranostic nanoemulsions (red) demonstrates that macrophages readily uptake nanoemulsions; (D) Least squares linear regression models the impact of radiolabeling conditions on the specific activity of nanoemulsions containing a positron emission tomography (PET) imaging moiety.

IMAGE CAPTION: (A) Proposed structure of a theranostic (therapeutic and diagnostic) nanoemulsion containing near infrared (NIR), 19F magnetic resonance (MR) and positron emission tomography (PET) imaging capabilities. Theranostic nanoemulsions are designed to provide image guided resveratrol delivery to macrophages as a treatment for inflammatory diseases; (B) The drug release profile of resveratrol loaded theranostic nanoemulsions with and without the 19F MRI agent perfluoropolyether PFPE demonstrates that incorporation of the MRI agent does not impact nanoemulsion drug release properties; (C) Composite z-stack fluorescent and DIC image of RAW 264.7 macrophages (blue) after 24h exposure to fluorescently labeled resveratrol loaded theranostic nanoemulsions (red) demonstrates that macrophages readily uptake nanoemulsions; (D) Least squares linear regression models the impact of radiolabeling conditions on the specific activity of nanoemulsions containing a positron emission tomography (PET) imaging moiety.

SESSION TITLE: Late Breaking Session 03: Preclinical, Probe Concepts & New Biology (all categories)

CONTROL ID: 2805364

TITLE: Regulation of Iron Export by Hepcidin is Detectable by Magnetic Resonance Imaging (MRI)

PRESENTER: Donna Goldhawk

AUTHORS (FIRST NAME, LAST NAME): Kobra Alizadeh[1, 2, 3], R T. Thompson[1, 2], Frank S. Prato[1, 2, 3], Neil Gelman[1, 2], Donna E. Goldhawk[1, 2, 3]

INSTITUTIONS (ALL):

1. Molecular Imaging, Lawson Health Research Institute, London, ON, Canada.
2. Medical Biophysics , Western University, London, ON, Canada.
3. Collaborative Graduate Program in Molecular Imaging, Western University, London, ON, Canada.

ABSTRACT BODY:

Abstract Body: Introduction: Using cell culture models, we established a direct linear relationship between total cellular iron content and transverse relaxation rates. Accordingly, one way to improve cell tracking using magnetic resonance imaging (MRI) is by increasing the amount of cellular iron. Alternatively, factors that increase the slope of the line correlating these measures should also improve the magnetic resonance signal. Using iron-exporting P19 cells and the endocrine hepcidin to attenuate ferroportin (iron export) activity, we demonstrate an increase in the slope of the line relating transverse relaxation and cellular iron, without altering total iron content. Methods: P19 cells were cultured in iron-supplemented medium containing 25 μM ferric nitrate for 7 days prior to removal of extracellular supplement and culture for an additional 1, 2, 4 and 24 hours. To examine interruption in iron export, hepcidin (200 ng/ml) was added either immediately or 1h after removal of iron supplement. Cells were harvested; mounted in gelatin phantoms; and scanned at 3 Tesla. Image-based measurements of total transverse relaxation rate (R_2*= 1/T_2*) and the irreversible component (R_2=1/T_2) were performed [1]. The reversible component, R2' aas calculated from the difference (R_2* - R_2). Total cellular iron content was measured by inductively-coupled plasma mass spectrometry. Linear regression modelling was performed in SPSS using relaxation rate, as the dependent variable, and cellular iron content, as the independent variable. Fisher Z transformation test and independent t-test were performed to compare the strength of correlations and linear regression slopes (β), respectively. The threshold of statistical significance was $p<0.05$. Results: Table 1 summarizes the correlation between transverse relaxation rates and total cellular iron content in P19 cells treated with and without hepcidin. In the whole data set (n=26), a significantly strong correlation was noted ($p<0.001$); however, there was no significant difference observed between relaxation rates. Separation of samples into non-hepcidin and hepcidin treatment groups revealed additional information. While the correlation between total cellular iron and either R_2 or R_2* was significant in both treatment groups, the slope of this linear regression relationship (β) in hepcidin-treated cells was significantly higher than in non-hepcidin treated samples ($p<0.05$). Discussion: Consistent with previous studies [2], a very strong correlation was observed between transverse relaxation rates and total cellular iron content in P19 cells. With respect to R_2* and R_2, the activity of hepcidin significantly increased the slope of this linear relationship approximately 3-4-fold over untreated samples. An insignificant contribution by R2' indicates that hepcidin activity is almost entirely explained by the change in R_2. These results suggest that regulation of iron export by hepcidin provides an MR-detectable signal. In addition, since macrophage are among the few cells subject to this type of regulation and hepcidin is stimulated by pro-inflammatory signalling, MRI may be an ideal platform for monitoring tissue inflammation.

(No Image Selected)

SESSION TITLE: Poster Session 01

CONTROL ID: 2686924

TITLE: In vivo visualization of HIV infection in humanized mice

PRESENTER: Won-Bin Young

AUTHORS (FIRST NAME, LAST NAME): Won-Bin Young[1, 2], Xiying Qu[1]

INSTITUTIONS (ALL):

1. Radiology, U of Pittsburgh, Pittsburgh, PA, United States.
2. Neuroscience, Lewis Katz School of Medicine at Temple University, Philadelphia, PA, United States.

ABSTRACT BODY:

Abstract Body: Introduction: Currently, the only functional cure for HIV is by suppressing the virus to an undetectable level via antiretroviral therapy (ART); however, the viremia could still rebound after ART withdrawal despite a life time use of ART. In vivo imaging can provide real time information and non-invasive images of deep tissues and organs for visualizing and quantifying HIV transmission and the tissue-resident infected cells as potential reservoirs. Knowing where the HIV-infected cells are allows for monitoring how the infection spreads from the primary infection site to others in real time over the course of infection. This also provides an opportunity for investigating where the HIV sanctuaries are during the suppressive ART and, when and where viremia rebound occurs after ART withdrawal. In vivo imaging can also be used as a readout for evaluating the efficacy of ART, vaccines and HIV eradication strategies, e.g. genome editing.

Materials and Methods: We previously demonstrated that in vivo bioluminescence imaging (BLI) based on an enhanced firefly luciferase is sensitive for visualizing as few as 5 single cells in a niche (Song, Cai et al. 2015). In this study, we engineered replication-competent HIV-BaL (CCR5/macrophage tropism) carrying this luciferase reporter for infecting humanized Bone marrow-Liver-Thymus (BLT) mice via vaginal mucosa or intraperitoneal injection. A combination of ART consisting of Truvada and Raltegravir was used to treat the infected BLT mice to reveal the HIV resistance in different tissues and organs.

Results: Compared to the intraperitoneal route, penetration of mucosal barrier by HIV vaginal transmission requires at least 17 fold more virus. Infection in the female reproductive tract (FRT) could be visualized in the vaginal vulva/canal 48 hrs post inoculation (p.i.). Robust infection from FRT to initiate a systemic infection was visualized as early as 21 days, p.i., an eclipse phase during local HIV expansion. Compared to intraperitoneal inoculation, the spatial-temporal dynamics of HIV mucosal transmission is significantly different, which is unlikely to be observed via conventional measurement of viral load in the blood. Treating the inoculated hu-BLT mice with combination ART, consisting of Truvada plus Raltegravir, resulted in declined HIV dissemination in only two weeks. HIV rebound was observed in the neck lymph node two weeks after ART withdrawal.

(No Image Selected)

SESSION TITLE: Poster Session 01

CONTROL ID: 2727283

TITLE: The accurate non-invasive staging of liver fibrosis using deep learning method on two-dimensional shear wave elastography

PRESENTER: Hui Zhou

AUTHORS (FIRST NAME, LAST NAME): Hui Zhou[1], Kun Wang[1], Jie Tian[1]

INSTITUTIONS (ALL):

1. Key Laboratory of Molecular Imaging of Chinese Academy of Sciences, Institute of Automation, Beijing, China.

ABSTRACT BODY:

Abstract Body: Introduction:

The clinical prognosis, surveillance and treatment of patients with liver fibrosis depend on the correct diagnostic of liver fibrosis staging. Traditionally, liver biopsy(LB) is the gold standard for staging liver fibrosis, but it is invasive and may cause complications. Therefore, it's necessary to develop a noninvasive but accurate method for staging liver fibrosis.

Two-dimensional shear wave elastography(2D-SWE) can calculate the speed of shear waves, which is directly related to tissue stiffness. Therefore, 2D-SWE is now widely recognized as a reliable method to assess liver fibrosis. There are few published studies which use the value from 2D-SWE as the threshold to assess liver fibrosis, and the result is good for single center. However, these studies also point out that this method is inadequate for staging liver fibrosis for multicenter.

We hypothesis that ultrasound images contain a wealth of information, which is essential to stage liver fibrosis. Therefore, a noninvasive method, which making full use of ultrasound images, applies to multicenter application.

Methods:

In this study, about 400 patients from twelve centers with liver fibrosis staging F0 to F4 were included. Five ultrasound images were obtained for each patient, namely, the dataset is consisted of two thousand pictures. The dataset was divided into training set (about 300 patients) and validation set (about 100 patients).

A convolutional neural network(CNN) model, as shown in the figure below, is built for the study. This CNN model can capture high-throughput information from medical ultrasound images, Furthmore it can give a better result for staging fibrosis compared with the clinical method.

Results:

Receiver operating characteristic (ROC) curves were obtained to assess the diagnostic performance on multicenter datasets. The CNN model was superior to the clinical model in diagnosis of significant fibrosis (score of F2 or greater) (AUC, 0.81 vs 0.77) and early cirrhosis (score of F4) (AUC, 0.97 vs 0.90).

Conclusions:

By using the CNN model we built, plenty of useful information from medical images can be acquired. Furthermore, a better result can be obtained for staging liver fibrosis compared with the clinical method. This CNN model can improve diagnostic accuracy on multicenter datasets, and benefit the clinical treatment.

Index Terms—Liver fibrosis, Two-dimensional shear wave elastography, Multicenter, Deep learning, Convolutional neural network

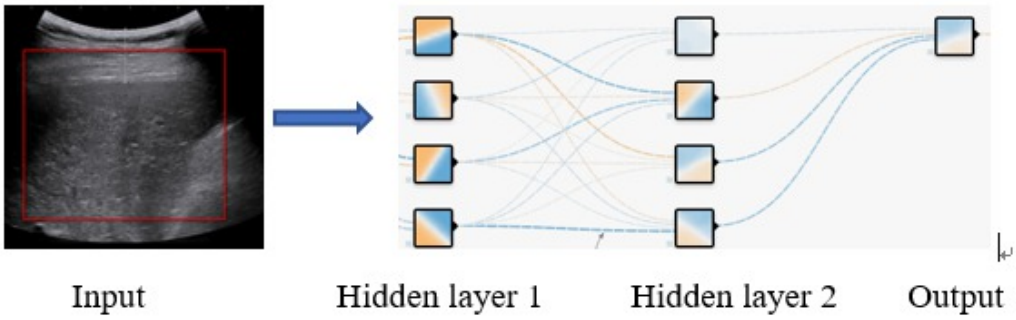

CNN model

IMAGE CAPTION: CNN model

SESSION TITLE: Poster Session 01

CONTROL ID: 2727703

TITLE: Translational imaging of B cells labeled with [^{18}F]FDG in non-human primate.

PRESENTER: Hiroshi Fushiki

AUTHORS (FIRST NAME, LAST NAME): Hiroshi Fushiki[1], Yoshihiro Murakami[1], Nobuhiro Umeda[1], Akihiro Noda[1]

INSTITUTIONS (ALL):

1. Astellas Pharma Inc., Tsukuba, Ibaraki, Japan.

ABSTRACT BODY:

Abstract Body: Cell tracking is one useful application of molecular imaging. However, only few reports have described the feasibility of cell tracking in large animals including monkey. Here we describe translational cell tracking experiments by PET imaging using 2-deoxy-2-[^{18}F]fluoro-D-glucose (FDG)-labeled B cells. Autologous B cells were isolated from the blood of cynomolgus monkeys using anti-CD20 antibody and MACS cell separation system. Isolated B cells were labeled with concentrated [^{18}F]FDG solution. The monkeys were received intravenously transplanted with [^{18}F]FDG labeled autologous B cells with and without rituximab administration, and then dynamic whole body PET imaging was conducted. PET imaging clearly indicated that transplanted B cells were mainly allocated into spleen and liver. Rituximab administration reduced the accumulation of [^{18}F]FDG labeled B cells in both the spleen and liver within one hour, indicating that rituximab rapidly affected the behavior of transplanted B cells. Taken together, cell tracking by [^{18}F]FDG labeling and PET imaging is feasible in non-human primates, and has showed a capability to detect drug responses as a translational research tool from rodents to primates.

(No Image Selected)

SESSION TITLE: Poster Session 01

CONTROL ID: 2728087

TITLE: In vivo Monitoring of Immune Response to Hepatitis B Vaccination by Noninvasive Imaging

PRESENTER: Ha Kim

AUTHORS (FIRST NAME, LAST NAME): Ha Kim[4], Myung Geun Song[4], Keon Wook Kang[3], June-Key Chung[3, 5], Byeong-Cheol Ahn[2], Jung Sun Yum[2], Hyewon Youn[4, 1]

INSTITUTIONS (ALL):

1. Cancer Imaging Center, Seoul National University Cancer Hospital, Seoul, Korea (the Republic of).
2. CHA Vaccine Institute, Seongnam-si, Gyeonggi-do, Korea (the Republic of).
3. Department of Nuclear Medicine, Biomedical Sciences, Cancer Research Institute, Seoul National University College of Medicine , Seoul, Korea (the Republic of).
4. Department of Nuclear Medicine, Cancer Research Institute, Seoul National University College of Medicine, Seoul, Korea (the Republic of).
5. Tumor Microenvironment Global Core Research Center, Seoul National University, Seoul, Korea (the Republic of).

ABSTRACT BODY:

Abstract Body: Purpose:

By taking advantage of Bioluminescence imaging (BLI) with luciferase expressing splenocytes, we monitored the enhancement of immune response against hepatitis B virus (HBV) vaccine with adjuvants in real time to evaluate their efficacy.

Methods:

To visualize antigen in vivo, large hepatitis B virus antigen (L-HBsAg) was labeled with radioiodine (^{125}I-L-HBsAg). B6 mice were vaccinated intramuscularly with ^{125}I-L-HBsAg, ^{125}I-L-HBsAg+adj1, ^{125}I-L-HBsAg+adj2 and ^{125}I-L-HBsAg+adj1+adj2. The localization of ^{125}I-L-HBsAg was monitored for 5 weeks using NanoSPECT/CT. To monitor the immune response in vivo, the luciferase expressing splenocytes from the luciferase transgenic mouse model (B6.Luc^{TG}) were transferred intravenously into immunized B6 mice. Bioluminescence signals from splenocytes were measured by IVIS 100 system. To examine the cellular/humoral response, B6 mice were immunized 3 times at 3 week intervals with L-HBsAg in combination with adj1, adj2 and adj1+adj2. A week after the final immunization, splenocytes were isolated and stimulated with L-HBsAg for 24-48hrs, and analyzed cell-mediated response by IFN-γ ELISPOT and ELISA assay. Mouse serum was analyzed for titers of L-HBsAg-specific IgG and its isotypes by ELISA.

Results:

Localization of inoculated L-HBsAg was successfully monitored using animal SPECT/CT. L-HBsAg was lasted for 5 weeks and diminished. In addition, the injected splenocytes were successfully visualized in immunized mice, homing to spleen within 30 minutes and were accumulated in lymph nodes within 5 hours. Accumulation of splenocytes at vaccination site was observed within 24 hours. 6 days later, mouse vaccinated with ^{125}I-L-HBsAg+adj1+adj2 showed increased accumulation of splenocytes at vaccination site and draining lymph nodes compared to mouse vaccinated with ^{125}I-L-HBsAg, ^{125}I-L-HBsAg+adj1 and ^{125}I-L-HBsAg+adj2. ELISPOT and ELISA assay showed that adj1+adj2 enhances IFN-γ secretion of L-HBsAg-specific T cell and production of L-HBsAg-specific antibodies by synergistic manner.

Conclusion:

In conclusion, in vivo real-time bioluminescent monitoring of splenocytes homing and proliferation against vaccination successfully provides efficiency of adjuvants. Our immune cell imaging system can be useful for evaluation of vaccine efficacy by monitoring enhanced the proliferation and activation of splenocytes near the vaccination site, reducing the development time and cost compared to the conventional methods.

Keyword : Hepatitis B virus, Adjuvant, Immune response, Bioluminescence imaging, Luciferase transgenic mouse model, SPECT/CT

(No Image Selected)

SESSION TITLE: Poster Session 01

CONTROL ID: 2728463

TITLE: A theranostic approach for the prevention of abdominal aortic aneurysms.

PRESENTER: Xiaowei Wang

AUTHORS (FIRST NAME, LAST NAME): Xiaowei Wang[1, 2], Amy K. Searle[1, 2], Yungchih chen[1, 2], Karlheinz Peter[1, 2]

INSTITUTIONS (ALL):

1. Atherothrombosis and Vascular Biology, Baker IDI Heart andDiabetes Institute, Melbourne, VIC, Australia.
2. Monash University, Melbourne, VIC, Australia.

ABSTRACT BODY:

Abstract Body: Background: Abdominal aortic aneurysm (AAA) is a major health concern, carrying an astonishingly high acute mortality rate. Current condition monitoring for high-risk patients is ultrasound imaging, without secondary prevention therapies available. Limited high-risk surgical interventions are available for severe cases.

Purpose: Targeted microbubbles for the delivery of microRNA-126 (miR126) mimics downregulate vascular cell adhesion molecule-1 (VCAM-1) expression, rectify endothelial inflammation and ameliorate the development of abdominal aortic aneurysm.

Methods: Single-chain antibodies against VCAM-1 were conjugated onto ultrasound enhancing microbubbles, and coated with miR126 for targeted delivery.

Results: Using the angiotensin II induced model of murine AAA, we observed that targeted delivery of mimic-miR126 hinder the dilation of the abdominal aorta both before (1.12 ± 0.11 vs. 1.36 ± 0.12; mm mean ± SD; $p>0.05$; N=5-9) and after (0.88 ± 0.06 vs. 1.05 ± 0.05; $p>0.001$; N=5-9) the renal arteries. Further confirmation using 3D ultrasound vessel reconstructions, immunohistological examination, and gene expression analyses ($p>0.01$; N=5-9) confer an overall decrease in VCAM-1 expression and aneurysm severity.

Conclusions: We describe a novel theranostic approach towards effective reestablishment of intravascular endothelial homeostasis under pro-inflammatory conditions. This technology holds immense potential for a safe, non-invasive, targeted treatment towards conditions driven by inflammation of the endothelial, including AAA.

(No Image Selected)

SESSION TITLE: Poster Session 01

CONTROL ID: 2733830

TITLE: Use of optical imaging method to compare PK/Biodistributions of the nanoparticles and therapeutic monoclonal antibodies labeled with near infrared fluorescence

1Cao J, 1Yang J, 8Ilyinskii P, 8O'Neil, C, 8Gao Y 2Johnson J, 2Bangari D, 3Stefano J, 3Chen Y, 3Qiu H, 4Zarazinski E, 4Norton K 5Cate J, 5Youd M, 6Greene B, 6Sabbagh Y, 7Majid T, 1Ying X

1Bioimaging, 2Pathology, 3Biologicals Research, 4In Vivo Research Center, 5Immuno Tolerance Cluster, 6Rare Disease, 7Project Management, Sanofi, Framingham, 8 Selecta Biosciences, Watertown,

PRESENTER: james cao

AUTHORS (FIRST NAME, LAST NAME): james cao[1]

INSTITUTIONS (ALL):

1. Bioimaging, Sanofi-Genzyme, Framingham, MA, United States.

ABSTRACT BODY:

Abstract Body: Introduction: The preclinical assessment of PK/biodistribution is important for prediction of the safety and efficacy of biotherapeutics. The rate and extent of biodistribution is wide and complex as it is dependent on many factors. Biotherapeutics have intrinsic properties such as format, size and charge that influence extravasation and elimination. In addition, not only antibody target binding and off targeting binding affects its PK/biodistribution, but also fragment crystallizable domain FC receptors regulate PK/biodistribution greatly through the immune effector functions of particular animal models. Optical imaging method with near infrared (NIR) fluorescent probe has been successfully used in nonclinical PK/biodistribution studies, complementary to traditional ELISA, LC-MS/MS and radionuclides method. We have used NIR fluorescent labeled antigen or antibody to image PK/Biodistrubution for many different formats of antigen and antibodies.

Methods: 1) Peanut antigen was labelled with Tide Fluorophore 7 and encapsulated into polymeric nanoparticles that previously demonstrated durable therapeutic efficacy in peanut allergic mice (Synthetic Vaccine Particles, SVP made by Selecta Biosciences, Watertown). Four different formulations were dosed through footpad injection into hairless SKH1 mice. 2) Various formats of targeted antibodies and control antibodies were labelled with either with AlexaFluor 680 or 750 and dosed IV or IP in various animal models. The PK/biodistribution of different antigen formulations and different form of antibodies were then determined by in-vivo (live animals), in-situ (lymph nodes) and ex-vivo (organ panels) with IVIS imager over the course of many days.

Results: We demonstrated that the optical imaging approach can be a very useful method to evaluate antigen/antibody PK/biodistribution in preclinical models through in vivo imaging, in situ imaging, blood micro sampling and organ panel imaging. For example: 1) Nanoparticle-encapsulated antigen showed targeted and extended lymph node uptake compared to free antigen with much less systemic exposure; 2) Various format antibodies had dramatic different serum half-life and distinct tissue targeting capacity.

Conclusions: Fluorescence-labeled antibody imaging provides timely PK/biodistribution data at reduced cost compared to traditional bioanalytical methods. Similar to radionuclide imaging method, we limit our fluorescence labeling between 2 to 4 to avoid the potential changes of antigen/antibody property. Both direct comparison of NIR fluorescence imaging and enzyme-linked immunosorbent analysis and its binding property analysis support application of our optical approach for initial PK/biodistribution analysis in preclinical animal models.

(No Image Selected)

SESSION TITLE: Poster Session 01

CONTROL ID: 2734041

TITLE: The Feasibility of ^{18}F-labeled Paeonol Derivative to Detect Neuroinflammation

PRESENTER: Yang-Yi Chen

AUTHORS (FIRST NAME, LAST NAME): Yang-Yi Chen[1], Jia-Jia Lin[1], Min-Ying Lin[1], Chun-Yi Wu[1]

INSTITUTIONS (ALL):

1. Department of Biomedical Imaging and Radiological Science, China Medical University, Taichung, Taiwan.

ABSTRACT BODY:

Abstract Body:

Objectives: In traumatic brain injury (TBI), the expression of 18-kDa translocator protein (TSPO) is upregulated in glial cells and macrophages while its expression is low under normal condition. This study aims to evaluate the potential of ^{18}F-2-(2-(3-(4-fluorophenyl)ureido)thiazol-4-yl)-5-methoxyphenyl 4-methoxybenzenesulfonate (^{18}F-MMBS) as a TSPO ligand in detection of neuroinflammation.

Methods: Starting from paeonol, the precursor 6 for ^{18}F-MMBS preparation was synthesized via a five-step reaction. Radiofluorination of 6 was carried out with [^{18}F]KF/K2.2.2 in the presence of $Cu(OTf)_2(Py)_4$. TBI was induced in adult male SD rats (body weight 300 – 400 g) by using a NYU weight-drop impactor. Briefly, a round tip was used to directly impact the dura matter (dropped from a height of 50 mm) after drilling a hole on the left side of skull (2.8 mm left of and 3.2 mm back from the bregma). In vivo biological studies of ^{18}F-MMBS including microSPCET/CT imaging, autoradiography, and immunohistochemistry (IHC) staining were performed with a neuroinflammation-induced rat model.

Results: The precursor 6 was synthesized in around 8% yield after multi-steps syntheses. After HPLC purification, ^{18}F-MMBS was prepared with acceptable radiochemical yield (≧15%, decay corrected) and high radiochemical purity (≧98%) from precursor 6 with a synthesis time of 155 mins. IHC staining for glial fibrillary acidic protein (GFAP) and CD68 was clearly observed in excised rat brain tissue slices, indicating that this animal model is appropriate for the study. For microPET/CT imaging, the radioactivity accumulation of ^{18}F-MMBS in lesion site was observed at 10-20 mins post-injection and then decreased with time in the inflammation-induced rat, while no significant accumulation was noticed in the cortex of controls. Autoradiography and IHC staining confirmed the results obtained from microPET/CT imaging. The high-uptake region seen in the inflammation-induced rat after ^{18}F-MMBS administration was inflammatory lesion.

Conclusion: In this study, we have successfully synthesized ^{18}F-MMBS with acceptable radiochemical yield and demonstrated the potential of ^{18}F-MMBS to noninvasively reflect the process of neuroinflammation.

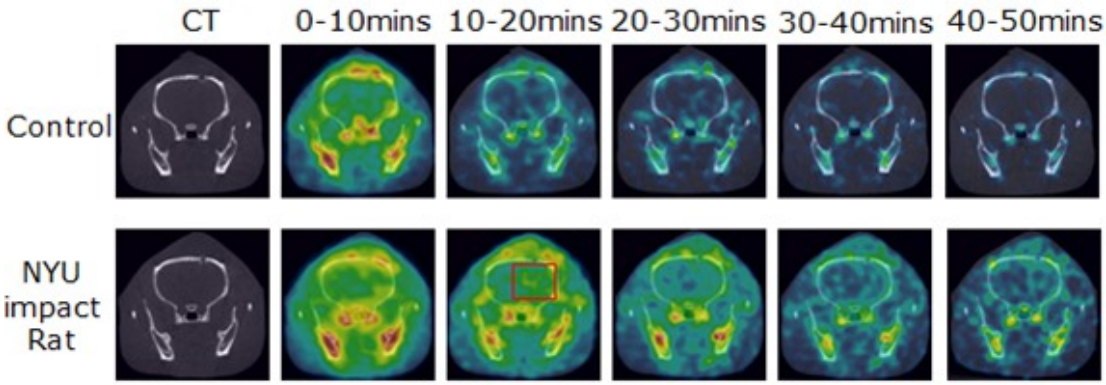
CT
0-10mins
10-20mins
20-30mins
30-40mins
40-50mins
Control
NYU impact Rat

IMAGE CAPTION:

SESSION TITLE: Poster Session 01

CONTROL ID: 2734657

TITLE: The Role of Hepcidin in Monitoring Inflammation by Magnetic Resonance Imaging (MRI)

PRESENTER: Donna Goldhawk

AUTHORS (FIRST NAME, LAST NAME): Kobra Alizadeh[1, 2], R T. Thompson[1, 2], Frank S. Prato[1, 2], Neil Gelman[1, 2], Donna E. Goldhawk[1, 2]

INSTITUTIONS (ALL):

1. Imaging, Lawson Health Research Institute, London, ON, Canada.
2. Medical Biophysics, Western University, London, ON, Canada.

ABSTRACT BODY:

Abstract Body: Introduction Magnetic resonance imaging (MRI) can be used to track cellular activities in the body using iron-based contrast agents[1, 2]. This suggests that a particular cell's iron handling mechanisms may influence the detection of magnetic resonance (MR) contrast [3]. For instance, inflammation involves downregulation of iron export in monocytes and macrophages by the hormone hepcidin [4], due to degradation of the iron export protein ferroportin [5].We therefore examined the effect of hepcidin on transverse relaxation rates in multipotent P19 cells, which provide a convenient model of molecular activities present during inflammation owing to their high iron import and export activities, similar to macrophage [6].

Hypothesis Pro-inflammatory signalling by hepcidin is detectable by MRI due to regulation of iron export.

Methods Iron-exporting P19 cells were cultured for 7 days in iron-supplemented α-minimal essential medium containing 25 μM ferric nitrate (+Fe) prior to removal of extracellular supplement and culture for an additional 1 (1h – Fe), 2 (2h – Fe), 4 (4h – Fe) and 24 (24h – Fe) hours. To examine interruption in iron export, hepcidin (200 ng/ml) was added at either 1h-Fe or +Fe. Cells were then harvested; mounted in a gelatin phantom; and scanned at 3 Tesla. Image-based measurements of total transverse relaxation rate ($R_2^* = 1/T_2^*$) and the irreversible component ($R_2 = 1/T_2$) were performed [7]. The difference between R_2^* and R_2 yields a reversible component ($R_2' = R_2^* - R_2$) that is closely correlated with cellular iron content [3], as measured by inductively-coupled plasma mass spectrometry. Analysis of variance identified significant differences ($p < 0.05$).

Results In the absence of hepcidin, R_2' in P19 cells decreased within hours of iron supplement withdrawal (Figure 1, black line), consistent with high iron export activity [3, 6]. However, hepcidin treatment resulted in stabilization of R_2' over 24 hours, despite the removal of iron supplement (orange line). These findings raise the possibility that cells treated concurrently with hepcidin and iron supplement (green circle), may provide substantial changes in the R_2' of target cells (i.e., monocytes and macrophages).

Discussion We have shown that hepcidin regulation of iron export is detectable by MRI in cells that exhibit high ferroportin expression [3] and actively export iron [6]. We anticipate that interruption of iron export, in combination with continued iron import, may transiently induce an iron retention phenotype, as described for macrophage responding to inflammatory signalling through hepcidin [4]. These findings provide a unique mechanism for monitoring inflammatory signalling and suggest that MRI may be an effective non-invasive imaging modality for the diagnosis of inflammatory diseases.

[1] Li et al (2013) Theranostics 3, 595
[2] Goldhawk et al (2012) Wiley Interdiscip Rev Nanomed Nanobiotechnol 4, 378
[3] Goldhawk et al (2015) Magnetic Resonance Insights 8, 9
[4] Theurl et al (2008) Blood 111, 2392
[5] Nemeth et al (2004) Science 306, 2090
[6] Liu (2015) MSc Thesis, Western University
[7] Sengupta et al (2014) Front Microbiol 5, 29

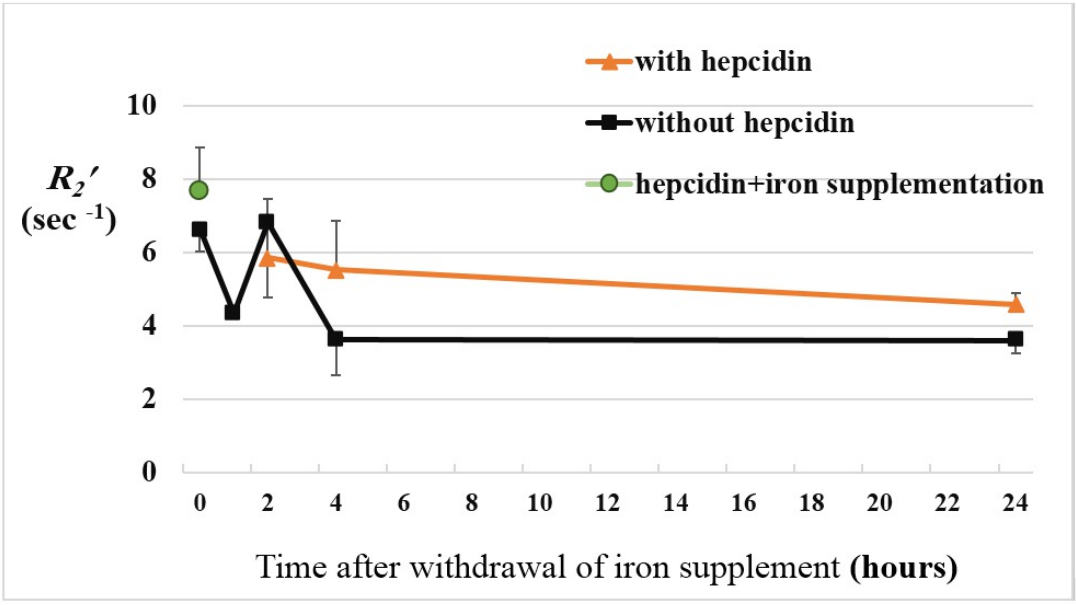

Figure 1. Comparison of R_2' transverse relaxation rates over time in P19 cells after iron supplementation withdrawal, with and without hepcidin treatment. Cells were cultured in iron-supplemented medium for 7 days, then harvested and scanned either immediately (0 hour), or 1, 2, 4 and 24 hours after removal of extracellular iron supplement. One hour after iron withdrawal, hepcidin was added to interrupt iron export. In the absence of hepcidin, R_2' decreased over the course of 24 hours (black line), consistent with ferroportin activity. However, hepcidin treatment resulted in stabilization of R_2' (orange line), suggesting that iron export activity was interrupted. The green circle shows R_2' for cells treated with hepcidin in the presence of iron supplementation. Data are the mean ± standard error (SE) where n=3-8. For 1h-Fe, n=1.

IMAGE CAPTION: Figure 1. Comparison of R_2' transverse relaxation rates over time in P19 cells after iron supplementation withdrawal, with and without hepcidin treatment. Cells were cultured in iron-supplemented medium for 7 days, then harvested and scanned either immediately (0 hour), or 1, 2, 4 and 24 hours after removal of extracellular iron supplement. One hour after iron withdrawal, hepcidin was added to interrupt iron export. In the absence of hepcidin, R_2' decreased over the course of 24 hours (black line), consistent with ferroportin activity. However, hepcidin treatment resulted in stabilization of R_2' (orange line), suggesting that iron export activity was interrupted. The green circle shows R_2' for cells treated with hepcidin in the presence of iron supplementation. Data are the mean ± standard error (SE) where n=3-8. For 1h-Fe, n=1.

SESSION TITLE: Poster Session 01

CONTROL ID: 2734917

TITLE: Synthetic imaging applied to infectious animal disease models for the purpose of improving efficiency in In Vivo studies

PRESENTER: Janie Liang

AUTHORS (FIRST NAME, LAST NAME): Janie Liang[1, 6], Jeffrey M. Solomon[5], Joseph R. Laux[7, 6], Richard S. Bennet[1, 6], David M. Thomasson[3], Peter Jahrling[2], Nadia M. Biassou[4]

INSTITUTIONS (ALL):

1. Virology, IRF, NIAID, Frederick, MD, United States.
2. Integrated Research Facility, NIAID, Frederick, MD, United States.
3. NIH NIAID, Frederick, MD, United States.
4. Department of Radiology and Imaging Sciences, National Insitutes of Health, Bethesda, MD, United States.
5. CIDI/RAD&IS, NIH, Potomac, MD, United States.
6. NIH, Bethesda, MD, United States.
7. IRF, NIAID, Frederick, MD, United States.

ABSTRACT BODY:

Abstract Body: Introduction: Imaging has been used in the past to search for markers of disease in clinical settings. MRI has been the imaging modality of choice in different types of cancers, however, it is possible to use MRI to look at disease progression in infectious diseases as well. One of the constraints of using MRI is the amount of time it takes to acquire an image. In an animal model study, more time translates to more parameters that need to be considered including the amount of extra anesthesia required and the number of animals that can imaged in a given time frame. Shifts in these important study parameters can affect critical time points and can have a negative impact on the study. Synthetic imaging is an MRI technique that can be applied to the evaluation of pathology of in vivo infectious disease models by increasing the efficiency of data generation. Synthetic imaging allows the user to create images using only equations based on a set of given values such as proton density, echo time (TE), repetition time (TR), T1 relaxation and T2 relaxation. This imaging technique was evaluated by physically acquiring an MPRAGE (Magnetization Prepared Rapid Acquisition Gradient Echo) and comparing it to a synthetically produced T1 weighted image.

Materials and Methods:
Images were acquired using a 3.0T clinical MRI scanner. Subject was a female Rhesus macaque, 10 years old, weighing 6 kg. The MPRAGE sequence was acquired with a repetition time of 9.7 msec, an echo time of 4.7 msec and a flip angle of 8.0. The image resolution was 0.5 x 0.5 mm/pixel with 1.0 mm slice thickness and 0.5 mm spacing between slices. Synthetic image created with the parameters of 70.0 degree flip angle, 2 msec repetition time and echo time of 1.8 msec. The image resolution was also 0.5 x 0.5 mm/pixel with 1.0 mm slice thickness and 0.5 mm spacing between slices. Images were processed in MIM (MIM Software Inc., Cleveland, OH). The synthetic image was created using the following equation for a spoiled gradient echo acquisition [1]:

Results: The acquired MPRAGE is a T1 weighted gradient echo sequence and the synthetic T1 weighted image are shown in figure 1. From visual inspection, the synthetic image has greater contrast than the acquired MPRAGE image. This is confirmed by the contrast ratio values; the MPRAGE image has a contrast ratio of 0.19 while the synthetic image has a contrast ratio of 0.384. The T1 weighted image has a contrast ratio of 0.19.

Conclusion: Synthetic imaging is a useful technique for producing comparable images to physically acquired images. They are useful for characterizing and detecting markers of disease as well as disease progression while simultaneously increasing efficiency of acquisition.
The next would be using filtering and processing techniques on these synthetic images and comparing the resulting images with images that have produced from physically acquired sequences.

References:
[1] Bernstein, M. A., King, K. F., & Zhou, X. J. (2004). Handbook of MRI pulse sequences. Amsterdam: Academic Press.

Note: Additional funding by the NCI Contract No. HHSN261200800001E

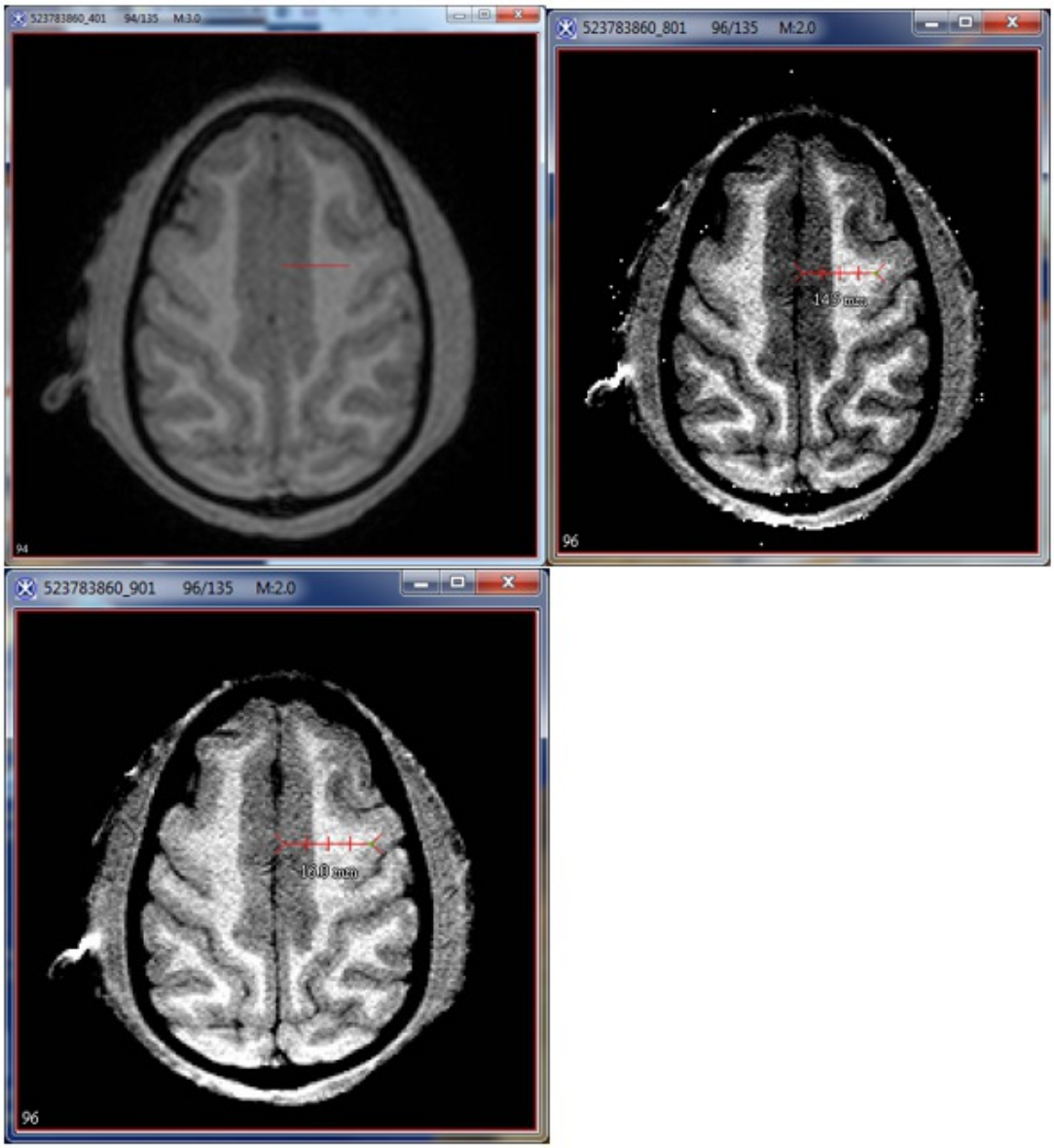

Figure 1: (top left) acquired MPRAGE image (top right) T1 weighted synthetic image (bottom) T1 weighted image

IMAGE CAPTION: Figure 1: (top left) acquired MPRAGE image (top right) T1 weighted synthetic image (bottom) T1 weighted image

SESSION TITLE: Poster Session 01

CONTROL ID: 2734973

TITLE: MicroMRI as a Tool for Assisting the Preclinical Development of Magnetic Resonance Sensors: Imaging of Myeloperoxidase Activity in Human Histopathology Samples.

PRESENTER: Alexei Bogdanov

AUTHORS (FIRST NAME, LAST NAME): Alexei A. Bogdanov[1], Youssef Z. Wadghiri[3], Matthew J. Gounis[4], Peter Caravan[2], Dung M. Hoang[3], John P. Weaver[5], Anita Leporati[1], Aurora Rodriguez-Rodriguez[2], Suresh Gupta[1], Julian Goding[1]

INSTITUTIONS (ALL):

1. Radiology, Laboratory of Molecular Imaging Probes, Worcester, MA, United States.
2. Radiology, Massachusetts General Hospital, Harvard Medical School, Charlestown, MA, United States.
3. Radiology, NYU School of Medicine, New York, NY, United States.
4. Radiology, University of Massachusetts, Worcester, MA, United States.
5. Neurosurgery, UMMS-Neurosurgery, Worcester, MA, United States.

ABSTRACT BODY:

Abstract Body: The pathway to clinical development of magnetic resonance imaging probes is complicated by the absence of early human feasibility data. We report here on one of the potential shortcut strategies that involved in situ imaging of human surgically resected samples of human brain vascular pathology. We performed MR imaging of myeloperoxidase (MPO) activity using MPO-specific imaging probes since MPO is an imaging marker reporting on local inflammatory response (1). We used a high-resolution 7T μMR imaging (μMRI) setup enabled by a set of dedicated micro-MRI histology coils providing a sealed water environment (2). The initial validation of μMRI setup in phantoms was followed by: 1) frozen tissue samples of human ruptured (n=2); 2) unruptured (n=3) aneurysms; and 3) a sample of arteriovenous malformation (AVM). The imaging with 57-100 μm resolution was performed by acquiring ultra-short TE pulse (UTE) sequences with multiple averages (NEX=16). We performed relaxometric and imaging testing of 5-hydroxytryptamide (5HT) of DOTAGAGd, a highly stable macrocyclic chelate of gadolinium (III) as an MPO imaging substrate for μMRI. 5H-DOTAGAGd is a negatively charged, highly soluble myeloperoxidase (MPO) imaging probe stable against trans-metallation. The probe showed 1.5-1.7 fold increase of molar relaxivity ($r_{1,2}$) mediated by MPO/hydrogen peroxide suggesting MPO substrate activity. MPO reaction showed a relaxivity change which strongly depended on magnetic field strength (B_0): despite a low r1 change at 7T, μMRI of tissue-like phantoms showed relaxation time shortening and MPO activity-dependent signal enhancement, which paralleled the intensity of fluorescent products of the MPO reaction with 5HT-Cy3 fluorescent substrate. μMRI of surgically resected samples enabled imaging of MPO activity by tracking the elevated local MR signal enhancement due to the presence of tissue-retained probe. We observed local increase of T1- and T2- weighted normalized signals in resected tissue that matched the elevated MPO levels revealed by using immunohistochemical (IHC) and immunofluorescent (IF) corroboration, i.e. MR signal largely correlated with the presence of MPO in the samples of high-risk unruptured aneurysms as established by IHC and IF (Figure 1). Therefore, 1) μMRI enables testing the efficacy of new MR imaging agents/biomarker targeted probes in non-fixed human tissues; 2) μMRI confirmed the presence of MPO in high-risk unruptured aneurysms (3). References: 1. Chen JW, et al. Radiology, 2006 240:473-81; 2. Hoang DM, et al., Magn Reson Med., 2014 71:1932-43; 3. Gounis MJ, et al., Stroke, 2014, 45:1474-77. Acknowledgement: supported by R01 NS091552 and R01 EB000858.

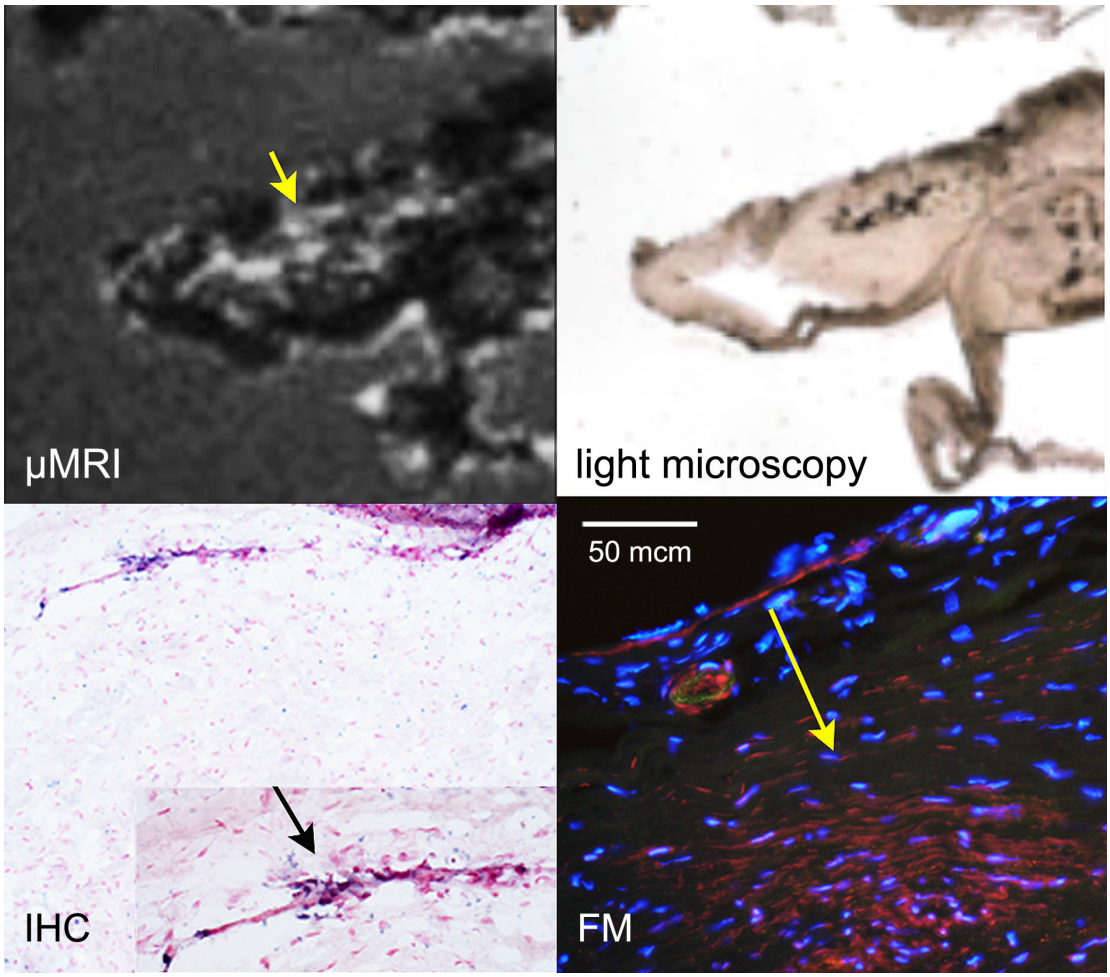

Figure 1. μMRI image of the left middle cerebral artery unruptured human aneurysm tissue sample obtained after incubating 0.1 mm-thick section in the presence of 0.5 mM paramagnetic substrate / 1 mM H_2O_2. Right - light microscopy image. IHC image (thin section) : MPO positive cells (blue, 20x magnification) are pointed to by an arrow. IF - red fluorescence of MPO+ cells and extracellular MPO after treating with 5HT-Cy3/ H_2O_2. Blue – DAPI (nuclei).

IMAGE CAPTION: Figure 1. μMRI image of the left middle cerebral artery unruptured human aneurysm tissue sample obtained after incubating 0.1 mm-thick section in the presence of 0.5 mM paramagnetic substrate / 1 mM H_2O_2. Right - light microscopy image. IHC image (thin section) : MPO positive cells (blue, 20x magnification) are pointed to by an arrow. IF - red fluorescence of MPO+ cells and extracellular MPO after treating with 5HT-Cy3/ H_2O_2. Blue – DAPI (nuclei).

SESSION TITLE: Poster Session 01

CONTROL ID: 2735406

TITLE: Hydrogel swelling-based sensor to radiographically detect pH on implant surfaces

PRESENTER: Md Arifuzzaman

AUTHORS (FIRST NAME, LAST NAME): Md Arifuzzaman[3], Yash Raval[2], Paul W. Millhouse[3], Thomas B Pace[4], Caleb J Behrend[5, 6], John Desjardins[6], Tzuen-Rong J. Tzeng[1], Jeffrey N. Anker[7, 8]

INSTITUTIONS (ALL):

1. Department of Biological Sciences, Clemson University, Clemson, SC, United States.
2. Department of Biological Sciences, Clemson University, Clemson, SC, United States.
3. Department of Chemistry, Clemson University, Clemson, SC, United States.
4. Greenville Health System, Greenville, SC, United States.
5. Virginia Tech Carilion School of Medicine and Research Institute, Roanoke, VA, United States.
6. Department of Bioengineering, Clemson University, Clemson, SC, United States.
7. Department of Chemistry, Clemson University, Clemson, SC, United States.
8. Center for Optical Materials Science and Engineering Technology (COMSET), Clemson University, Clemson, SC, United States.

ABSTRACT BODY:

Abstract Body: A simple biomedical sensor is constructed to noninvasively measure pH on the surfaces of implanted devices using standard X-ray radiography. In the United States over 2 million fracture fixation implants are installed in patients annually, and these fixation surgeries sometimes (~5%) lead to bacterial biofilm formation [1]. Bacterial biofilms are resistant to antibiotics and the host's innate immune system [2]. Fully established bacterial biofilms are almost impossible to eradicate and one of the major reasons for internal implant failure. If the biofilm initiating bacterial infection can be identified at earlier post-operative stages, a less aggressive but effective treatment is possible to give comfort to patients. At early stages, bacteria are often localized near implant surfaces which bring challenges to currently available almost all detection methods. X-ray imaging is routinely used to monitor bone healing, and can detect bone erosion or sinus tracts resulting from infection but does not directly measure pH [3]. Herein we describe a pH sensor which is read with X-ray imaging, comprising a gel with pH-dependent swelling, a radiopaque indicator-dial embedded in the gel, and a scale that the dial position is read against in the radiographs.

The pH-dependent gel sensor was fabricated from a covalently cross-linked poly-acrylic acid hydrogel film which possesses carboxylic acid groups in the backbone of networked polymer chains and exhibits pH-dependent swelling/deswelling. A radiopaque tungsten indicator-dial is embedded in the hydrogel film. Therefore, the swelling/deswelling induced expansion/contraction of the gel-sensor causes the embedded indicator-dial to move against the scale such that the dial position can be seen and pH determined using plain film radiography. The sensor was characterized in standard pH buffers, a bacterial growth culture, and also tested on an orthopedic plate fixed onto a human cadaver tibia. Gel-sensor swelling in neutral to high pH and deswelling in acidic pH causes reversible movement of the radiopaque indicator-dial against an internal scale which is recorded via standard X-ray imaging both in vitro and in a cadaver model. The sensor responded almost identically in bacterial growth culture and in standard pH buffer and had an acceptably rapid response time (~ 30 minutes).

The constructed sensor can detect local pH changes non-invasively on implanted device surfaces using standard X-ray imaging. Hydrogel swelling based sensor provides a simple approach to obtain chemical information through standard radiography, a technique routinely used in patient follow-up.

References:

1. Zimmerli, W., Clinical presentation and treatment of orthopaedic implant-associated infection., J. Intern. Med., 2014, 276(2), 111.

2. Stewart, P. S., Costerton, J. W., Antibiotic resistance of bacteria in biofilms., Lancet, 2001, 358 (9276), 135.

3. Chen, H., Rogalski, M. M., Anker, J. N., Advances in functional X-ray imaging techniques and contrast agents., Phys. Chem. Chem. Phys., 2012, 14 (39), 13469.

Acknowledgement: This research was supported by the grants R-01 (5R01AR070305) and SCBioCRAFT, COBRE (5P20GM10344407) awarded from NIH.

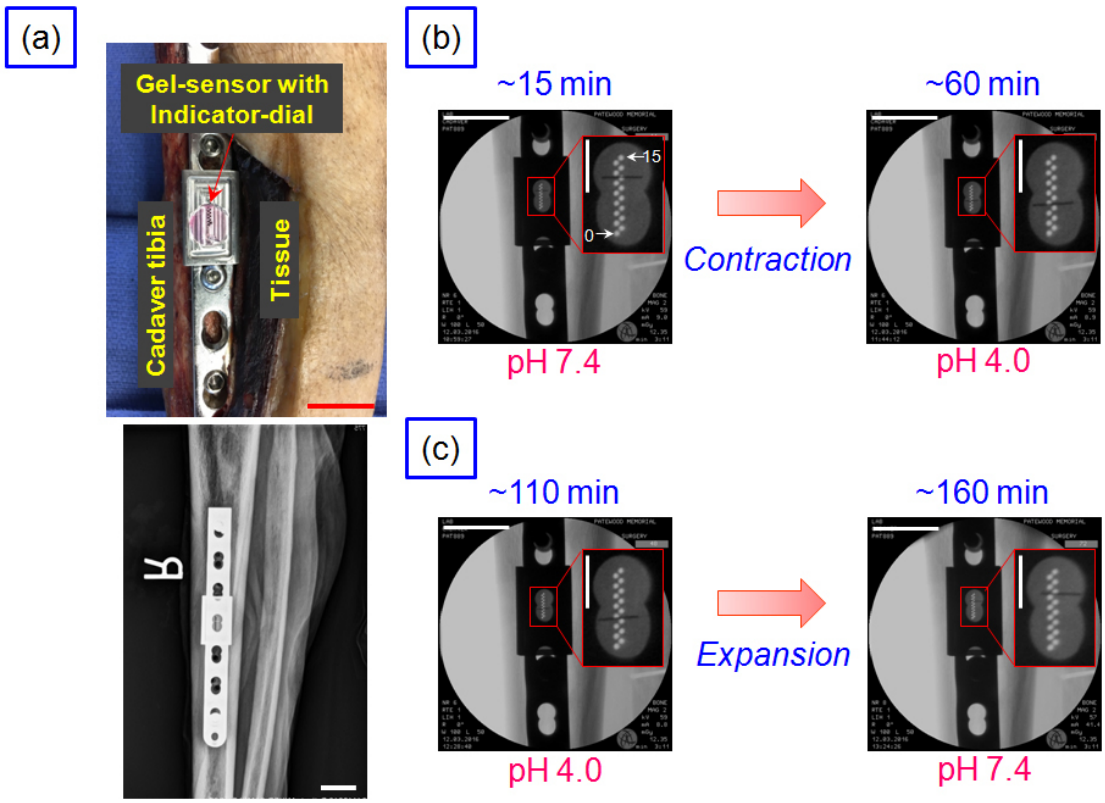

Figure: Testing the pH sensor response on a cadaver tibia. In (a), the above image represents the gel-sensor (incubated in pH 7.4) with an immobilized radiopaque indicator-dial (pointed by using an arrow) attached on a fixed cadaver tibia plate and the image below shows a standard radiograph of the same setup. And in (b) and (c), individual set of radiographs indicate the translated position of the indicator-dial in a radiographic scale made out of constant 250 micron radius holes while deswelling and swelling of the sensor was being occurred towards low and high pH, accordingly. Very bottom hole is counted as hole #1 and very top one is #15. Center to center distance between two adjacent holes is 500 micron. Horizontal and vertical scale bar in the individual images is equivalent to 20 mm and 5 mm, respectively.

IMAGE CAPTION: **Figure:** Testing the pH sensor response on a cadaver tibia. In (a), the above image represents the gel-sensor (incubated in pH 7.4) with an immobilized radiopaque indicator-dial (pointed by using an arrow) attached on a fixed cadaver tibia plate and the image below shows a standard radiograph of the same setup. And in (b) and (c), individual set of radiographs indicate the translated position of the indicator-dial in a radiographic scale made out of constant 250 micron radius holes while deswelling and swelling of the sensor was being occurred towards low and high pH, accordingly. Very bottom hole is counted as hole #1 and very top one is #15. Center to center distance between two adjacent holes is 500 micron. Horizontal and vertical scale bar in the individual images is equivalent to 20 mm and 5 mm, respectively.

SESSION TITLE: Poster Session 01

CONTROL ID: 2735491

TITLE: Quantitative Bioluminescent Tomographic Murine Model to Monitor Antimicrobial Treatment of Staphylococcus aureus Osteomyelitis

PRESENTER: Neal Paragas

AUTHORS (FIRST NAME, LAST NAME): Elizabeth Y. Flores[3], Sabrina Khan[3], Michael Yin[3], Roger D. Plaut[4], Neal Paragas[2], Alexander D. Klose[1], Lowy Franklin[3]

INSTITUTIONS (ALL):

1. In Vivo Analytics Inc, New York, NY, United States.
2. Medicine, University of Washington, Seattle, WA, United States.
3. Columbia University, New York, NY, United States.
4. FDA, Silver Spring, MD, United States.

ABSTRACT BODY:

Abstract Body: Here we monitor a murine model of osteomyelitis using an automated cloud-based software system, InVivoPLOT, that allows for the detection and reliable determination of bacterial density in mice using a bioluminescent (BLI) USA300 strain of Staphylococcus aureus. Osteomyelitis remains among the most difficult infections to manage. Damaged bone, diminished vascular supply and poor antimicrobial penetration into affected tissues has been further exacerbated by the emergence of methicillin-resistant S. aureus (MRSA) strains that are relatively resistant to the traditional treatment, vancomycin. New antimicrobials have demonstrated efficacy in treating MRSA infections. This study will examine the efficacy of current standard of therapy vancomycin using a novel quantitative bioluminescent method to screen the efficacy of these new drugs.

BLI is the best technique to monitor an infection in real-time and its response to therapy over the full course. Current BLI methods for measuring the luminescent bacterial organ burden as colony forming units (CFU) in vivo assume that the measured light intensity at the tissue surface (photons $s^{-1}cm^{-2}$) directly correlates to CFU. However, light is strongly attenuated by tissue and the measured signal is dependent on (i) the spatial location of bacteria, (ii) the heterogeneous optical tissue properties the bacteria reside in, and (iii) the animal's size and shape. Here we use the InVivoPLOT system to overcome those barriers to quantify bioluminescent bacteria and overlay the signal to a high definition anatomical map for longitudinal organ burden monitoring.

The strain used in these initial studies was a MRSA [NRS384 (USA300)-lux] with an integrated plasmid vector containing the luxBACDE operon (SAP231). The bioluminescent construct has been validated in both in vitro and in vivo studies. USA300 is the epidemic strain that has become the most common cause of skin and soft tissue infections in the community and is now also an important nosocomial pathogen. To model osteomyelitis, anesthetized mice (C3H, female, 12-weeks old) had both femurs exposed and, with a 21g needle, a 1mm defect was created. Bacterial inocula of $1x\ 10^6$ bacteria was inoculated into the opening and the wound closed.

Here we used spectral images of the BLI light intensity distribution at the animal's tissue surface for four different views, and transformed them into 3D data sets of the light source inside the animal. InVivoPLOT calculated the bacterial distribution inside the mouse and overlaid these to a novel digital mouse atlas. Tomographic images are represented by coronal slices with 1 mm spatial separation. The bacterial infection could clearly be identified in both femurs. Integrating over the entire ROI of the femur, we calculated the total CFU count at given time points (1, 4, 7, and 14 d) of the longitudinal study in both femurs. Finally, a correlation coefficient for the microbiological versus the bioluminescent data range from 0.79 to 0.99, demonstrating that bioluminescence tomography can be used for the in vivo determination of the bacterial load in both femurs for longitudinal studies without the need for sacrificing the animal.

(No Image Selected)

SESSION TITLE: Poster Session 01

CONTROL ID: 2735733

TITLE: First In Vivo Neutrophil Imaging with Noninvasive Magnetic Particle Imaging (MPI)

PRESENTER: Prashant Chandrasekharan

AUTHORS (FIRST NAME, LAST NAME): Prashant Chandrasekharan[1], Jason Lewis Luke[1], Prarthana Joshi[1], Sneha Balan[1], Elaine Yu[1], Bo Zheng[1], Steven Conolly[2]

INSTITUTIONS (ALL):

1. Bioengineering, UC Berkeley, Berkeley, CA, United States.
2. Bioengineering & EECS, UC Berkeley, Berkeley, CA, United States.

ABSTRACT BODY:

Abstract Body: Aim: Neutrophils are the first line of defense in the body from foreign substances and play a significant role in early tumor development [1,2,3]. Leukocyte scintigraphy is medicine's most powerful imaging tool for highlighting the WBCs as they concentrate at sites of infection, osteomyelitis, and inflammation. MPI [4,5,6], a new and completely non-invasive imaging technique has enormous potential for noninvasive (zero radiation) tracking of WBCs. MPI has already shown exquisite, quantitative sensitivity for in vivo cell tracking (20-200 cells) anywhere in an animal [5,6]. Here, we report the first in vivo MPI scans of prelabeled neutrophils using MPI. Materials and Methods: Neutrophils were isolated from peripheral blood of C57BL6 mice. In brief, RBCs were removed from the isolated blood by lysing. Then neutrophils were isolated by negative selection using magnetic activated cell sorting. Isolated neutrophils were labeled with SPIOs by electroporation. Cell viability assay using trypan blue, iron labeling assay using prussian blue and neutrophil characterization using FACS were performed to ensure the quality of the neutrophils. MPI was carried out with a 6.4T/m gradient homebuilt vertical bore field-free line Berkeley scanner [7]. C57BL/6 mouse was injected with 75,000 SPIO-labeled neutrophils. 3D MPI scans with 21 projections were acquired with respiratory gating. Images were reconstructed with x-space method and filtered back projection algorithm [8,9]. Results: 300,000 neutrophils were isolated from 1.2 mL of the blood sample and the neutrophils were confirmed by CD11b and Ly6G surface markers. Neutrophils without electroporation were 66% viable, whereas only 33.3% of cells were viable when electroporated in the presence of SPIO. Of the total cell sample, 26.7% were labeled cells. The MPI signal was found to be linear with cell number (r2=0.967), as expected. The injected cells quickly concentrated in the liver of the mice. Discussion: MPI tracking of neutrophil could soon provide a completely radiation-free diagnostic complement to Indium111-WBC and Tc99m-WBC scans. Because the magnetic reporter persistence is permanent, there is no tradeoff between radioactive half-life, SNR and time constant for optimal pathophysiologic contrast. In the future, we hope that this platform could help screen early-stage tumors, which are thought to have intact immune response. References: [1] Bar-Shalom R, et al.Journal of nuclear medicine: official publication, SNM. 2006;47(4):587-94. Epub 2006/04/06. [2] Coffelt SB, Wellenstein MD, de Visser KE. NatRevCancer. 2016;16(7):431-46. [3] Lewis SS, et al. Open Forum Infectious Diseases. 2014;1(2):ofu089. doi: 10.1093/ofid/ofu089. [4] Gleich B, Weizenecker J. Nature. 2005;435(7046):1214-7. [5] Zheng, B. et al. Sci. Rep. 5, 14055; doi: 10.1038/srep14055 (2015). [6] Zheng B, et al. Theranostics 2016; 6(3):291-301. doi:10.7150/thno.13728. [7] Yu, E. et al. WMIC 2016. [8] Konkle JJ, Goodwill PW, Hensley DW, Orendorff RD, Lustig M, Conolly SM (2015), PLoS ONE 10(10): e0140137. [9] Konkle JJ et al, Biomedizinische Technik Biomedical engineering. 2013;58(6):565-76.

Field Free Line – MPI scanner

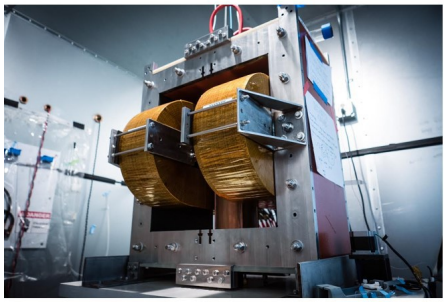

Characterization of isolated neutrophils

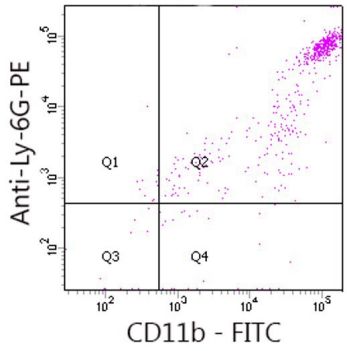

MPI-MIP images of labeled neutrophils

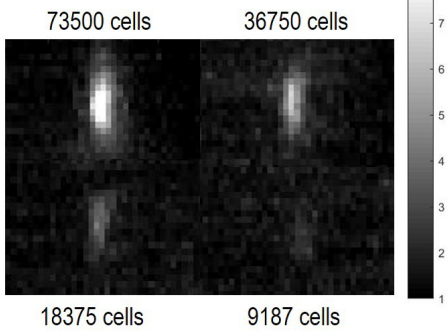

MPI image of 75000 neutrophils injected in C57BL/6 mouse

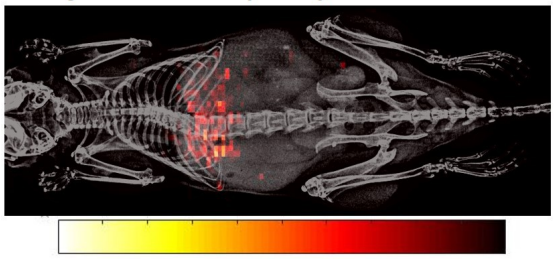

IMAGE CAPTION:

SESSION TITLE: Poster Session 02

CONTROL ID: 2756826

TITLE: Elastin-based molecular magnetic resonance imaging of kidney fibrosis

PRESENTER: Twan Lammers

AUTHORS (FIRST NAME, LAST NAME): Twan Lammers[1], Maike Baues[1], Qinxue Sun[1], Barbara M. Klinkhammer[1], Rene M. Botnar[2], Josef Ehling[1], Fabian Kiessling[1], Peter Boor[1]

INSTITUTIONS (ALL):

1. RWTH Aachen, Aachen, Germany.
2. King's College London, London, United Kingdom.

ABSTRACT BODY:

Abstract Body:

Introduction: Millions of people suffer from chronic kidney disease (CKD) [1]. Biopsies remain to be the gold standard for diagnosis and staging of CKD and renal fibrosis, but suffer from multiple drawbacks, including their invasive nature, painful procedure, sampling variability and limited spatial information . Based on the notion that renal fibrosis refers to the excessive deposition of extracellular matrix components, we here set out to (1) assess the suitability of elastin as a biomarker for kidney fibrosis, and (2) evaluate the potential of elastin-based molecular magnetic resonance imaging (MRI) for non-invasive staging and longitudinal treatment monitoring.

Methods: We have already shown the usefulness of the elastin-specific MRI contrast agent ESMA for molecular imaging of atherosclerosis and liver fibrosis [2,3]. In the present study, ESMA was employed in three established mouse models suffering from kidney fibrosis, i.e. unilateral ureteral obstruction (UUO), unilateral ischemia/reperfusion injury (I/R) and adenine-containing diet (ADE) [4]. In vivo MRI findings were validated using microscopy and laser ablation inductively coupled mass spectrometry (LA-ICP-MS).

Results: Both in human and in rodent tissues, western blotting and immunohistochemistry confirmed the gradual deposition of elastin in the kidney during fibrosis progression (Fig. 1A-B). Elastin expression, localization and upregulation were confirmed using transmission electron microscopy (Fig. 1C). ESMA-enhanced T1-weighted MRI revealed a significant difference in signal intensity in fibrotic vs. healthy kidneys at 24 h after i.v. injection, which was significantly larger than the difference observed upon injecting unspecific Gd-DTPA (Fig. 1D-E). In ADE mice, the MRI signal intensity closely reflected the degree of fibrosis in the time-course of adenine nephropathy, enabling accurate assessment of disease progression as well as efficient treatment monitoring upon CRID3-based anti-inflammasome therapy. Evidence for the repeatability of ESMA-based molecular MRI was also obtained (Fig. 1F). Metal quantification via LA-ICP-MS was in line with the observed MRI signal intensities and identified the highest levels of Gd in fibrotic kidneys in mice injected with ESMA (Fig. 1G-H).

Conclusion: Our findings show that ESMA-based molecular MRI holds promise for non-invasive and quantitative staging and treatment monitoring of kidney fibrosis.

Acknowledgements: This work is supported by the DFG (SFB/TRR57), the ERC (StG309495-NeoNaNo), and the START programme (124/14, 152/12).

References:

[1] Boor P, et al. Nat Rev Nephrol 2010, 6:643-656
[2] Makowski M, et al. Nat Med 2011, 17:383-388
[3] Ehling J, et al. Hepatology 2013, 4:1517-1518
[4] Ehling J, et al. J Am Soc Nephrol 2016, 27:520-532

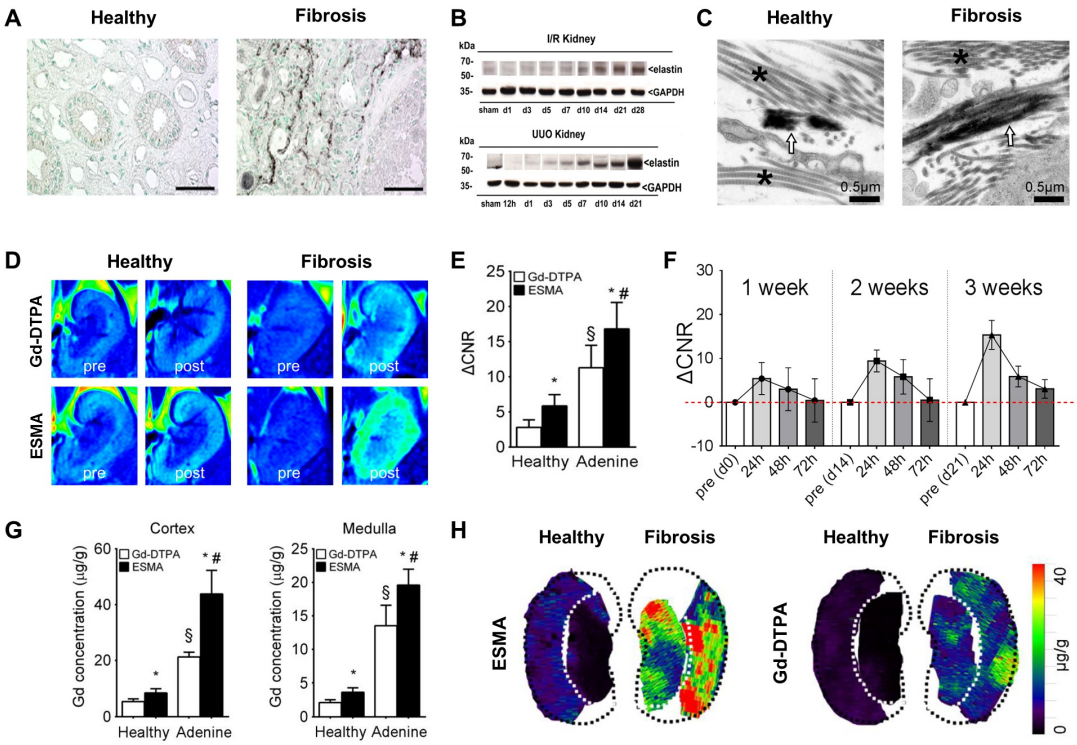

Figure 1: ESMA-based molecular magnetic resonance imaging of kidney fibrosis. A-C: Validation of elastin expression as a biomarker for staging kidney fibrosis by means of immunohistochemistry (A), western blotting (B) and transmission electron microscopy (C; arrows indicate elastin). D-E: Elastin-based molecular MRI of kidney fibrosis, showing strong and specific contrast enhancement in diseased kidneys for ESMA, resulting in significantly changes in the contrast-to-noise-ratios (CNR) than for unspecific Gd-DTPA. F: Longitudinal assessment of fibrosis development in ADE mice using EMS-based MRI, demonstrating the possibility of performing multiple ESMA injections and repeated MRI measurements. G-H: *Ex vivo* Gd quantification using standard ICP-MS (G) and spatial Gd distribution using LA-ICP-MS (H).

IMAGE CAPTION: Figure 1: ESMA-based molecular magnetic resonance imaging of kidney fibrosis. A-C: Validation of elastin expression as a biomarker for staging kidney fibrosis by means of immunohistochemistry (A), western blotting (B) and transmission electron microscopy (C; arrows indicate elastin). D-E: Elastin-based molecular MRI of kidney fibrosis, showing strong and specific contrast enhancement in diseased kidneys for ESMA, resulting in significantly changes in the contrast-to-noise-ratios (CNR) than for unspecific Gd-DTPA. F: Longitudinal assessment of fibrosis development in ADE mice using EMS-based MRI, demonstrating the possibility of performing multiple ESMA injections and repeated MRI measurements. G-H: *Ex vivo* Gd quantification using standard ICP-MS (G) and spatial Gd distribution using LA-ICP-MS (H).

SESSION TITLE: Poster Session 02

CONTROL ID: 2761827

TITLE: Ultrasound Imaging based on Molecular Targeting for Quantitative Evaluation of Hepatic Ischemia Reperfusion Injury

PRESENTER: Chen Qiu

AUTHORS (FIRST NAME, LAST NAME): Chen Qiu[1], Tinghui Yin[1], Rongqin Zheng[1]

INSTITUTIONS (ALL):

1. ultrasound, 3rd affiliated hospital of Sun-yat sen university, Guangzhou, Guangdong, China.

ABSTRACT BODY:

Abstract Body: Objective To prepare intracellular adhesion molecule 1 (ICAM-1) targeted microbubbles (MBs) and obtain molecular imaging of hepatic ischemia reperfusion injury (IRI) inflammation with contrast-enhanced ultrasound (CEUS). Moreover a precise quantitative method of US molecular imaging was established to diagnose different degrees of IRI and monitor anti-inflammatory effect of IRI rats.

Method (1) Preparation of targeted MBs. The binding efficacy of ICAM-1 antibodies to the surface of MBs and the specific affinity of MB_{ICAM-1} in vitro was observed under confocal laser scanning microscope and florescence imaging. (2) Establishment of targeted US imaging evaluating different degrees of IRI inflammation. Rats were divided into 3 groups: normal group, mild IRI group and moderate-severe group. Targeted US imaging was applied in a destruction-replenishment manner after MB_{ICAM-1} was injected via tail vein. Molecular images of each animal was colorfully coded and further qualitative data was expressed as normalized intensity difference (NID, %) by calculating the ratio of the attached MBs imaging signal and total MBs imaging signal. Furthermore a linear regression analysis was performed between NID of each animal and its relative ICAM-1 mRNA expression. (3) Monitoring of IRI inflammation by US molecular imaging. Andrographolide was used to attenuate IRI inflammation in treated group. Both ICAM-1 US molecular images and quantitative data (NID) were acquired in each animal to monitor anti-inflammatory efficacy.

Result (1) Preparation of targeted MBs. Excellent binding efficacy of ICAM-1 antibodies to the surface of MBs and specific affinity of MB_{ICAM-1} in vitro was observed under confocal laser scanning microscope and florescence imaging. (2) Establishment of targeted US imaging evaluating IRI inflammation. In moderate to severe IRI group, molecular images of ICAM-1 exhibited more abundant signal than those of mild IRI group and control group. Consistently, NID in moderate to severe IRI group was significantly higher than that of mild group and control group (38.74±15.08%，21.07±9.65%, 10.26±3.06%，$P < 0.05$). Further statistical analysis showed that there was a good linear correlationship between normalized intensity difference (%) and ICAM-1 mRNA expression ex vivo of each animal（a coefficient of determination $R^2 = 0.7947$, $P < 0.05$). (3) Monitoring of IRI inflammation by targeted US imaging. In treated group, signal of ICAM-1 molecular images was weaker than that without treatment. Additionally, NID of treated group depressed（16.44 ± 5.72%，38.74 ± 15.08%，$P < 0.05$）. Statistical test of NID obtained from images and predicted from equation established previously proved no difference（$P = 0.352$).

Conclusion We have successfully developed ICAM-1 targeted MBs. With this contrast agent, inflammation of IRI in rats was visualized following CEUS. Quantitative molecular imaging data (NID) was proved an accurate and specific quantitative indicator evaluating IRI inflammation .Using this quantitative ICAM-1 targeted US imaging method, anti-inflammatory treatment effects of IRI rats were monitored precisely, which made preparation for clinical trials of IRI therapy.

(No Image Selected)

SESSION TITLE: Poster Session 02

CONTROL ID: 2784342

TITLE: Dynamic PET Imaging to Study the Spatial Biodistribution of ^{11}C-Rifampin in a Rabbit Model of Pediatric TB meningitis

PRESENTER: Elizabeth Tucker

AUTHORS (FIRST NAME, LAST NAME): Elizabeth W. Tucker[1, 2, 3], Brittaney Ritchie[1, 2, 4], Mariah Klunk[5, 2, 4], Alvaro A. Ordoñez[5, 2, 4], Yong S. Chang[5, 2, 4], Sujatha Kannan[1, 6], Sanjay K. Jain[5, 2, 4]

INSTITUTIONS (ALL):

1. ACCM, Johns Hopkins University School of Medicine, Baltimore, MD, United States.
2. Center for Tuberculosis Research, Johns Hopkins University School of Medicine, Baltimore, MD, United States.
3. Division of Pediatric Critical Care Medicine, Johns Hopkins All Children's Hospital, St. Petersburg, FL, United States.
4. Center for Infection and Inflammation Imaging Research, Johns Hopkins University School of Medicine, Baltimore, MD, United States.
5. Department of Pediatrics, Johns Hopkins University School of Medicine, Baltimore, MD, United States.
6. Center for Nanomedicine, Johns Hopkins University School of Medicine, Baltimore, MD, United States.

ABSTRACT BODY:

Abstract Body: Background:

Central nervous system (CNS) tuberculosis (TB) is the most devastating form of extra-pulmonary TB and disproportionately affects young children. TB meningitis is fatal without treatment and, even with treatment, it is associated with high morbidity and mortality. Optimal dosing of drugs for treating TB in privileged compartments such as the CNS is unknown. Rifampin is a first-line TB drug that is critical for sterilization and is required to prevent disease relapse. However, rifampin has limited penetration into the CNS and recent studies demonstrate that treatment could be optimized by specific information about rifampin penetration at the site of infection in the brain. We used a pediatric rabbit model of TB meningitis and performed dynamic positron emission tomography (PET) and computed tomography (CT) imaging to study disease as well as penetration of rifampin into infected brain tissues.

Objective:

To noninvasively determine rifampin penetration in a rabbit model of pediatric TB meningitis using PET bioimaging.

Methods:

TB meningitis in young rabbits (corresponding to toddler age) was established by injecting live Mycobacterium tuberculosis (H37Rv) into the subarachnoid space. Treatment with isoniazid and rifampin began 3 weeks post-infection and animals were serially imaged using ^{18}F-fluorodeoxyglucose (^{18}F-FDG) and ^{11}C-rifampin PET/CT at various time-points. Regions of interest were drawn to determine rifampin penetration into brain tissues versus the blood compartment (carotid artery). Neurobehavioral studies were performed in the imaged animals throughout treatment.

Results:

Imaging demonstrated that the rabbits developed both diffuse (meningitis) and localized (TB lesions) disease in the CNS. ^{18}F-FDG localized to regions of infection in the brain. Motor deficits initially progressed despite treatment, but there was delayed improvement after 4 weeks of treatment in those that survived. The penetration of ^{11}C-rifampin into the brain tissues was limited and local. Area under the curve $(AUC)_{0\text{-}15\ min}$ for ^{11}C-rifampin in brain tissues versus blood was 0.02 ± 0.01 and 0.01 ± 0.01 for infected and uninvolved brain respectively.

Conclusions:

TB meningitis in the rabbit model produces diffuse and localized disease. Overall, ^{11}C-rifampin penetration into the brain is limited, but there is increased at the sites of infection versus uninvolved brain tissues. ^{11}C-Rifampin imaging could be used to noninvasively study the biodistribution of rifampin and penetration into infected brain tissues, where optimal drug concentrations are most important. These studies could be used to optimize treatment dosing in TB meningitis, the most serious and devastating form of TB.

This work was funded by the NIH Director’s Transformative Research R01-EB020539 (S.K.J.), NIH R01HD069562 (S.K.), NIH NICHD K12 PCCTSDP 2K12HD047349-11(E.W.T), StAAR grant from JHH ACCM (E.W.T) and Johns Hopkins ACHF IRGP (E.W.T).

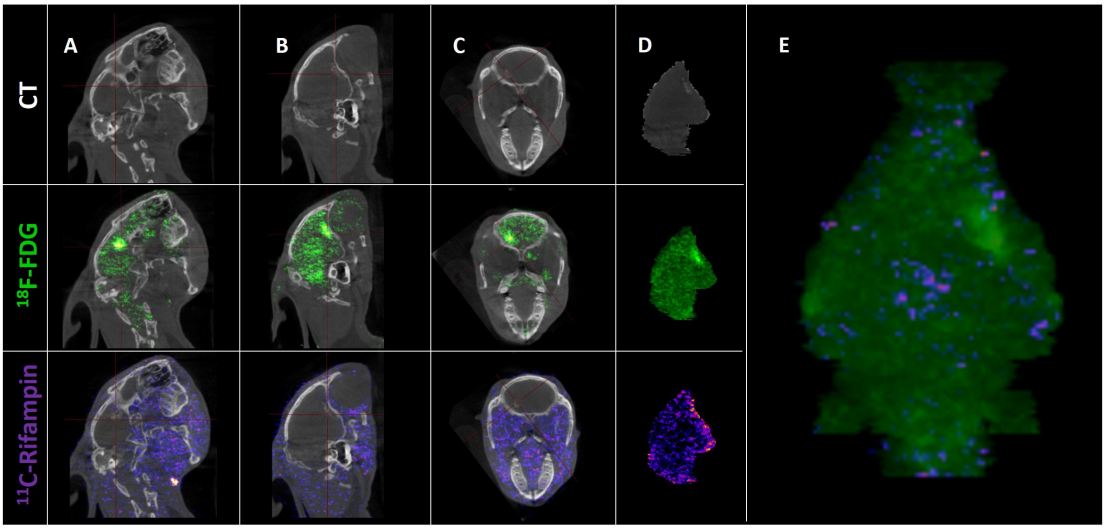

A) Sagittal, B) Coronal, C) Transverse, D) Isolated brain region of interest (ROI) views of CT (top panel), ^{18}F-FDG (middle panel) and ^{11}C-rifampin (bottom panel) and E) 3-D brain ROI reconstruction of ^{18}F-FDG and ^{11}C-rifampin in an infected kit 4 weeks post-treatment with isoniazid and rifampin. CNS lesion with hypodensity on CT (top panel) corresponds with increased ^{18}F-FDG PET signal (middle panel) is noted at the site of the CNS lesion in the infected animal (red cross-hair). There is a paucity of ^{11}C-rifampin PET signal (bottom panel) in the brain, though there is a slight increase at the site of CNS lesion and increased ^{18}F-FDG PET signal which is seen with the3-D brain ROI reconstruction overlay (E).

IMAGE CAPTION: A) Sagittal, B) Coronal, C) Transverse, D) Isolated brain region of interest (ROI) views of CT (top panel), ^{18}F-FDG (middle panel) and ^{11}C-rifampin (bottom panel) and E) 3-D brain ROI reconstruction of ^{18}F-FDG and ^{11}C-rifampin in an infected kit 4 weeks post-treatment with isoniazid and rifampin. CNS lesion with hypodensity on CT (top panel) corresponds with increased ^{18}F-FDG PET signal (middle panel) is noted at the site of the CNS lesion in the infected animal (red cross-hair). There is a paucity of ^{11}C-rifampin PET signal (bottom panel) in the brain, though there is a slight increase at the site of CNS lesion and increased ^{18}F-FDG PET signal which is seen with the3-D brain ROI reconstruction overlay (E).

SESSION TITLE: Poster Session 02

CONTROL ID: 2784553

TITLE: Dynamic in vivo assessment of immune cell infiltration in models of pulmonary Aspergillus infection using ^{19}F MRI

PRESENTER: Shweta Saini

AUTHORS (FIRST NAME, LAST NAME): Shweta Saini[1], Jennifer Poelmans[1], sayuan liang[1, 2], Rein Verbeke[3], Hannelie Korf[4], Ine Lentacker[3], Stefaan Desmedt[3], Katrien Lagrou[5], Uwe Himmelreich[1]

INSTITUTIONS (ALL):

1. Biomedical MRI/Imaging and pathology, KU Leuven, Leuven, Flanders, Belgium.
2. Bio-imaging lab, University of Antwerp, Antwerp, Belgium.
3. General Biochemistry and Physical Pharmacy, University of Ghent, Ghent, Belgium.
4. Hepatology laboratory, KU Leuven, Leuven, Belgium.
5. Clinical Bacteriology and Mycology, Department of Microbiology and Immunology, KU Leuven, Leuven, Belgium.

ABSTRACT BODY:

Abstract Body: Host pulmonary defense mechanisms play a pivotal role in healthy people eliminating Aspergillus fumigatus inhaled spores. Albeit, depending on type of immunosuppressive (IS) drug's mode of action in immunocompromised subjects, progression of fungal hyphae can lead to invasive pulmonary aspergillosis (IPA) & recruitment of certain types of innate immune cells to the lungs . Hence, it's crucial to know interplay between host immune competence &pathogenicity of Aspergillus to better understand dynamics of disease progression and migration of immune cells to lungs. For this, we followed-up A. fumigatus infection in mouse models using two clinically applied IS drugs by fluorine (^{19}F) MRI.

For IS in male Balb/c mice, either hydrocortisone acetate (9mg/mouse) was injected s.c. on day-3/day-1 to develop a nonneutropenic model (HCA group, n=5) or cyclophosphamide (200mg/mouse) was i.p. injected to induce neutropenia on day-4/day-1 (CY group, n=5) prior to fungal infection. On day0, 4h prior to MRI acquisition, intranasal A. fumigatus ($fluc^+$ spores) infection was done in HCA group with 10^6 & CY group with $5x10^5$ spores. Non-infected immunocompetent mice (n=2) served as control group. Longitudinal tracking of immune cells in lungs was done daily using ^{19}F MRI. First MRI was done post 4h infection and 1h after i.v. injection of PFCE particles [doi.org/10.1016/j.jconrel.2013.03.022] (day0/day1) incorporated with surfactant Zonyl® FSP (Z-PFCE) in all murine groups. ^{19}F & ^{1}H MR images were acquired on Bruker Biospec 9.4T MRI system with home-built surface coil & spin echo sequence (TSE). In vivo Computed Tomography was done on day1/day3 post infection. For quantification of fungal load, ex vivo BLI was performed on day3 post administration of D-luciferin into the excised lungs.

We showed HCA group with higher pulmonary ^{19}F MRI signal intensity (SI) compared to CY group, corresponding to higher in vivo Z-PFCE labeled immune cell infiltration post A. fumigatus infection Fig.A. No detectable ^{19}F MRI signal was observed in lungs of mice from control group. We also observed differences in ex vivo BLI from two different immunocompromised groups where a significantly larger SI increase in BLI from lungs was observed in CY group as compared to HCA group Fig.B. Quantitative CT data confirmed lesion development in both infected groups with differences in terms of lesion volume & SI from lungs between HCA and CY groups.

We studied in vivo Z-PFCE labeling of immune cells in 3 different experimental groups using ^{19}F MRI. We demonstrated distinctive interactions between host and pathogen in pulmonary aspergillosis models by tracking cyclic pulmonary recruitment of immune cells (^{19}F MRI) and correlation with accumulation of A. fumigatus (CT and BLI). Our findings showed that HCA treated animals developed excessive inflammation and less fungal infection in contrast to CY model [dx.doi.org/10.1155/2013/693023], depicting peculiar immune environment created by different clinical IS drugs. This clearly indicates the potential of ^{19}F MRI for non-invasive preclinical imaging in providing sensitive in vivo quantitative data on immune cells infiltration in infectious diseases models.

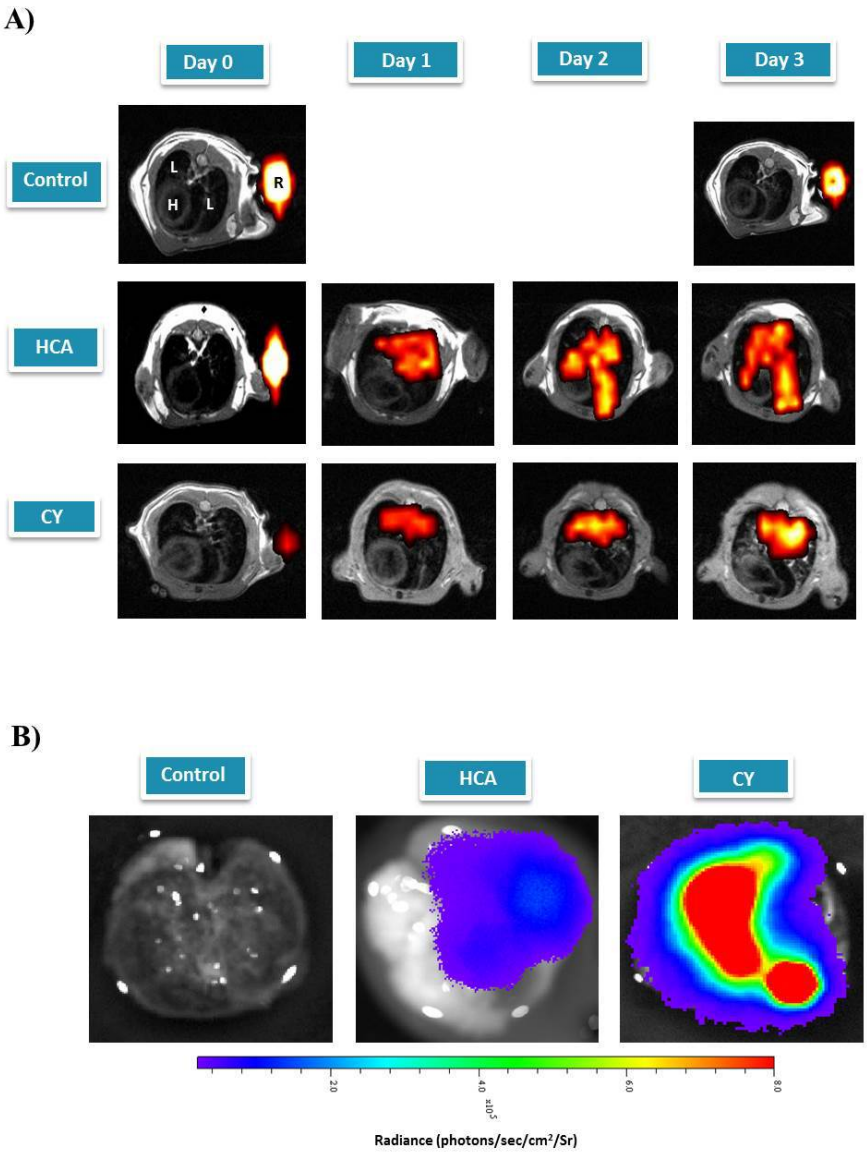

Fig. A; *In vivo* longitudinal ^{19}F MRI images showing recruitment of immune cells in lungs upon pulmonary *A. fumigatus* infection; ^{19}F MRI signal is shown as hot spots and was overlaid on anatomical MRI (^{1}H) images from hydrocortisone acetate (HCA) and cyclophosphamide (CY) groups. The non-infected control group (scanned on Day 0/Day 3) did not show detectable ^{19}F MR signal in the lungs. (**L**=lungs, **H**= heart, **R**= reference with known fluorine spins). **Fig. B, *Ex vivo* bioluminescence imaging (BLI);** On day 3, BLI was performed in all 3 experimental groups. Images acquired show luciferase-expressing *A. fumigatus* fungal burden in the lungs.

IMAGE CAPTION:

SESSION TITLE: Poster Session 02

CONTROL ID: 2790905

TITLE: Multi-Channel In Vivo Imaging of Biomarker Changes in a Mouse Collagen Antibody Induced Model of Rheumatoid Arthritis

PRESENTER: Jeffrey Morin

AUTHORS (FIRST NAME, LAST NAME): Jeffrey Morin[1], Rao Varada[2]

INSTITUTIONS (ALL):

1. Comparative Medicine Global Science & Technology, Pfizer, Andover, MA, United States.
2. Lab Animal Science Center, Boston University, Boston , MA, United States.

ABSTRACT BODY:

Abstract Body: Rheumatoid arthritis (RA), an auto-immune inflammatory disorder affecting close to 2 million Americans, is a progressive disease hallmarked by joint inflammation, pain and stiffness which ultimately lead to bone and cartilage destruction and functional loss of the affected joints. Animal models that reproducibly exhibit signs of the human disease and at the same time allow for non-invasive monitoring of disease severity and progression, will be invaluable to discover and validate novel therapies for RA patients. The mouse collagen antibody induced arthritis (CAIA) model is used to evaluate novel anti-inflammatory drugs, is created by administering an initial injection of a collagen II antibody cocktail, followed by lipopolysaccharide injection three days later which results in acute inflammation of multiple joints. Animals develop classic RA symptoms (e.g., joint swelling, inflammatory cell infiltration) as early as 7 days after initial animal induction, compared to the more established models that develop symptoms much later. CAIA disease progression follows a two part process, with an acute phase driven mostly by innate immune inflammatory arm, followed by a chronic phase dominated by adaptive immune cells of the host. The activity of several joint-destructive enzymes, including Cathepsin K (cat K) and members of the matrix metalloproteinase (MMP) family known to be elevated in RA, was monitored using activatable, near infra-red fluorescent imaging probes. Clinical observations of disease severity correlated with in vivo assessment of cat K and MMP levels. It was found that peak disease symptoms occurred 10 days after model initiation, coincident with increased levels of cat K and MMP activity reaching their maximum ratios compared to signal from the control mice. As the disease progressed to more chronic stage (21 days), the mice showed less severe signs of joint inflammation and disease. A significant reduction in the cat K but not in MMP produced signal was observed, indicating the lasting presence of one or more MMPs in the affected tissues. Furthermore, when mice were treated with oral prednisolone (10 mg/kg BID), a reduction in both cat K and MMP produced signals was observed on both Day 10 and Day 21. The reduced levels of these biomarkers correlated with clinical observations such as paw swelling and clinical scores. These findings highlight both cat K and MMP as useful non-invasive in vivo imaging biomarkers of arthritis and suggest that optical imaging is a valuable approach to longitudinally assess arthritis and other autoimmune disorders in mice during drug discovery and development.

(No Image Selected)

SESSION TITLE: Poster Session 02

CONTROL ID: 2796473

TITLE: Defining the sites of regulatory T cell trafficking in pre-clinical humanised mouse models of transplantation using SPECT/CT imaging.

PRESENTER: Jacinta Jacob

AUTHORS (FIRST NAME, LAST NAME): Jacinta Jacob[1], Gilbert O. Fruhwirth[2], Robert I. Lechler[1], Lesley Smyth[3, 1], Giovanna Lombardi[1]

INSTITUTIONS (ALL):

1. MRC Centre for Transplantation, Division of Transplantation Immunology and Mucosal Biology, King's College London, London, United Kingdom.
2. Department of Imaging Chemistry and Biology, King's College London, London, United Kingdom.
3. School of Health, Sport and Bioscience, University of East London, London, United Kingdom.

ABSTRACT BODY:

Abstract Body:

Introduction

Solid organ transplantation is the current gold standard therapy for end stage organ failure. Although results are excellent in initial years, the recipient's immune system gradually attacks the graft and leads to rejection [1]. Transplantation tolerance can be achieved by favouring a regulatory environment via adoptive transfer of ex-vivo expanded regulatory T-cells (Tregs). This subset of T cells has been shown to suppress excessive immunological activation in many pathological conditions, as well as promoting graft survival [2]. Despite ongoing clinical trials using polyclonal Tregs, details of transferred Treg longevity and trafficking remain elusive.

Methods

To address these questions in vivo, whole body nuclear imaging was employed to visualise radiolabelled human Tregs longitudinally following administration. The human sodium iodide symporter (hNIS), which facilitates radioactive uptake, was expressed on Tregs via lentiviral transduction. Cells were then characterised and tested for suppressive functionality. To visualise Tregs using SPECT/CT imaging, $hNIS^{+}$Tregs and CD25 negative PBMCs were adoptively transferred into immunodeficient BRG (BALB/cRag2$^{-/-}$gc$^{-/-}$) and NSG (NOD/scid/IL-2Rg$^{-/-}$) mice transplanted with human skin. Additionally, BRG mice were treated with or without anti-Gr1 to see whether the presence of mouse granulocytes could impact Treg migration and localisation. $hNIS^{+}$Tregs were tracked with Tc99m pertechnetate (i.v.) on days 0, 3, 8, 16 and 30.

Results

After 3 weeks in culture, 90% of Tregs continued to express hNIS (Fig.1A). Importantly, when labelled with Tc99m pertechnetate, $hNIS^{+}$Tregs exhibited significantly more radioactive uptake in comparison to untransduced Tregs (Fig. 1A). Ex vivo expanded $hNIS^{+}$Tregs also retained their phenotype and suppressive ability following radioactive uptake (Fig. 1B). In BRG mice without anti-Gr1 administration, $hNIS^{+}$Tregs were observed day 3 post transfer in the skin graft and remained visible until day 30 (Fig. 1C). Subsequent retrieval of $hNIS^{+}$Tregs from tissues revealed initial trafficking to the lymph node like structures followed by an increase in $hNIS^{+}$Treg number in the skin graft at day 8 (Fig. 1D). In contrast, BRG mice injected with anti-Gr1 and NSG mice displayed signal in the skin graft only after day 25, suggesting a contribution of innate cells to Treg migration.

Conclusions

This is the first study to show that SPECT-CT imaging using human $hNIS^{+}$Tregs allows longitudinal tracking in a transplant setting and can be employed in future clinical trials to direct Treg cell therapy.

References

1. Nankivell , B.J. and S.I. Alexander Rejection of the Kidney Allograft. New England Journal of Medicine, 2010. 363(15): p. 1451-1462.

2. Safinia, N., et al., Regulatory T Cells: Serious Contenders in the Promise for Immunological Tolerance in Transplantation. Frontiers in Immunology, 2015. 6(438).

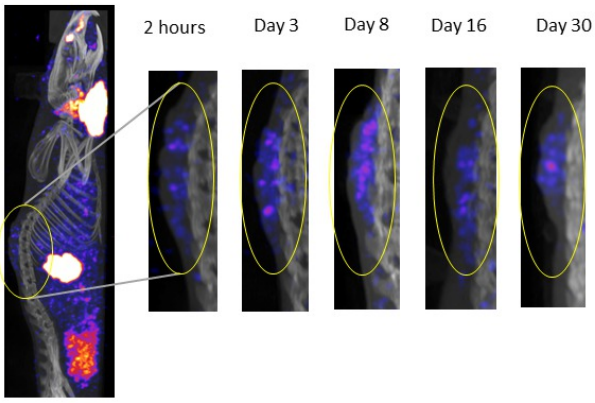

SPECT/CT maximum intensity projections of human skin transplanted mouse imaged longitudinally, following adoptive transfer of hNIS⁺ Tregs; skin graft is circled in yellow.

SPECT/CT maximum intensity projections of human skin transplanted mouse imaged longitudinally, following adoptive transfer of hNIS+ Tregs; skin graft is circled in yellow.

IMAGE CAPTION: SPECT/CT maximum intensity projections of human skin transplanted mouse imaged longitudinally, following adoptive transfer of hNIS+ Tregs; skin graft is circled in yellow.

SESSION TITLE: Poster Session 02

CONTROL ID: 2804481

TITLE: Different imaging pattern between TSPO targeting PET and conventional imaging modalities in murine rheumatoid arthritis model

PRESENTER: Seock-jin Chung

AUTHORS (FIRST NAME, LAST NAME): Seock-jin Chung[1], Hyewon Youn[1], June-Key Chung[1], Gi Jeong Cheon[1]

INSTITUTIONS (ALL):

1. Nuclear Medicine, Seoul National University Hospital, Seoul, Korea (the Republic of).

ABSTRACT BODY:

Abstract Body: Purpose: We visualized murine rheumatoid arthritis with several molecular imaging modalities having different imaging mechanisms, and compared imaging patterns of both conventional imaging modalities and TSPO targeting PET.

Methods: Collagen-induced arthritis (CIA) were developed in DBA/1 mice and the degree of arthritis was measured using severity score (0 to 4). For evaluation of inflammatory response in CIA mice, bioluminescence imaging was performed after injection of luciferase transfected splenocytes in CIA mice. ^{99m}Tc-MDP bone scintigraphy and magnetic resonance imaging (MRI) reflecting osteoblast activity and exudate respectively, were performed in CIA mice. PET/CT and MRI scans were performed with ^{18}F-FDG and F-18 labeled TSPO ligand (FEDAC) reflecting glucose metabolism and activated macrophages. All images were evaluated depending on their severity scores. Histological examinations with immunofluorescence were performed to evaluate TSPO expressions.

Results: Arthritis induced within one week after first immunization of CIA mice and their severity score were increased to the day 40. Splenocytes accumulation measured by bioluminescence imaging was related well with arthritis development in CIA mice. ^{99m}Tc-MDP bone scintigraphy and MRI showed less signal in the non-induced state (Score 0). Both images showed increased signal in the moderate state (Score 1 to 2) and significantly increased in the severe state (Score 3 to 4). ^{18}F-FDG showed no signals in non-induced and moderate state. However, ^{18}F-FEDAC showed slight signals in the non-induced state and strong signals in inflammatory region of the moderate state. ^{18}F-FDG and ^{18}F-FEDAC PET images showed strong and extension signals in the severe state. Immunofluorescence staining of the arthritic joint demonstrated increasing TSPO compared to normal joints.

Conclusions: These findings revealed different characteristic of pathogenesis in rheumatoid arthritis can be visualized by molecular imaging modalities. These results can be used valuably in the research of pathogenesis and in the development of medication for RA.

(No Image Selected)

SESSION TITLE: Poster Session 02

CONTROL ID: 2804548

TITLE: Differentiating acute interstitial nephritis from acute tubular necrosis in a rodent model with ^{18}F-fluorodeoxysorbitol.

PRESENTER: Christopher Palestro

AUTHORS (FIRST NAME, LAST NAME): Christopher J. Palestro[1, 2], Silvat Sheikh-Fayyaz[3, 4], Stephen L. Dewey[7, 5], Kenneth J. Nichols[1, 2], Pravin C. Singhal[6, 5], Matthew J. Hellman[5], Kuldeep K. Bhargava[1, 2]

INSTITUTIONS (ALL):

1. Radiology, Hofstra Northwell School of Medicine of Hofstra University, Hempstead, NY, United States.
2. Radiology, Long Island Jewish Medical Center, New Hyde Park, NY, United States.
3. Pathology, Hofstra Northwell School of Medicine of Hofstra University, Hempstead, NY, United States.
4. Pathology, Long Island Jewish Medical Center, New Hyde Park, NY, United States.
5. Feinstein Institute for Medical Research, Manhasset, NY, United States.
6. Medicine, Hofstra Northwell School of Medicine, Hemstead, NY, United States.
7. Molecular Medicine, Hofstra University School of Medicine, Manhasset, NY, United States.

ABSTRACT BODY:

Abstract Body: Background/Objectives: Acute tubular necrosis (ATN) is the most common cause of acute kidney injury (AKI). Acute interstitial nephritis (AIN) accounts for 5%-15% of all AKI cases. Early diagnosis is important so that the causal agent can be removed & appropriate therapy can be instituted promptly. Differentiating AIN & ATN can be difficult because the clinical presentation of these two entities can be similar. The reference standard for diagnosis is the presence of an intense interstitial infiltrate of mononuclear cells, T lymphocytes, plasma cells, & eosinophils on renal biopsy. Biopsy, however, is invasive with side effects such as pain, hematuria, bleeding, & occasionally nephrectomy. Gallium-67 (^{67}Ga), which has limited resoltuion & requires 2 days between injection & imaging, is used as a non-invasive alternative to biopsy to differentiate AIN & ATN. The positron-emitting analog of a sugar free sweetener, sorbitol, 2-[^{18}F]-fluorodeoxysorbitol (^{18}F-FDS) has been used to image certain infections. The objective of this investigation was to determine, in a rodent model, if ^{18}F-FDS, which is imaged shortly after injection & has superior resolution could differentiate AIN & ATN.

Methods: 3 groups of rats were studiedl: Controls (C, n=16), ATN (n=13) & AIN (n=15). ATN animals were imaged 8 days after intraperitoneal injection of 6 mg /kg cisplatin. AIN animals were imaged 14 days after intraperitoneal injection of 150 mg/kg puromycin aminonucleoside. Imaging was performed on a Micro-PET, 3 hours after injection of approximately 11.1 MBq (300 µCi) ^{18}F-FDS, which was derived from commercial ^{18}F-FDG. Kidney & spine SUV's were determined & kidney/spine SUV ratios were generated. 1 nuclear medicine physician reviewed all images; images in which renal activity was more intense than lumbar spine activity were classified as positive for AIN. Animals were euthanized & organs were removed for tissue counting; kidney/spine tissue ratios were generated. Renal tissue samples were evaluated by a pathologist for evidence of mononuclear cellular infiltration (MNC) & tubular damage (TD). Statistical analysis was performed with “Medcalc” software. The Chi-square test indicated that none of the continuous variables were normally distributed, so significance of differences of means was assessed by the Wilcoxon unpaired test. Analysis of variance assessed significance of differences by the Student-Newman-Keuls test for all pairwise comparisons. Correlations between continuous variables were assessed by linear regression of log-transformed variables. P value of < 0.05 was considered significant.

Results: MNC was significantly higher in AIN than in ATN & C. TD was significantly higher in ATN than in AIN & C. Mean kidney SUV & kidney:spine SUV ratios were significantly higher in AIN than in C & ATN. Kidney: spine tissue ratio was higher for AIN than for ATN & C; the difference was significant for AIN vs. C. Visually, AIN was accurately differentiated from ATN & C; ATN & C could not be differentiated from each other.

Conclusion:These results indicate that in an animal model ^{18}F-FDS reliably differentiates acute interstitial nephritis from acute tubular necrosis.

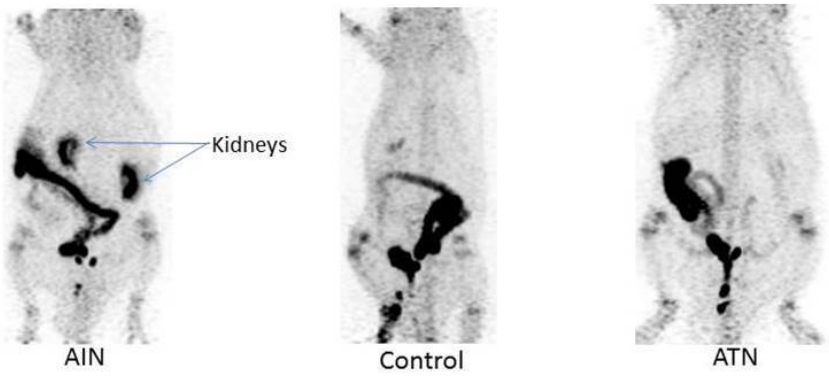

There is intense renal uptake of ^{18}F-FDS in AIN, with little or no renal uptake in the Control or in ATN.

IMAGE CAPTION: There is intense renal uptake of ^{18}F-FDS in AIN, with little or no renal uptake in the Control or in ATN.

SESSION TITLE: Poster Session 02

CONTROL ID: 2805024

TITLE: Fluorinated nanoparticles for the in vivo tracking of inflammation in a mouse model of Spinal Cord Injury

PRESENTER: Francesca Garello

AUTHORS (FIRST NAME, LAST NAME): Francesca Garello[1], Marina Boido[2, 3], Marco Zenzola[1], Matilde Ghibaudi[2, 3], Lorena Consolino[1], Enzo Terreno[1]

INSTITUTIONS (ALL):

1. Department of Molecular Biotechnology and Health Sciences, Molecular & Preclinical Imaging Centers, University of Torino, Torino, Italy.
2. Department of Neuroscience Rita Levi-Montalcini, University of Torino, Torino, Italy.
3. Neuroscience Institute Cavalieri Ottolenghi, Orbassano, TO, Italy.

ABSTRACT BODY:

Abstract Body: The pathophysiology of spinal cord injury (SCI) is described as biphasic: the occurring cellular events are time-dependent and involve the early activation of inflammatory cytokines followed by the glial cyst and scar formation.[1] Therefore, the success of any therapeutic treatment strictly depends on the timing of SCI therapy.[2] Moreover, every cure (e.g. anti-inflammatory drugs,stem cells) is generally limited to symptomatic treatment,and its success is difficult to assess. Here, we tested the possibility to in vivo image inflammation in SCI mice by ^{19}F-MRI/MRS using perfluoro-15-crown-5-ether-based nanoemulsion (PFCE-NE) in order to gain more information about monocyte/macrophage recruitment and investigate the best timing for the therapeutic intervention.

Methods

PFCE-NE was obtained by emulsifying PFCE with Rhodamine-DOPE and Pluronic F-68 by direct sonication. The efficiency of the system in labeling immune system cells was investigated first in vitro in primary macrophages, and then in vivo in a model of SCI in C57BL/6J mice (n=9). The half-life time of the system was determined by ^{19}F MR spectroscopy.The in vivo monitoring of inflammation was performed both by 19F MRI and by Point RESolved Spectroscopy (PRESS). Mice were either once or sequentially injected with PFCE-NE (20 mmol fluorine/kg) at different time points after injury.Pre-saturation of Kupffer cells with a lipid mixture was tested in order to increase targeting efficiency while reducing unspecific uptake.Ex-vivo investigation of PFCE-NE homing to the injured site was carried out by immunofluorescence (IF).

Results

PFCE-NE suspension contained particles with a hydrodynamic size of 170±20nm with a total fluorine concentration of around 3.2 M. In vitro FACS experiments proved the strong avidity of M0, M1 and M2 phenotypes towards PFCE-NE (95% labeling efficiency). In vivo, the 19F signal in blood displayed a bi-exponential decay with very different time constants (t_1=70 min, t_2=20 hours).The recruitment of macrophages at the lesion site was successfully followed for 2 weeks, both by ^{19}F PRESS and MRI (Fig.1),displaying the higher signal enhancement in the first days post injury (pi) even if, when multiple administrations of the contrast agent were repeated, a constant and faint fluorine accumulation was detectable throughout the 14 days of monitoring. At days 3 and 14 pi, the amount of fluorine at the lesion site was 0.85 µmol and 1.9 µmol, respectively. Pre-saturation of Kupffer cells did not result in a significant enhancement of the signal at the lesion site. Ex-vivo validation by IF displayed a massive accumulation of particles in the injured region. In conclusion, PFCE-NE assures the in vivo monitoring of macrophage recruitment in a SCI model both by MRI and PRESS, allowing to identify the best therapeutic time window and to evaluate the treatment success. Moreover, this method may contribute to resolve how immune cells act in SCI as well as in other neuroinflammatory and neurodegenerative diseases.

Acknowledgements

“FUV” is gratefully acknowledged for the support.

References

1. Rowland JW et al. Neurosurg Focus. 2008;25(5):E2.
2. Garbossa D et al. Neurosurg Rev. 2012;35(3):293-311.

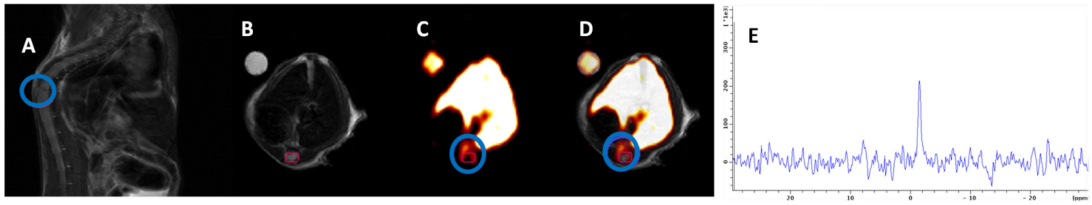

Figure 1. A) 1H high resolution MR sagittal image of the SCI; B) 1H and C) 19F MR axial image of the SCI; D) merge of 1H and 19F MRI of SCI; E) PRESS of a 43 mm^3 voxel located in the site of injury. Blue circles indicate the lesion site, red line delineates the vertebral column.

IMAGE CAPTION: Figure 1. A) 1H high resolution MR sagittal image of the SCI; B) 1H and C) 19F MR axial image of the SCI; D) merge of 1H and 19F MRI of SCI; E) PRESS of a 43 mm^3 voxel located in the site of injury. Blue circles indicate the lesion site, red line delineates the vertebral column.

SESSION TITLE: Poster Session 02

CONTROL ID: 2805132

TITLE: In vivo imaging of mRNA based vaccine antigen in non-human primates using PET reporter mRNA-probe combination

PRESENTER: Talakad Lohith

AUTHORS (FIRST NAME, LAST NAME): Talakad G. Lohith[1], Kerry Riffel[1], Mona Purcell[1], Stephen T. Spagnol[2], Susan Secore[2], Thomas Graham[1], Andrew J. Bett[2], Manishkumar Patel[1]

INSTITUTIONS (ALL):

1. Translational Imaging Biomarkers, Merck & Co.,, West Point, PA, United States.
2. Infectious Diseases and Vaccines, Merck & Co.,, West Point, PA, United States.

ABSTRACT BODY:

Abstract Body: Messenger RNA (mRNA) based vaccines are of great interest recently because of their potential to induce both strong humoral and cellular immune response following transient expression of mRNA-encoded antigen [1,2]. Understanding the tissue types and location of expression is important from both an efficacy and safety standpoint. To characterize the distribution and quantify the expression of an mRNA-encoded antigen non-invasively, a well characterized positron emission tomography (PET) reporter gene-tracer combination of mutant herpes simplex virus type-1 thymidine kinase (HSV1-sr39tk) and 9-(4-(18)F-Fluoro-3-[hydroxymethyl]butyl)guanine ([^{18}F]FHBG) was used in non-human primates (NHP) as in vivo model [3].

The reporter mRNA construct consisting of HSV1-sr39tk was synthesized and formulated in lipid nanoparticles (LNP). The HSV-1 sr39tk and control mRNA-LNP formulations were injected into the right and left deltoid muscles respectively of a rhesus monkey. Twenty four hours later, a 2 h dynamic PET scan covering head to lower abdomen was performed after injection of 5 mCi of [^{18}F]FHBG along with arterial input function for metabolite analysis. Test and retest baseline scans were obtained in the same monkey a few weeks before mRNA-LNP injection. Radioactivity uptake was quantified in terms of regional area under the time activity curve during the clearance phase ($AUC_{30\text{-}120\ min}$) and total distibution volume (V_T) derived from two-tissue compartment model, and compared between ipsilateral and contralateral injection sides as well as between baseline and post-mRNA injection for periphery.

One day after HSV1-sr39tk mRNA/LNP injection, a strong PET signal with higher peak standardized uptake values (SUV) and radioactivity retention were observed in ipsilateral compared to contralateral deltoid muscles and axillary/cervical lymph nodes. The area under-time activity curve of SUV ($AUC_{30\text{-}120}$ min) and V_T values in ipsilateral vs contralateral were ~1.5 and 3 fold higher in muscle and lymph nodes respectively (Figure). However, the PET signal change in the periphery, such as liver, was only 1.2-1.4 fold relative to baseline and was close to the test-retest variability of baseline scans. A strong PET signal change indicates expression of HSV1-sr39TK enzyme localized to muscle tissue as well as its draining lymph nodes. Although there is slight change in the liver PET signal, it could be influenced by nucleoside transporter activity, flow and metabolism between baseline and post-mRNA scans, and therefore may not represent changes due to mRNA expression.

A PET-reporter mRNA imaging method based on a [^{18}F]FHBG as PET probe and HSV1-sr39tk delivered as mRNA could successfully image and quantify distribution and magnitude of mRNA expression in an NHP model. Such non-invasive imaging and quantification of mRNA expression in vivo could play a critical role to understand the distribution and efficacy of mRNA based therapeutics in the clinic.

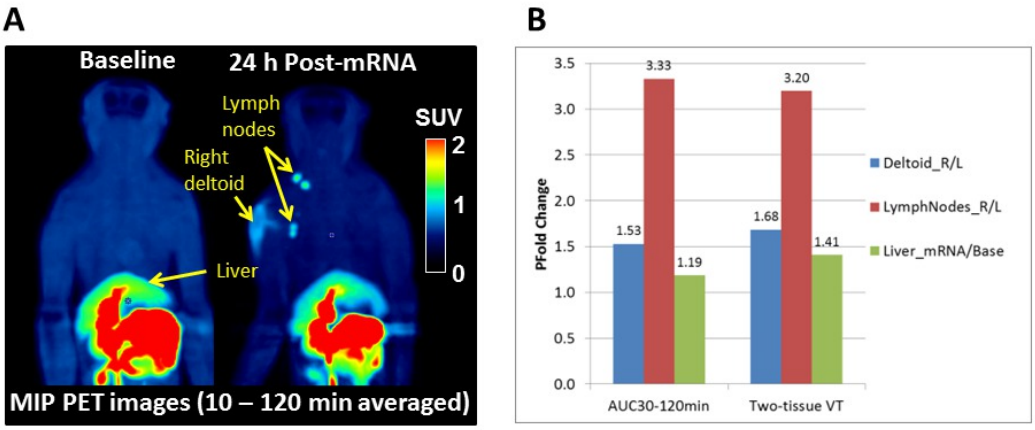

Figure: PET imaging of HSV1-sr39TK mRNA in a rhesus monkey. (A) Baseline and 24 h post-mRNA PET images showing intense radioactivity signal in right deltoid muscle (injection site) and axillary/cervical lymph nodes. The images are maximum intensity projection (MIP) averaged from 10 to 120 min scan time. (B) Regional radioactivity uptake quantified as $AUC_{30\text{-}120\ min}$ and Two-tissue V_T showing similar fold change with highest (~3-fold), moderate (~1.5-1.7 fold), and lowest (~1.2-1.4 fold) in lymph nodes, muscle and liver respectively. The R/L for deltoid and lymph nodes represent ratio between right and left from the post-mRNA scan. The mRNA/Base for liver represents ratio between mRNA and averaged baseline scans.

IMAGE CAPTION:

SESSION TITLE: Poster Session 02

CONTROL ID: 2805163

TITLE: Bioluminescence imaging detects a “viable but non-culturable” state in an in vivo model of catheter colonization by Candida albicans.

PRESENTER: Beatriz Salinas Rodríguez

AUTHORS (FIRST NAME, LAST NAME): Beatriz Salinas Rodríguez[1, 3], Lorena Cussó[1, 2, 3], María Guembe[4], Ana Villarejo[1], Jesús Guinea[4], Patricia Muñoz[4, 5, 6], Emilio Bouza[4, 6, 5], Manuel Desco[1, 3, 2]

INSTITUTIONS (ALL):

1. Biomedical Imaging and Instrumentation Group, Instituto de Investigación Sanitaria Gregorio Marañón, Madrid, Spain , Madrid, Madrid, Spain.
2. Departamento de Bioingeniería e Ingeniería Aeroespacial,, Universidad Carlos III de Madrid, Madrid, Madrid, Spain.
3. Imagen Avanzada, Centro Nacional de Investigaciones Cardiovasculares Carlos III (CNIC), Madrid, Madrid, Spain.
4. Instituto de Investigación Sanitaria Gregorio Marañón, Madrid, Spain.
5. CIBER Enfermedades Respiratorias- CIBERES , Madrid, Spain.
6. Medicina, Universidad Complutense de Madrid, Madrid, Spain.

ABSTRACT BODY:

Abstract Body: Aim:Several bacterial species have been found to exist in a so-called ‘viable but non-culturable’ (VBNC) state as reported in 1982 by Xu and coworkers [1]. This VBNC state implies that some bacteria that do not form morphologically-identifiable spores or cysts are, nonetheless, able to turn into dormant cells. Although this behaviour has been observed in different bacteria strains [2-4], there are no data in the field of fungal pathogens such as Candida albicans. Although VBNC cells are characterized by a loss of culturability on routine media, which impairs their detection by conventional plate count techniques, we have observed by bioluminescence (BL) the existence of a VBNC state in vitro and in vivo in a C. albicans biofilm model

Material and methods: In order to confirm the effectivity of a new antifungal therapeutic approach of catheter colonization (micafungin catheter sealing), we conducted in vitro and in vivo studies using a genetically-modified bioluminescent C. albicans strain SKCA23-ACTgLuc [5]. For in vitro evaluation, microtiter plates were incubated at 37C for 72 hours with 100 µL C albicans (10^6 CFU/mL), and 100 µl of micafungin (16 µg/ml), together with parallel controls of buffer. Metabolic activity of C. albicans was assessed by XTT assay and also by measuring BL. In vivo studies were carried out in animal model employing Wistar rats (n=9) with an intravascular infected catheter. From day one after the surgery, catheters were daily treated and sealed with micafungin (160 µg /ml) during 7 days and kept 7 days more without lock treatment in order to evaluate the progression of the infection. BL assays of each animal were carried out on days 1, 3, 5 and 14. Surviving animals were sacrificed after the last imaging session and the catheters were obtained for microbiological culture.

Results: In the in vitro experiment, after 24 hours on antifungal treatment the BL signal slightly decreased (27%), while metabolic C. albicans activity was markedly reduced (99.7%). After 72 hours of treatment, no metabolic activity was detected by XTT and CFU count was reduced by 99.9%, while the BL signal was reduced (75.4%) but still present. Similar results were observed in in vivo experiments, where micafungin treatment reduced catheter fungal load leading to only 25% of the subjects being positive in catheter culture at day 14. However, bioluminescence was still detectable at day 14 in all the animals, although with significant reduction between days 1 and 5 ($p = 0.018$).

Conclusions: Although in vitro experiments showed that micafungin treatment drastically reduced C. albicans activity and CFU counts after 72 hours of treatment, bioluminescence signal was still present, suggesting that bioluminescence imaging may be a more sensitive technique than current clinical procedures (culture and XTT). The results obtained by BL in the in vitro and in vivo studies support the hypothesis of a VBNC state and could justify the persistence of the fungi observed in the in vivo imaging. Although this work presents promising initial results, further research is warranted to confirm the existence of such VBNC state for C albicans.

(No Image Selected)

SESSION TITLE: Poster Session 02

CONTROL ID: 2805178

TITLE: 2-[^{18}F]F-PABA, a Novel PET Radiotracer for Imaging Bacterial Infection

PRESENTER: Yong Li

AUTHORS (FIRST NAME, LAST NAME): Zhou Zhang[1], Alvaro A. Ordonez[2, 3], Hui Wang[1], Kayla Gogarty[1], Edward A. Weinstein[2], Fereidoon Daryaee[1], Yong Li[1], Jonathan Merino[1], James N. Iuliano[1], EunBin Yoon[4], Alvin Kalinda[2, 3], Ronnie C. Mease[5], Peter Smith-Jones[4], Sanjay K. Jain[2, 3], Peter Tonge[1]

INSTITUTIONS (ALL):

1. Institute for Chemical Biology & Drug Discovery, Department of Chemistry and Radiology, Stony Brook University, Stony Brook, NY, United States.
2. Center for Infection and Inflammation Imaging Research, Johns Hopkins University School of Medicine, Baltimore, MD, United States.
3. Department of Pediatrics, Johns Hopkins University School of Medicine, Baltimore, MD, United States.
4. The Facility for Experimental Radiopharmaceutical Manufacturing, Department of Psychiatry, Stony Brook University, Stony Brook, NY, United States.
5. Russell H. Morgan Department of Radiology and Radiological Science, Johns Hopkins University School of Medicine, Baltimore, MD, United States.

ABSTRACT BODY:

Abstract Body: Staphylococcus aureus is a major contributor to human disease and death and a leading cause of deep-seated and fulminant infections in hospitalized patients as well as those with surgical implants and devices. Methicillin-resistant S. aureus (MRSA) continues to be one of the most prevalent antimicrobial-resistant pathogens, often requiring prolonged intravenous antibiotic therapy. Positron emission tomography (PET) is an imaging tool with exquisite sensitivity and commonly used in the clinic for noninvasive whole-body analysis. In the current work, we developed a method to synthesize a radiofluorinated analog of p-amino benzoic acid (2-[^{18}F]F-PABA), a radiotracer that selectively detects S. aureus in a soft-tissue infection model. Compared to FDG, 2-[^{18}F]F-PABA can discriminate between infection and inflammation, and can be used to quantify changes in bacterial burden upon administration of oxacillin in both MRSA and MSSA infections.

(No Image Selected)

SESSION TITLE: Poster Session 02

CONTROL ID: 2805297

TITLE: Novel neutrophil-specific PET probes targeting formyl peptide receptor type 1: ^{64}Cu-labeled CB-TE1A1P- and NODAGA conjugates of PEG$_{12}$-cBLCLF

PRESENTER: Jaeyeon Choi

AUTHORS (FIRST NAME, LAST NAME): Jaeyeon Choi[1], Lea Nyiranshuti[2], Joseph Latoche[2], Kathryn Day[2], Carolyn J. Anderson[2, 1, 3]

INSTITUTIONS (ALL):

1. Bioengineering, University of Pittsburgh , Pittsburgh , PA, United States.
2. Medicine, University of Pittsburgh, Pittsburgh, PA, United States.
3. Radiology, University of Pittsburgh, Pittsburgh, PA, United States.

ABSTRACT BODY:

Abstract Body:

Objectives: The overall goal of the research is to develop neutrophil specific PET tracers targeting formyl peptide receptor type 1 to provide detailed information about tuberculosis (TB) granulomas. We originally performed PET imaging studies with antagonist ^{64}Cu-CBTE1A1P-PEG$_{12}$-Cinnamoyl-Phe-$_{(D)}$Leu-Phe-$_{(D)}$Leu-Phe(cFLFLF). Although this tracer showed high uptake in the Complete Freund's Adjuvent (CFA) paw inflammation mouse model, it also showed high liver uptake due to the lipophilicity of the peptide structure. To address this problem, we developed a new antagonist, replacing Phe in the 1 and 3 positions to 4-Benzoyl-Lphenylalanine (Bpa) and 3-cyclohexyl-L-alanine (Cha), respectively. In addition, we conjugated the CBTE1A1P and NODAGA chelators, to PEG$_{12}$-Cinnamoyl-$_{(D)}$Bpa-Leu-$_{(D)}$Cha-Leu-Phe(cBLCLF)[1] for ^{64}Cu labeling.

Methods: The final compounds CB-TE1A1P-PEG$_{12}$-cBLCLF and NODAGA-PEG$_{12}$-cBLCLF were successfully synthesized as confirmed by ESI mass spectrometry and HPLC. For Cu-64 labeling to both agents, 4 nmol of conjugate were reacted with 2 mCi of Cu-64 in 0.1 M ammonium acetate buffer (pH 4.1 and 6.8 for the NODAGA and CB-TE1A1P conjugates, respectively) for 30 min at 70° C. For the paw inflammation model, mice (6 to 8 weeks old) were injected subcutaneously in the right paw with CFA (50 µL). Mice were assayed 24 h after CFA injection, while images were obtain at 6 and 18 h post-tracer injection.

Result: The radiolabeling efficiency of both BLCLF analogs was 99% and showed > 98% stability in PBS at 37° C out to 6 h. Both BLCLF analogs showed significant uptake in the CFA paw inflammation site. For the CB-TE1A1P analog, the SUV$_{mean}$ of the inflamed site was 2.6 ± 0.09 at 6 h, and 1.1 ± 0.06 at 18 h. The SUV$_{mean}$ of the liver was 4.5 ± 0.14 at 6 h, and 2.4 ± 0.07 at 18 h. The inflammation/muscle ratio was 12 at 6 h, and 10 at 18 h. Inflamed paw/normal paw ratio was 8.5 at 6 h, and 7.7 at 18 h. For the NODAGA analog, the SUV$_{mean}$ of the inflamed site was 1.9 ± 0.06 at 6 h, and 1.1 ± 0.11 at 18 h. The SUV$_{mean}$ of the liver was 3.9 ± 0.27 at 6 h, and 2.3 ± 0.10 at 18 h. The inflammation/muscle ratio was 7.1 at 6 h, and 6.1 at 18 h, while the inflamed paw/normal paw ratio was 7.6 at 6 h, and 9.7 at 18 h.

Conclusion: We have developed novel neutrophil-targeted PET imaging probes, ^{64}Cu-NODAGA-BLCLF and ^{64}Cu-CB-TE1A1P-BLCLF. The CB-TE1A1P conjugate showed higher SUV in the inflammation site and higher inflammation/muscle ratio compared to the NODAGA agent, and the CB-TE1A1P agent will likely move forward into a macaque model of tuberculosis to provide insight into the disease progression and the response to treatment.

Acknowledgements: This research was supported by by NIAID grant R01AI118195 and NCI P30CA047904 (UPCI In Vivo Imaging Facility).

References:

1. Hayashi, R., et al. Bioorganic & medicinal chemistry, 2014. 22(15): p. 3824-3828.
2. LOCKE, L. W., et al. Journal of Nuclear Medicine, 2009. 50: p. 790-797.

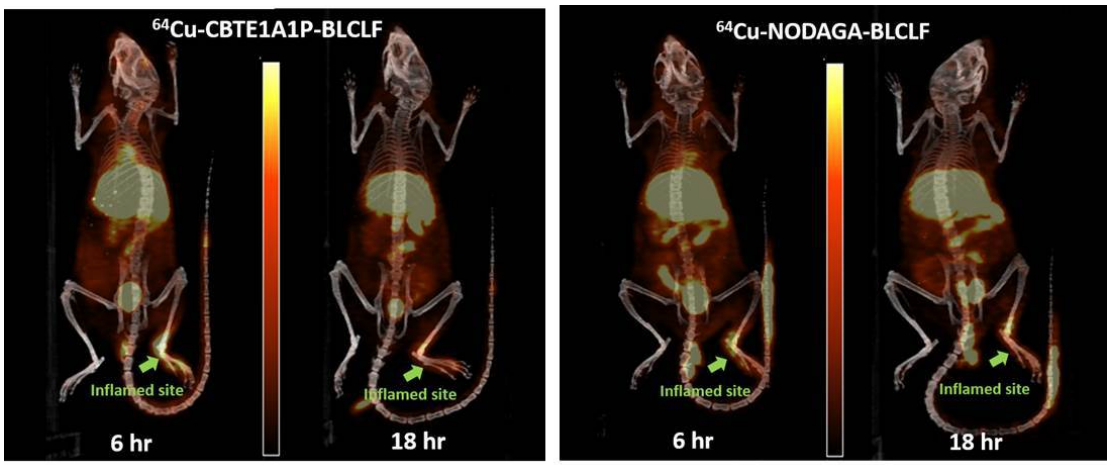
^{64}Cu-CBTE1A1P-BLCLF
Inflamed site
Inflamed site
6 hr
18 hr
^{64}Cu-NODAGA-BLCLF
Inflamed site
Inflamed site
6 hr
18 hr

IMAGE CAPTION:

SESSION TITLE: Scientific Session 06: Infection

CONTROL ID: 2715322

TITLE: Assessing severity of Staphylococcus aureus-induced infective endocarditis by MRI

PRESENTER: Christian Schwarz

AUTHORS (FIRST NAME, LAST NAME): Christian N. Schwarz[1], Verena Hoerr[1, 3], Silke Niemann[4], Carina Hillgruber[5], Tobias Goerge[5], Georg M. Peters[2], Cornelius Faber[1]

INSTITUTIONS (ALL):

1. Department of Clinical Radiology, University Hospital Muenster, Muenster, North Rhine-Westphalia, Germany.
2. Institute of Medical Microbiology, University of Muenster, Muenster, NRW, Germany.
3. Institute of Medical Microbiology, University Hospital Jena, Jena, Thuringia, Germany.
4. Institute of Medical Microbiology, University Hospital Muenster, Muenster, North Rhine-Westphalia, Germany.
5. Institute of Dermatology , University Hospital Muenster, Muenster, North Rhine-Westphalia, Germany.

ABSTRACT BODY:

Abstract Body: Introduction:

Staphylococcus aureus induced infective Endocarditis (IE) is a life threatening disease. To investigate and characterize IE in vivo, an established mouse model and appropriate MRI techniques were used [1], [2]. IE is induced by placing a permanent catheter into the right carotid artery to irritate the aortic valves. Upon systemic infection, S. aureus settles on the damaged endothelial layer of the aortic valves and subsequently infects the endocardium. S. aureus uses a number of adhesion proteins (adhesins), the exact role of each adhesin, however, is still under investigation. Using our mouse model, the role of bacterial fibronectin binding proteins (FnbpA/B) was investigated, using S. aureus strain Newman. FnbpA/B are responsible for invasion and activation of the adjacent endothelium, resulting in endothelial inflammation and procoagulant activity, including platelet activation [3]. Further, the role of host blood von-Willebrand-factor (vWF) was assessed by using a vWF-deficient C57BL/6-mice (Vwf^{tm1Wgr}). It is known, amongst other things, that protein A binds with high affinity to vWF, which mediates platelet aggregation at sites of endothelial damage [3].

Methods:

CD1 mice were infected with 10^5 colony-forming units (CFU) of S. aureus 6850 (n=5) or S. aureus Newman which is deficient in FnbpA/B function (n=17). Further, Vwf^{tm1Wgr} (n=8, 10^5 CFU 6850) were used to examine the interaction of bacteria with the host vWF.

MRI at 9.4T was performed 48h, 96h and 144h after surgery to observe the progression of IE. Cardiac MRI using a self-gated ultra-short echo time (UTE) sequence (TR/TE, 5/0.31ms; in-plane resolution/slice thickness, 0.125/1mm; duration: 12:08min) was applied to obtain high resolution, artifact-free cinematic images of the valves. Severity of IE was assessed in MR images as described previously [1]. After MRI, mice were sacrificed and heart, lung, spleen, kidneys and liver were homogenized to count the bacterial load in each organ.

Results:

Compared to 6850-infected CD1-mice, Newman-infected CD-1mice resulted in a milder course of the IE, as observed by lower clinical scores (Fig. 1A). In the MRI, only two mice out of 14 6850-infected Vwf^{tm1Wgr} showed altered contrast on the heart valves, while all 6850-infected CD1 mice showed alterations (Fig. 1B). Five out of 25 Newman-infected CD1 mice showed altered contrast in the MRI in comparison to 6850-infected CD1-mice (Fig. 1B).

Conclusions:

MRI is a suitable tool to assess severity of S. aureus-induced IE.

Acknowledgement:

This work was funded by the DFG (SFB/TR34).

References:

[1] Ring J et al. (2014). PLoS ONE 9(9): e107179. [2] Hoerr V et al. (2013). J Cardiovasc Magn Reson.15:59. [3] Werdan, K., et al. (2014). Nat Rev Cardiol,. 11(1): p. 35-50.

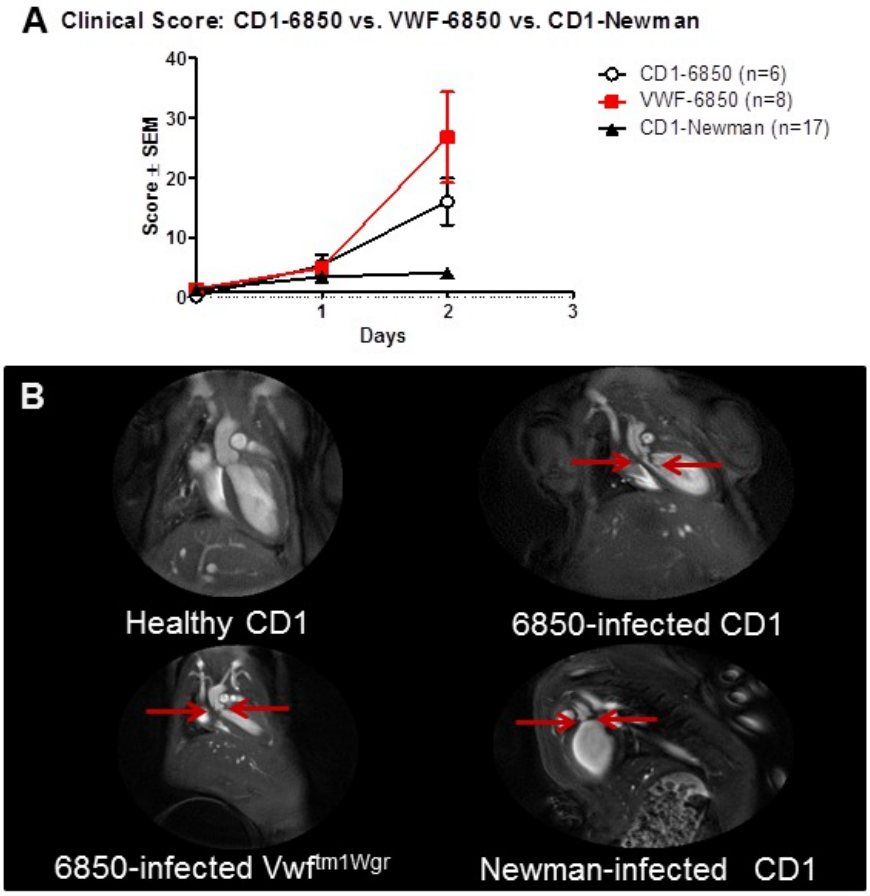

Figure 1: (A) Clinical Score of the three models over three days. Animals reaching a score of 20 were taken out of the experiment. (B) Exemplary MR-images of a healthy heart and IE in the three models. Bacterial vegetations on the valves (dark contrast) are highlighted by red arrows.

IMAGE CAPTION:

SESSION TITLE: Scientific Session 06: Infection

CONTROL ID: 2727857

TITLE: ^{18}F-FDG/PET kinetic modeling for evaluation of pathophysiological alterations after Ebola virus infection

PRESENTER: Svetlana Chefer

AUTHORS (FIRST NAME, LAST NAME): Svetlana Chefer[1], Katie R. Hagen[8], David M. Thomasson[6], Sayre Philip[9], Jurgen Seidel[2], Jeffrey M. Solomon[3], Mark A. Ahlman[4], Lisa Hensley[10], Peter Jahrling[7, 5], Reed F. Johnson[5]

INSTITUTIONS (ALL):

1. Integrated Research Facility, NIAID, NIH, Frederick, MD, United States.
2. Molecular Imaging Program, NIH/NCI , Bethesda, MD, United States.
3. CIDI/RAD&IS, NIH, Potomac, MD, United States.
4. Radiology and Imaging Sciences, National Institutes of Health, Bethesda, MD, United States.
5. EVPS, NIH, Ft. Detrick, MD, United States.
6. NIH NIAID, Frederick, MD, United States.
7. Integrated Research Facility, NIAID , Frederick, MD, United States.
8. National Institute of Allergy and Infectious Diseases, National Institutes of Health , Frederick, MD, United States.
9. IRF, NIAID, NIH, Frederick, MD, United States.
10. IRF, NIAID, NIH, Frederick, MD, United States.

ABSTRACT BODY:

Abstract Body: Introduction: ^{18}F-FDG/PET imaging detects inflammatory processes with high sensitivity[1,2]. In inflamed tissues, increased tissue perfusion and high glucose utilization rate of activated inflammatory cells form the pathophysiological basis of elevated ^{18}F-FDG SUVs. ^{18}F-FDG/PET applied to the Ebola virus (EBOV) nonhuman primate (NHP) model may provide critical data to understand pathogenesis and provide a biomarker that translates to human disease. In this study, ^{18}F-FDG kinetic modeling was utilized to characterize normal tissue and peripheral and systemic host response to EBOV infection via transfer rate constants in the EBOV NHP model.

Methods: Whole body CT and ^{18}F-FDG/PET images were acquired in six rhesus monkeys on a Gemini PET/CT clinical scanner (Philips Healthcare) modified to operate in a biosafety level 4 environment before and after intramuscular challenge with EBOV.

Dynamic PET data were reconstructed with 2–240 sec frame intervals. Volumes of interests for the bone marrow (BM), spleen, liver and left ventricle of the heart (LV) were placed on PET fused with CT images. Time-activity curves from the LV served as the arterial blood input function to calculate K_1, k_2, and k_3 and to produce parametric maps by two tissue compartmental modeling using PMOD and MIM (Fig. 1). From the calculated constants, measured blood glucose concentration (C_{bl}), and a lumped constant LC=0.36, the regional glucose metabolic rate was computed as $MRGlu=C_{bl}x(K_1k_3/(k_2+k_3)]/LC$[3,4].

Results: Pre-infection spleen, BM and liver SUVs averaged from six animals ranged from 2.2 to 3.2. Spleen and liver K_1 were comparable (1.21±0.25 and 1.1±0.61 mL/cm^3/min, respectively), but were almost 10-fold lower in the BM (0.17±0.029 mL/cm^3/min). Spleen and BM k_3 was relatively high (0.073±0.019 and 0.05±0.011 1/min, respectively). SUVs were reproducible with <0.7% (spleen and liver) and <6% (BM) difference between the mean values from two pre-infection scans. Similar reproducibility were demonstrated for K_1, k_3, and MRGlu in the BM and K_1 in the spleen and the liver. Due to low values and high variability up to 30% difference between two pre-infection scans were shown for mean spleen and liver k_3 and MRGlu rate (19.4±8.8 and 13.3±2.9 umol/min/100g). EBOV causes up to a 2-fold SUV increase in the spleen and BM and at the injection site on the arm on day 4 and 5 post-exposure. A 3- to 7-fold increase in K_1, k_3 and MRGlu was detected in the BM and at the site of EBOV injection on day 5 post-exposure. Similar increases in k_3 and MRGlu rate were found in spleen without changes in K_1. None of the liver parameters were altered up to day 5 post-exposure.

Conclusion: This is the first application of compartmental modeling to characterize normal tissue and host response to EBOV infection. The method has proved to be useful converting time-dependent SUVs into physiologically meaningful parameters that could serve as imaging biomarkers (tissue perfusion, glycolytic activity). Compared with contrast-enhanced CT and magnetic resonance imaging, ^{18}F-FDG/PET represents an alternative single examination that provides an information on both vascular and metabolic processes in pathological state.

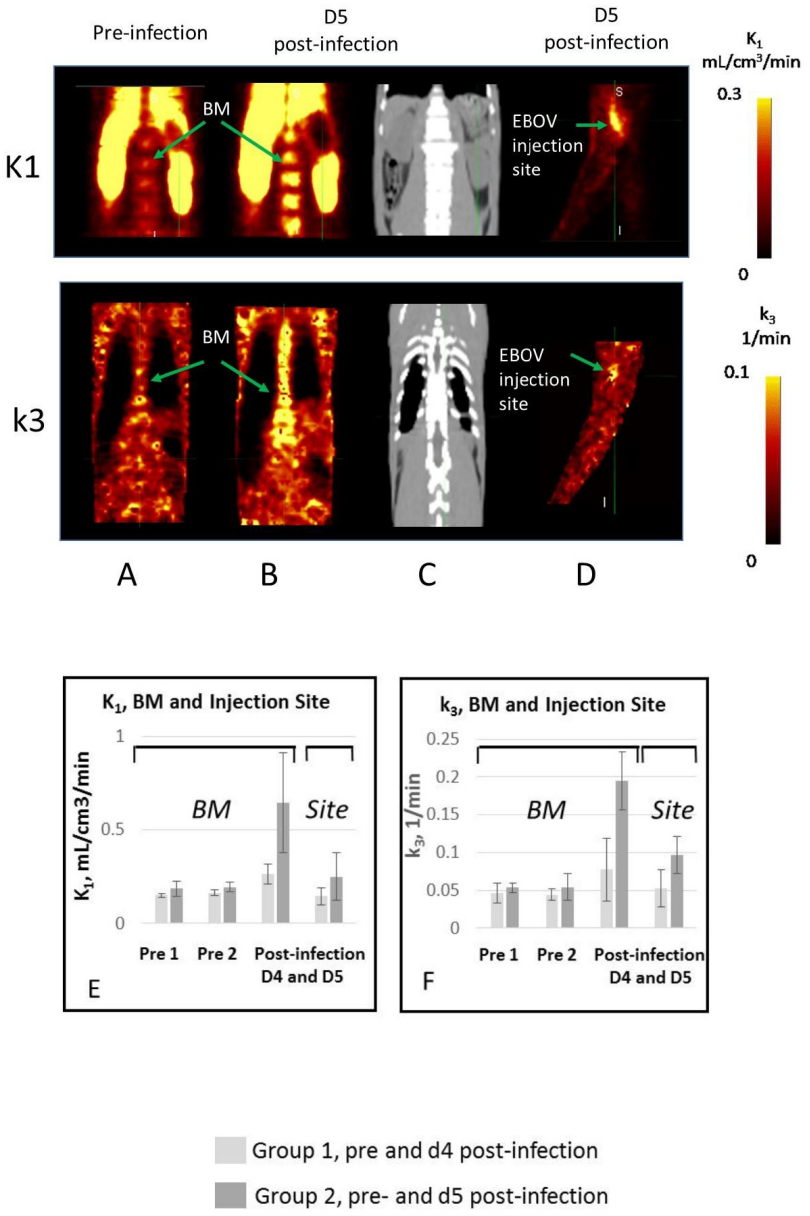

Fig. 1. K_1 and k_3 parametric maps derived from ^{18}F-FDG-PET dynamic data of rhesus monkeys and quantitative analysis of the changes post-exposure to Ebola virus. Parametric maps of K_1 and k_3 pre- and post-injection with EBOV were generated by MIM using image-derived input function computed from the VOI in the left ventricle. **A**, **B**, **D**. Parametric maps of K_1 and k_3 kinetic constants of a representative animal show an increase in tissue perfusion (K_1) and glucose utilization rate (k_3) in the BM and at the injection site on day 5 post-exposure. **C**. CT image aligned with parametric maps images. **E**, **F**. Quantitative analysis of the changes in tissue perfusion, **E**, and glucose utilization rate, **F**, on day 4 (group 1,) and day 5 (group 2) post-exposure assessed by K_1 and k_3 kinetic constants.

IMAGE CAPTION: Fig. 1. K_1 and k_3 parametric maps derived from ^{18}F-FDG-PET dynamic data of rhesus monkeys and quantitative analysis of the changes post-exposure to Ebola virus. Parametric maps of K_1 and k_3 pre- and post-injection with EBOV were generated by MIM using image-derived input function computed from the VOI in the left ventricle. **A**, **B**, **D**. Parametric maps of K_1 and k_3 kinetic constants of a representative animal show an increase in tissue perfusion (K_1) and glucose utilization rate (k_3) in the BM and at the injection site on day 5 post-exposure. **C**. CT image aligned with parametric maps images. **E**, **F**. Quantitative analysis of the changes in tissue perfusion, **E**, and glucose utilization rate, **F**, on day 4 (group 1,) and day 5 (group 2) post-exposure assessed by K_1 and k_3 kinetic constants.

SESSION TITLE: Scientific Session 06: Infection

CONTROL ID: 2727971

TITLE: ^{8}F-FDG/PET imaging to characterize Ebola virus infection and to evaluate the effect of potential therapeutics in a nonhuman primate model.

PRESENTER: Svetlana Chefer

AUTHORS (FIRST NAME, LAST NAME): Svetlana Chefer[2], Larry Zeitlin[3], James Pettitt[2], David M. Thomasson[2], Philip Sayre[2], Jurgen Seidel[4, 2], Mark A. Ahlman[5], Lisa Hensley[2], Peter Jahrling[1]

INSTITUTIONS (ALL):

1. Integrated Research Facility, NIAID, Frederick, MD, United States.
2. Integrated Research Facility, NIAID, NIH, Frederick, MD, United States.
3. Mapp BIopharmaceutical, Inc, San Diego, CA, United States.
4. Molecular Imaging Program, NIH/NCI , Bethesda, MD, United States.
5. Radiology and Imaging Sciences, National Institutes of Health, Bethesda, MD, United States.

ABSTRACT BODY:

Abstract Body: Introduction: In the aftermath of the 2014 Ebola virus disease (EVD) outbreak in Western Africa, major efforts have been undertaken to develop innovative methods for studying the virus in animal models. Characterized by high sensitivity to detect infectious and inflammatory processes, ^{18}F-FDG/PET imaging can play a critical role in researching the EVD process and evaluating potential treatment in pre-clinical settings[1,2]. In this study using a nonhuman primate model, ^{18}F-FDG/PET imaging is utilized to characterize Ebola virus (EBOV) infection and to monitor the response to ZMapp, a cocktail of well-characterized EBOV-specific monoclonal antibodies directed against EBOV glycoprotein[3,'4/sup>.

Methods: Twelve Rhesus monkeys underwent a series of ^{18}F-FDG-PET/CT scans (up to 9 scans over 48 days) of the upper body on a Gemini PET/CT clinical scanner (Philips Healthcare) modified to operate in a biosafety level 4 environment. These monkeys were imaged before and after challenge with aerosolized EBOV Makona C05 isolate with a target dose of 100 plaque forming units. Control groups 1 (n=3) and 2 (n=3) received no treatment or were treated with non-EBOV specific monoclonal antibody, respectively. Groups 3 (n=3) and 4 (n=3) received ZMapp twice (30 min and day 3 post-virus exposure) or three times (30 min, days 3 and 6 post-exposure).

^{18}F-FDG/PET whole body images were acquired between 50 to 60 min after an FDG injection and were fused with CT images. Based on the observed elevated SUVs in the bone marrow (BM), spleen, liver, and lymph nodes (LNs) in the chest following EBOV exposure, volumes of interests were placed on these organs to determine the SUVs pre-and post-exposure.

Results: All animals treated with ZMapp post-exposure survived aerosol challenge up to 48 days while all control animals in both groups succumbed to challenge by day 7-10. Control groups 1–2 displayed consistently elevated SUVs in the spleen, liver, BM and LNs in the chest that were noticeable on day 3 post-challenge and progressed to the disease endpoint (Fig. 1A). Increases in BM, spleen, and liver SUVs were not seen in NHPs treated with EBOV-specific antibodies, although all animals had increased uptake in the LNs in the chest after day 9 post-challenge. NHPs treated twice with ZMapp had slightly higher elevations in the LNs SUVs compared with that observed in NHPs treated three times (Fig. 1B). All ZMapp-treated but one NHP treated with 2 doses developed an adaptive response to EBOV nucleoprotein as evidenced by antibody titer by day 14 post-exposure. The pattern of SUV changes is this animal was distinct from the rest of ZMapp-treated NHPs. Some consolidation was observed via CT in animals treated with 3 doses but resolved by day 28 post-exposure.

Conclusion: This study is the first application of ^{18}F-FDG/PET imaging to characterize host response to aerosolized EBOV challenge and to monitor the effect of ZMapp. The technology suggests to be sensitive identifying the development of adaptive immune response and could be useful in augmenting conventional efficacy studies and correlating imaging results with tissue pathological evaluation.

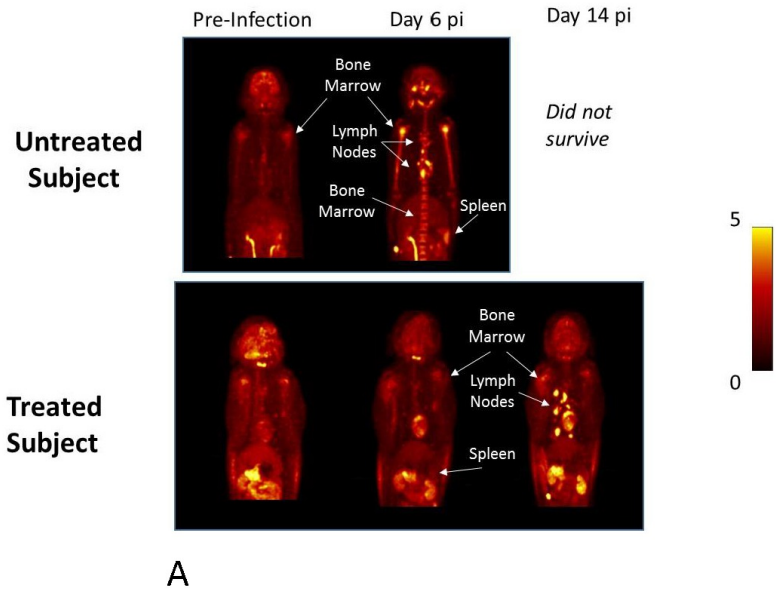

A

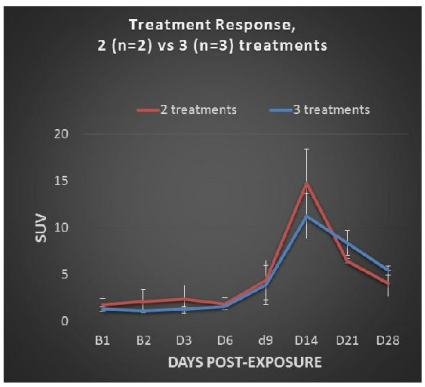

B

Fig.1 Changes in FDG uptake by the spleen, bone marrow and lymph nodes after ZMapp treatment. (**A**) MIP SUV FDG/PET images of upper body of two representative NHPs, NHP 1, top images, and NHP 2, bottom images, challenged with aerosolized Ebola virus (EBOV) and scanned pre-challenge and on days 6 and 14 post-challenge. Elevated SUVs in the bone marrow (BM) at multiple locations, the spleen and the lymph nodes (LNs) in the chest are noticeable on day 6 post-challenge in non-treated animal but not in NHP 2 treated with ZMapp. Elevated SUVs in the LNs were observed in NHP 2 on day 14 post-challenge, suggesting involvement of these LNs in developing adaptive immune responses to treatment. **(B)** Mean SUVs averaged from 3 animals treated with 2 ZMapp doses and 3 animals treated with 3 ZMapp doses. Each data point represent mean ± SD from two scans pre-challenge (B1 and B2) and scans on days 3, 6, 9, 14, 21, 28 post-challenge.

IMAGE CAPTION: Fig.1 Changes in FDG uptake by the spleen, bone marrow and lymph nodes after ZMapp treatment. (**A**) MIP SUV FDG/PET images of upper body of two representative NHPs, NHP 1, top images, and NHP 2, bottom images, challenged with aerosolized Ebola virus (EBOV) and scanned pre-challenge and on days 6 and 14 post-challenge. Elevated SUVs in the bone marrow (BM) at multiple locations, the spleen and the lymph nodes (LNs) in the chest are noticeable on day 6 post-challenge in non-treated animal but not in NHP 2 treated with ZMapp. Elevated SUVs in the LNs were observed in NHP 2 on day 14 post-challenge, suggesting involvement of these LNs in developing adaptive immune responses to treatment. **(B)** Mean SUVs averaged from 3 animals treated with 2 ZMapp doses and 3 animals treated with 3 ZMapp doses. Each data point represent mean ± SD from two scans pre-challenge (B1 and B2) and scans on days 3, 6, 9, 14, 21, 28 post-challenge.

SESSION TITLE: Scientific Session 06: Infection

CONTROL ID: 2734069

TITLE: Vascular adhesion protein-1 targeting positron emission tomography visualizes Borrelia burgdorferi-induced arthritis in mice

PRESENTER: Riikka Siitonen

AUTHORS (FIRST NAME, LAST NAME): Riikka Siitonen[1], Annukka Pietikäinen[2], Heidi Liljenbäck[1, 3], Meeri Käkelä[1], Mirva Söderström[4], Sirpa Jalkanen[5], Jukka Hytönen[2], Anne Roivainen[1, 3]

INSTITUTIONS (ALL):

1. Turku PET Centre, University of Turku, Turku, Finland.
2. Institute of Biomedicine, University of Turku, Turku, Finland.
3. Turku Center for Disease Modeling, University of Turku, Turku, Finland.
4. Department of Pathology, University of Turku, Turku, Finland.
5. MediCity Research Laboratory, University of Turku, Turku, Finland.

ABSTRACT BODY:

Abstract Body: Background: Lyme borreliosis (LB) is a human tick-borne infectious disease caused by spirochete of Borrelia burgdorferi. Infection begins with erythema migrans skin lesions at the tick bite site, and disseminate via the blood into distant organs. (1) Mouse models are widely used to study LB especially joint manifestations resembling human disease. Vascular adhesion protein-1 (VAP-1) is an inflammation-inducible endothelial adhesion molecule involved in leukocyte recruitment to the inflamed tissue. Previously, we have found that sialic-acid binding IgG-like lectin 9 (Siglec-9) is a leukocyte ligand of VAP-1, and gallium-68-labeled Siglec-9 motif containing peptide can be used for positron emission tomography (PET) imaging of inflammation and cancer (2). Purpose of this study was to evaluate the feasibility of VAP-1 targeting PET for assessment of Borrelia burgdorferi infection induced inflammation in mice.

Methods: C3H/He mice (n=22) were infected with intracutaneous (i.c.) injection of wild type Borrelia burgdorferi bacteria to induce LB, and their littermates (n=4) were injected i.c. with equal volume of phosphate-buffered saline as an uninfected controls. A subgroup of infected mice (n=8) was treated with ceftriaxone starting at four weeks after infection (25 mg/kg, twice a day for five days). During seven week follow-up period, progression of arthritis was monitored weekly with [^{68}Ga]DOTA-Siglec-9 PET/computed tomography (CT) and measurement of tibio-tarsal joint swellings. Starting at two weeks after infection, the radioactivity concentration of excised tissue samples was measured using a gamma counter. In addition, tibio-tarsal joint samples were subjected to borrelia culturing and one tibio-tarsal joint/mouse was collected for histological analysis.

Results: Explicit joint swelling and [^{68}Ga]DOTA-Siglec-9 uptake could be demonstrated in the affected joints from Borrelia burgdorferi infected mice. In contrast, no obvious accumulation of [^{68}Ga]DOTA-Siglec-9 was detected in joints of uninfected mice (Fig. 1). According to PET, the highest standardized uptake value in the affected joints was observed at four weeks after infection (0.68 ± 0.17), which was significantly higher compared to uninfected mice (0.36 ± 0.065, $P = 0.0037$). In spite of short-term antibiotic treatment, the arthritis still persisted and the PET signal was as high as that of non-treated mice. In vivo [^{68}Ga]DOTA-Siglec-9 uptake in joints correlated well with swelling ($r = 0.73$, $P < 0.001$) and histological scoring of inflammation ($r = 0.61$, $P = 0.020$).

Conclusion: [^{68}Ga]DOTA-Sigec-9 is able to accurately detect Borrelia burgdorferi infection induced arthritis in mice. Longitudinal PET/CT imaging allowed the monitoring of arthritis development and therapy response over time.

References:

1. Stanek G. et al. Lancet 379(9814):461-73, 2012.

2. Aalto K. et al. Siglec-9 is a novel leukocyte ligand for vascular adhesion protein-1 and can be used in PET imaging of inflammation and cancer. Blood 118(13):3725-33, 2011.

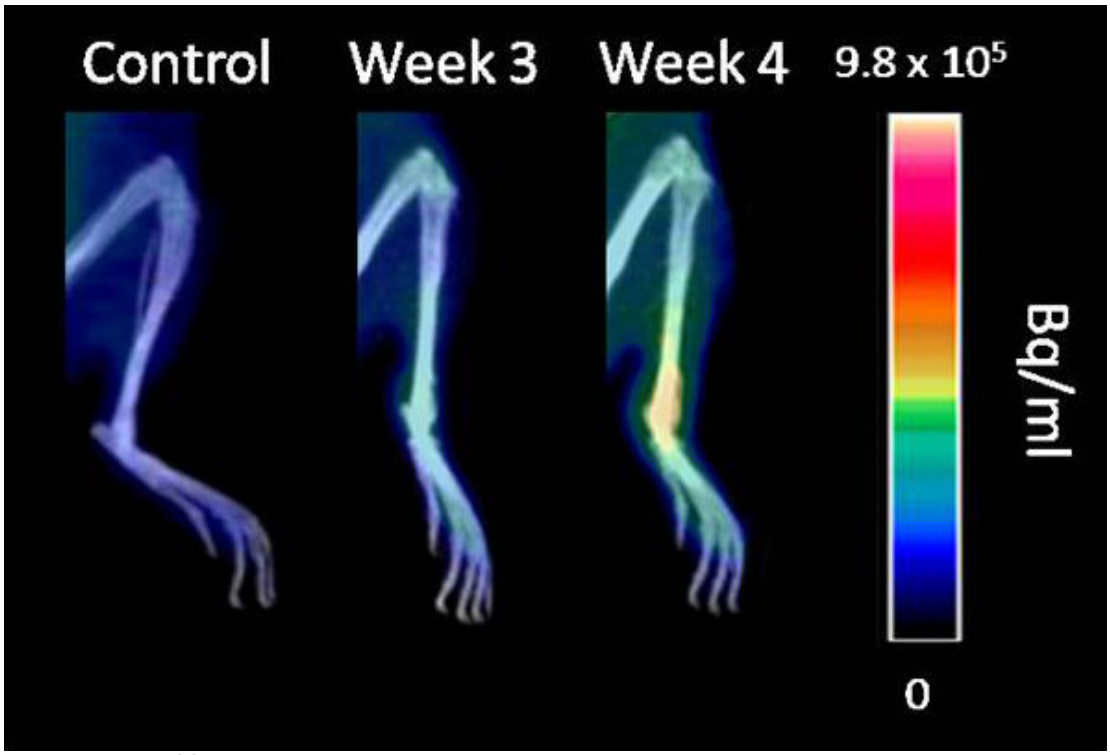

Figure 1. Representative [^{68}Ga]DOTA-Siglec-9 PET/CT images of hind legs of a uninfected control mouse and a *Borrelia burgdorferi*-infected mouse. Images are displayed in the same color scale.

IMAGE CAPTION: Figure 1. Representative [^{68}Ga]DOTA-Siglec-9 PET/CT images of hind legs of a uninfected control mouse and a *Borrelia burgdorferi*-infected mouse. Images are displayed in the same color scale.

SESSION TITLE: Scientific Session 06: Infection

CONTROL ID: 2735047

TITLE: [^{18}F]DPA-714 PET imaging provides a very sensitive and early indicator of Zika-related neuroinflammation in the brains of infected mice

PRESENTER: Kyle Kuszpit

AUTHORS (FIRST NAME, LAST NAME): Kyle Kuszpit[1], Bradley S. Hollidge[2], Robert G. Stafford[1], Darci R. Smith[2], Thomas Bocan[1]

INSTITUTIONS (ALL):

1. Molecular and Translational Sciences, US Army Medical Institute for Infectious Diseases (USAMRIID), Ft. Dterick, MD, United States.
2. Virology, US Army Medical Research Institute of Infectious Diseases (USAMRIID), Ft. Detrick, MD, United States.

ABSTRACT BODY:

Abstract Body: The development of effective therapeutic countermeasures against Zika virus (ZIKV) infection has become a high research priority, one in which in vivo, non-invasive imaging could play a key role. Mounting evidence suggests that ZIKV is neurotropic and neurovirulent in humans and is capable of causing severe congenital and adult neuropathology. Several ZIKV animal models have recently been developed which recapitulate many of the hallmarks of the human disease including congenital defects, neuroinflammation and viral replication in several organs including the brain. [^{18}F]DPA-714 is a promising new fluorinated positron emission tomography (PET) radiotracer that is specific for the 18 kDa translocator protein (TSPO), a biochemical marker of neuroinflammation which is highly upregulated in activated microglia and CNS macrophages. Here, we show for the first time that [^{18}F]DPA-714 PET imaging provides a very sensitive and early indicator of ZIKV-related neuroinflammation in the brains of infected mice. By as early as day 3-post infection, we show in a mouse model of ZIKV infection a modest yet significant ~2-fold increase in mean whole-brain [^{18}F]DPA-714 uptake (~2.21 %ID/g) compared to PBS-only controls (~1.06 %ID/g) ($p<0.001$). By days 6 and 10 post-infection, the increase in mean whole brain [^{18}F]DPA-714 binding was ~4 and ~6-fold greater, respectively (~4.48 %ID/g and ~5.70 %ID/g), compared to PBS-only controls (~1.06 %ID/g) ($p<0.001$). These results were confirmed in the brains of our imaging mice at the late, day 10 time point by infrared (IR) and immunofluorescent detection of Iba-1, a microglia/macrophage-specific calcium-binding protein which is highly upregulated during neuroinflammation. Significant neuroinflammation could not, however, be detected by Iba-1 labeling at the earlier day 3 and day 6 time points, indicating a level of sensitivity to detect ZIKV-induced neuroinflammation by in vivo PET imaging not achievable by IR or immunofluorescent imaging. These results demonstrate the usefulness of [^{18}F]DPA-714 PET as a means to monitor very early stages of ZIKV infection and as a very sensitive, non-invasive tool to evaluate therapy-induced changes in neuroinflammation in the development of novel therapeutics against ZIKV infection.

(No Image Selected)

SESSION TITLE: Scientific Session 06: Infection

CONTROL ID: 2735318

TITLE: Positron emission tomography imaging of human tumor necrosis factor alpha using ^{89}Zr-certoluzimab pegol.

PRESENTER: Denis Beckford-Vera

AUTHORS (FIRST NAME, LAST NAME): Denis R. Beckford-Vera[1], Catherine Fu[1], Joseph E. Blecha[1], Tony L. Huynh[1], Benjamin L. Franc[1], Xiaojuan Li[1], Henry VanBrocklin[1]

INSTITUTIONS (ALL):

1. Radiology and Biomedical Imaging, University of California San Francisco, San Francisco, CA, United States.

ABSTRACT BODY:

Abstract Body: Rheumatoid arthritis (RA) is a chronic inflammatory disorder that affects an estimated 1.3 million Americans and constitutes an important cause of long-term disability (1). Some RA patients experience a rapid clinical response to tumor necrosis factor alpha (TNFα) inhibitors such as Certolizumab pegol (CZP), an anti-TNFα antibody fragment (2). Other patients exhibit delayed response or no response at all (2). This disparate response might be due to the complexity of the immune-mediated processes underlying the development and progression of RA. Current standard methods for imaging RA are limited in their sensitivity for the detection and evaluation of treatment response and do not assist in the selection of the type of immune-mediated therapy. SPECT imaging of TNF-α using ^{99m}Tc-CZP has been recently reported but this modality still has limitations (3). Hence, a robust PET method for predicting response to TNFα inhibitors would serve an unmet clinical need.

Certolizumab pegol was modified with 1-(4-isothiocyanatophenyl)-3-[6,17-dihydroxy-7,10,18,21-tetraoxo-27-[N-acetylhydroxylamino)-6,11,17,22-tetrazaheptaeicosine]-thiourea (DFO-CNS) and radiolabeled with Zr-89. Quantification of the number of DFO per CZP molecule was determined by isotopic dilution. Immunoreactivity fraction of DFO-CZP conjugate and ^{89}Zr-DFO-CZP was evaluated using size-exclusion high performance liquid chromatography (HPLC). Affinity and specificity of ^{89}Zr-DFO-CZP to TNFa was evaluated by radioimmunoassay. PET imaging in Sprague Dawley rats was used to study the biodistribution and dosimetry of ^{89}Zr-DFO-CZP. GMP preparation of ^{89}Zr-DFO-CZP and FDA authorization, seeking first-in-human ^{89}Zr-DFO-CZP PET-MRI imaging in patients with RA.

^{89}Zr-DFO-CZP was isolated with radiolabeling yields 85 ± 6 % (n=5) and specific activities ranged from 74 – 185 MBq/mg (n=5). Following size exclusion purification, the radiochemical purity of ^{89}Zr-DFO-CZP was greater than 97%. After conjugation and radiolabeling, ^{89}Zr-DFO-CZP exhibited specific binding to TNFα (Fig 1 B). As seen in Fig 1A ^{89}Zr-DFO-CZP retained high immunoreactivity with more than 95% of the radioactivity shifted into higher molecular weight complexes. PET/CT images in normal Sprague-Dawley rats revealed uptake of ^{89}Zr-DFO-CZP in the heart, liver, lungs, and kidneys at 24h post-injection that decreased in heart and lungs while increasing in the liver and kidneys by 48h post-injection (Fig 1C).

Non-invasive immuno-PET imaging of TNFα with ^{89}Zr-DFO-CZP may be useful for monitoring and predicting anti-TNFα treatment response in RA.

[1]Helmick C, Felson D, Lawrence R, Gabriel S, Hirsch R, Kwoh C, et al. Estimates of the prevalence of arthritis and other rheumatic conditions in the United States. Part I. Arthritis Rheum. 2008;58(1):15-25

[2]McDonnel T, Ioannou Y, Rahman A. PEGylated drugs in rheumatology--why develop them and do they work? Rheumatology (Oxford). 2014 Mar;53(3):391-6.

[3]Bieke Lambert et al. ^{99m}Tc-labelled S-HYNIC certolizumab pegol in rheumatoid arthritis and spondyloarthritis patients: a biodistribution and dosimetry study. Lambert et al. EJNMMI Research (2016) 6:88

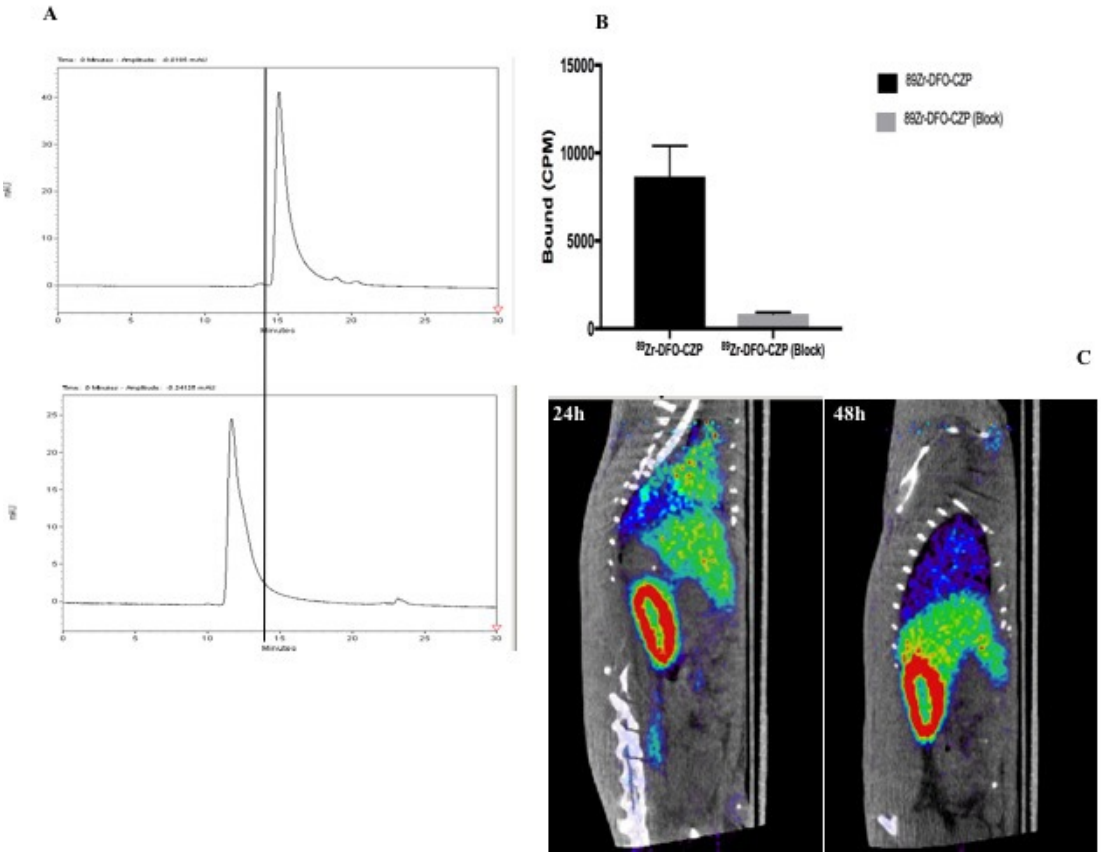

Figure 1(A) Size-exclusion HPLC chromatograms of DFO-CZP(top) and DFO-CZP incubated with TNF-α (bottom). (B) Incubation of ^{89}Zr-DFO-CZP with excess of unlabeled CZP significantly decreased the signal associate with ^{89}Zr-DFO-CZP binding to TNFα, demonstrating specific binding of ^{89}Zr-DFO-binding to TNFα antigen. (C) PET/CT images of ^{89}Zr-DFO-CZP at 24 and 48h post-injection in healthy Sprague Dawley rats.

IMAGE CAPTION: Figure 1(A) Size-exclusion HPLC chromatograms of DFO-CZP(top) and DFO-CZP incubated with TNF-α (bottom). (B) Incubation of ^{89}Zr-DFO-CZP with excess of unlabeled CZP significantly decreased the signal associate with ^{89}Zr-DFO-CZP binding to TNFα, demonstrating specific binding of ^{89}Zr-DFO-binding to TNFα antigen. (C) PET/CT images of ^{89}Zr-DFO-CZP at 24 and 48h post-injection in healthy Sprague Dawley rats.

SESSION TITLE: Scientific Session 09: Infection & Inflammation

CONTROL ID: 2732492

TITLE: Monitoring Anti-Inflammatory Treatment Effects in Porcine Acute Ileitis using Ultrasound Molecular Imaging

PRESENTER: Huaijun Wang

AUTHORS (FIRST NAME, LAST NAME): Huaijun Wang[1], Stephen Felt[2], Jean-Marc Hyvelin[3], Ismayil Guracar[4], Samir Cherkaoui[3], Thierry Bettinger[3], Juergen K. Willmann[1]

INSTITUTIONS (ALL):

1. Radiology, Stanford, Stanford, CA, United States.
2. Comparative Medicine, Stanford , Stanford, CA, United States.
3. Research, Bracco Suisse SA, Geneva, Switzerland.
4. Advanced Development, Siemens Medical Solutions, Ultrasound Business Unit, Mountain View, CA, United States.

ABSTRACT BODY:

Abstract Body: Purpose: Inflammatory bowel disease (IBD) is a life-long disease and noninvasive monitoring of treatment response is crucial for patient management. Ultrasound molecular imaging (USMI) using P- and E-selectin targeted microbubbles ($MB_{selectin}$) has been shown to accurately quantify inflammation at the molecular level in rodent and porcine models of IBD. This study aimed to assess whether dual selectin-targeted USMI allows longitudinal monitoring of anti-inflammatory treatments in a swine model of IBD.

Materials and Methods: Fourteen female swine with chemically-induced acute terminal ileitis using an intraluminally administered TNBS/ethanol solution at day 0 were randomized into 1) an anti-inflammatory treatment group (n=8; treatment with meloxicam at 0.25 mg/kg and prednisone at 0.5 mg/kg; oral or i.v. twice daily) and 2) a control group (n=6; treatment with saline only). USMI was performed in contrast pulse sequencing mode using a clinical machine (Acuson Sequoia 512; 15L8W, 7MHz; Siemens) after i.v. injection of clinically translatable $MB_{selectin}$ ($5x10^8$/kg b.w.). Four minutes after injection, USMI datasets were acquired for 10 sec, followed by a 5-sec high power destruction pulse; this was followed by another 10-sec data acquisition. Three bowel segments per swine were imaged each at baseline, day 1, 3 and 6 after ileitis induction. Linearized imaging signal was quantified as the difference between pre- and post-destructive signal intensity by using a pre-clinical dedicated prototype version of VueBox quantification software (Bracco) and normalized to day 1 signal intensity. After the last imaging session, scanned ileal segments were analyzed ex vivo for both inflammation grading on H&E staining and for expression of selectins using immunofluorescence staining.

Results: Background USMI signals were shown at baseline day 0 and were not significantly different (P=0.09) between treatment and control groups. At day 1 after acute ileitis induction, USMI signals significantly (P<0.05) increased in both groups compared to baseline imaging and imaging signal was not significantly different (P=0.9) between the two groups. In contrast, at day 3, USMI signal significantly (P=0.02 vs. day 1) decreased in the treatment group, while it remained high in the control group (P=0.25 vs. day 1) and the signal was significantly higher (P=0.001) in the control group compared to the treatment group. At day 6, USMI signal further decreased in the treatment group. While USMI signal also dropped in the control group at day 6 due to known spontaneous decrease of inflammation in this porcine animal model, the imaging signal remained significant higher (P=0.046) compared to the treatment group (Figure). H&E staining confirmed higher inflammation in control tissues compared to the treatment group and immunofluorescence demonstrated higher P- and E-selectin expression in control versus treated ileum (Figure).

Conclusions: Dual-selectin targeted USMI allows longitudinal monitoring of anti-inflammatory treatment effects in a porcine model of acute ileitis. This study paves the way for clinical translation of this radiation-free technique for monitoring IBD in patients.

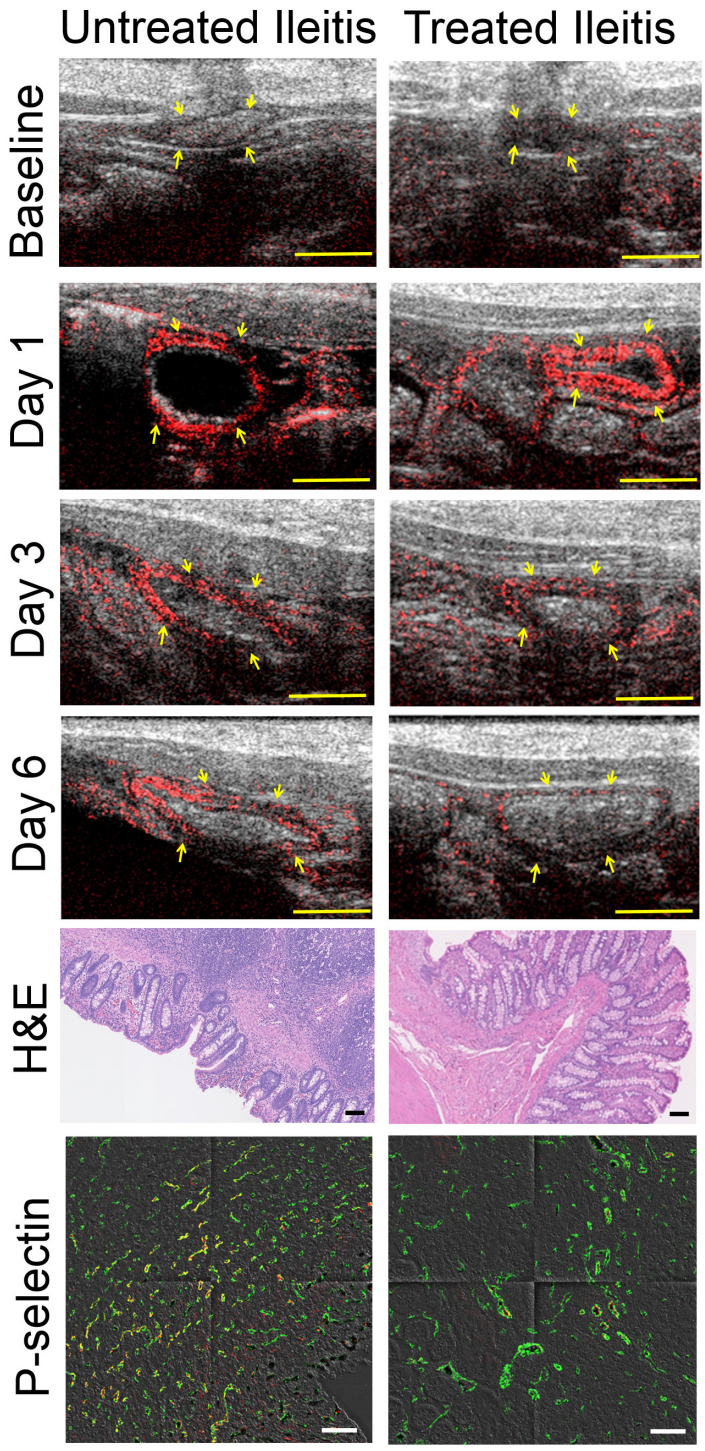

Figure. Effects of anti-inflammatory treatment on dual selectin-targeted USMI signal (arrows) in inflamed terminal ileum in swine imaged at different time points before (baseline) and at day 1, 3, and 6 after induction of inflammation. USMI signals substantially increase from day 0 to day 1 after ileitis induction in both control and treated swine and then quickly decreased in treated animals (right) while remaining increased in control swine (left). Photomicrographs of H&E stained tissue and immunofluorescence staining confirmed anti-inflammatory treatment effects in the treatment group with decreased inflammation grade and P-selectin expression in the treated versus control group. Scale bar = 1cm in ultrasound images and 100μm in photomicrographs respectively.

IMAGE CAPTION: **Figure.** Effects of anti-inflammatory treatment on dual selectin-targeted USMI signal (arrows) in inflamed terminal ileum in swine imaged at different time points before (baseline) and at day 1, 3, and 6 after induction of inflammation. USMI signals substantially increase from day 0 to day 1 after ileitis induction in both control and treated swine and then quickly decreased in treated animals (right) while remaining increased in control swine (left). Photomicrographs of H&E stained tissue and immunofluorescence staining confirmed anti-inflammatory treatment effects in the treatment group with decreased inflammation grade and P-selectin expression in the treated versus control group. Scale bar = 1cm in ultrasound images and 100μm in photomicrographs respectively.

SESSION TITLE: Scientific Session 09: Infection & Inflammation

CONTROL ID: 2733939

TITLE: In vivo imaging to explore the respiratory tract in a model of Bordetella pertussis infection using non-human primates

PRESENTER: Catherine Chapon

AUTHORS (FIRST NAME, LAST NAME): Thibaut Naninck[1, 5], Céline Mayet[1, 5], Vanessa Contreras[1, 5], Sébastien Langlois[1, 5], Néla Klimova[1, 2], Peter Sebo[2], Camille Locht[4], Loïc Coutte[4], Roger Le Grand[3, 5], Catherine Chapon[1, 5]

INSTITUTIONS (ALL):

1. DRF/ImVA U1184/IDMIT, CEA, Fontenay-aux-Roses, France.
2. Instituteof Microbiology CAS, Prague, Outside U.S. & Canada, Czech Republic.
3. DRF/IMETI/IMVA U1184/IDMIT, CEA, Fontenay-aux-Roses, France.
4. Inserm U1019, CNRS UMR8204 , Institut Pasteur de Lille, Lille, France.
5. Université Paris-Sud, Orsay, France.

ABSTRACT BODY:

Abstract Body: Introduction

Non-invasive and longitudinal imaging approaches are required to study host/pathogens interactions in relevant animal models. Whooping cough or pertussis, resulting from infection with the bacteria Bordetella pertussis, is a contemporary medical and public health problem. The deficiencies of current acellular vaccines are well documented [1], including the striking observation that acellular vaccination of non-human primates only protects against disease symptoms but not colonization or transmission [2]. To enable the development of more effective vaccine strategies, a better understanding of mechanisms of action of the bacteria during infection is needed. We thus developed fluorescence imaging techniques including Fibered Confocal Fluorescence Microscopy (FCFM) [3] to explore the respiratory tract for visualizing the interactions between the bacteria Bordetella pertussis and antigen presenting cells (APCs) in baboons.

Methods

GFP-expressing B. pertussis was inoculated by intranasal and intra-tracheal routes in young baboons. Besides, monoclonal anti-HLA-DR antibody (mAb), labelled with Alexa-Fluor647, was administered by topical application in the trachea to specifically target and label APCs. FCFM (Cellvizio® DualBand, Mauna Kea Technologies), coupled with bronchoscopy, was performed in the lower respiratory tract 2 days prior to and 2, 7, 14 and 27 post-infection. In addition, immunohistofluorescence was performed in lungs, trachea and bronchus to finely characterize the interactions between B. pertussis and APCs.

Results

We were able to specifically detect by in vivo FCFM the bacterial and APCs localizations and interactions in the lower respiratory tract of young baboons after infection (Figure 1).

Conclusions

These findings confirm previous published in vitro data about strong interactions between Bordetella pertussis and dendritic cells and macrophages [4]. This approach using fluorescence imaging will then be a useful tool to describe the mechanisms of action of the bacteria during infection to develop more effective vaccines against pertussis.

1. Klein, N.P., et al., N Engl J Med, 2012.
2. Warfel, J.M., et al., Proc Natl Acad Sci U S A, 2014.
3. Thiberville, L., et al., Am J Respir Crit Care Med, 2007.
4. Lamberti, Y.A., et al., Infect Immun, 2010.

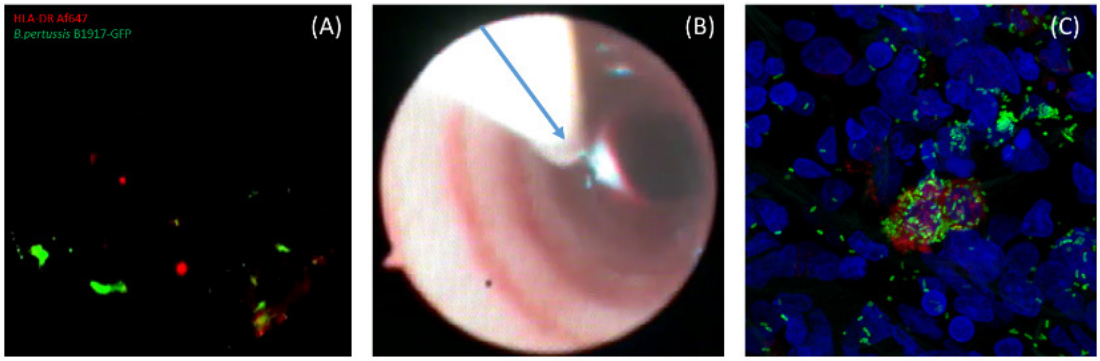

Figure 1: (A) FCFM detection of GFP-expressing *B.pertussis* (green) and APCs with anti-HLA-DR AF647 (red). (B) *In vivo* bronchoscopy on young baboon lower respiratory tract, visualization of the trachea and FCFM probe (blue arrow) with the camera. (C) Lung slices after 24h ex-vivo co-culture with GFP-expressing *B.pertussis* (green). Nuclei are stained with DAPI (blue) and alveolar macrophages with anti-CD163 AF594 antibody (red).

IMAGE CAPTION:

SESSION TITLE: Scientific Session 09: Infection & Inflammation

CONTROL ID: 2734287

TITLE: Imaging Changes in pH on the Surface of Implanted Medical Devices in order to Detect and Monitor Implant-associated Infection using X-ray Excited Luminescent Chemical Imaging (XELCI).

PRESENTER: Unaiza Uzair

AUTHORS (FIRST NAME, LAST NAME): Unaiza Uzair[1], Donald Benza[1, 5], Fenglin Wang[1], Chloe Johnson[4, 1], Yash Raval[2], Tzuen-Rong J. Tzeng[2], Caleb J. Behrend[3], Jeffrey N. Anker[1]

INSTITUTIONS (ALL):

1. Chemistry, Clemson University, Clemson, SC, United States.
2. Biological Sciences, Clemson University, Clemson, SC, United States.
3. Virginia Tech Carilion School of Medicine and Research Institute, Roanoke, VA, United States.
4. Materials Science & Engineering, Clemson University, Clemson, SC, United States.
5. Electrical and Computer Engineering, Clemson University, Clemson, SC, United States.

ABSTRACT BODY:

Abstract Body: To non-invasively image bacterial colonization of medical implants, a pH sensor is being developed to indicate implant associated infection based on changes in pH. It consists of a bottom layer of scintillator particles (Gd_2O_2S:Eu) and a pH sensing top layer. The scintillator layer acts as an in situ X-ray irradiated light source emitting red light which is differentially absorbed by the pH sensitive film on the top depending on the pH of the area. There is evidence of low pH associated with infection contributed to the acidic products from bacterial metabolism and inflammatory responses of the body. Implant-associated infection is the leading cause of fixation failures and is often challenging to detect due to lack of symptoms and specific tests to detect localized infection, therefore, early diagnosis is the key to better treatment in such an infection. X-ray Excited Luminescent Chemical Imaging (XELCI) allows to noninvasively detect and image changes in pH at implant surface through the tissue with high spatial and pH resolution while minimizing tissue scattering effects. It allows point by point mapping of the surface with minimum background and high spatial resolution mainly limited by the X-ray beam width. pH changes on the device surface were imaged through tissue in vitro and ex vivo (human cadaver studies). A pre-pilot rabbit study was also conducted to test the sensor in vivo. Further studies are planned to image the pH changes on the device surface during infection and antibiotic treatment in animal models. In summary, the pH sensor will provide a novel approach to noninvasively image surface pH to diagnose implant associated infection and assess treatment.

References:

1.Kottinen et al., J. Bone & Mineral Res. 16, 1780-1786(2001)

2.Wang et al., Adv. Healthcare. Mater., 3, 197-204(2014)

3.U. Uzair, D. Benza, et al., Proc. SPIE 10081, Frontiers in Biological Detection: From Nanosensors to Systems IX, 100810K(2017)

Acknowledgements:

This research was supported in part by National Science Foundation (NSF) CAREER award CHE1255535, a Fulbright Scholarship award to the graduate student (presenter), fluorescence imaging and plain film x-ray funded through the South Carolina Bioengineering Center of Regeneration and Formation of Tissues (SCBioCRAFT) under NIH grant 5P20GM103444-07 and animal studies funded by an R01 grant.

(No Image Selected)

SESSION TITLE: Scientific Session 12: Inflammation

CONTROL ID: 2715157

TITLE: Multimodal Imaging Reveals an Activin-A Dependent Growth of Nascent Heterotopic Ossification in Fibrodysplasia Ossificans Progressiva

PRESENTER: Jaymin Upadhyay

AUTHORS (FIRST NAME, LAST NAME): Jaymin Upadhyay[1], Sarah Hatsell[1], Rachel Stewart[2], Morgan C. Lyon[2], Keryn Palmer[2], Saathyaki Rajamani[1], Chris Graul[2], Merryl Lobo[2], Tyler J. Wellman[2], Lily Huang[1], LiQin Xie[1], Nanditha M. Das[1], Kalyan Nannuru[1], Vincent Idone[1], Edward J. Soares[3], Matt Silva[2], Jacob Hesterman[2], Aris Economides[1]

INSTITUTIONS (ALL):

1. Regeneron Pharmaceuticals, Tarrytown, NY, United States.
2. Contract Research, inviCRO LLC, Boston, MA, United States.
3. College of the Holy Cross, Worcester, MA, United States.

ABSTRACT BODY:

Abstract Body: Fibrodysplasia Ossificans Progressiva (FOP) is a rare autosomal dominant disorder that arises from missense mutations in the type I Bone Morphogenetic Protein (BMP) receptor, ACVR1. Individuals with FOP develop heterotopic ossification (HO) in skeletal muscles, tendons, and ligaments due to activation of mutant ACVR1 by Activin A (Huning, 2014). Here, a combination of T2-MRI (detection of inflammation, edema and cartilage formation), ^{18}F-NaF-PET (detection of active bone formation/remodeling) and CT (informing on HO volume) was implemented in an FOP mouse model (Hatsell, 2015) in order to elucidate the dependence of Activin A upon the growth of nascent HO. Moreover, an adaptive design was employed where administration of an anti-Activin-A antibody (REGN2477) or an isotype control antibody (REGN1945 – akin to placebo) was initiated only after HO lesions could be detected with ^{18}F-NaF-PET/CT.

To assess T2-MRI data and inform on the level of inflammation, edema and cartilage formation, a visual severity score (Lesion Severity Scale (0-3): No Lesion (0), Mild (1), Moderate (2), Severe (3). Increments of 0.5.) based on signal intensity and volume was attributed to each lesion by 3 blinded readers. In addition to this semi-quantitative assessment, FOP lesions identified with T2-MRI were segmented by a single blinded reader, yielding an account of lesion volume. A blinded manual segmentation of each region of enhanced tracer ^{18}F-NaF uptake or region of HO identified by CT was performed, allowing calculation of lesion specific ^{18}F-NaF mean standard uptake values (SUV) and HO volume (mm^3). A Mann Whitney U test was used to test for significance.

HO presence was detectable in 17 FOP mice by day 15 post-model induction, and in turn, treatment was started at day 18. From the baseline condition (day 15), in mice receiving REGN1945, the T2-MRI lesion severity was held constant and then slightly decreased (Fig. 1A-B), while the MRI lesion volume increased and then stabilized (Fig. 1C). In ^{18}F-NaF-PET data, the mean SUV increased from baseline to day 30 under REGN1945 treatment (Fig. 1F-G). In contrast, there was a reduction in both MRI lesion severity (Fig. 1A-B), MRI lesion volume (Fig. 1C) and ^{18}F-NaF-PET uptake (Fig. 1F-G) after a single dose of REGN2477. Single-subject T2-MRI and ^{18}F-NaF-PET data from both dosing group have been depicted in Fig. 1D-E and Fig. 1H-I, respectively. Compared to REGN1945 treatment, where HO volume (measured by CT) steadily increased from days 9 to 37, REGN2477 resulted in significant suppression of HO volume progression (Fig. 1J-L). The halting of HO volume increases in FOP mice within a delayed treatment paradigm was detectable by calculating the mean HO volume across all subjects (Fig. 1J-K) and total HO volume across each cohort (Fig. 1L).

These results not only verify that inhibition of Activin A induces stasis of the growth of mineralizing HO lesions in FOP, but demonstrate that Activin A plays a role in the inflammation, edema and cartilage formation (as visualized by T2-MRI). Furthermore, we demonstrate the requirement for Activin A for the initial steps of HO formation as well as for sustained growth of nascent HO.

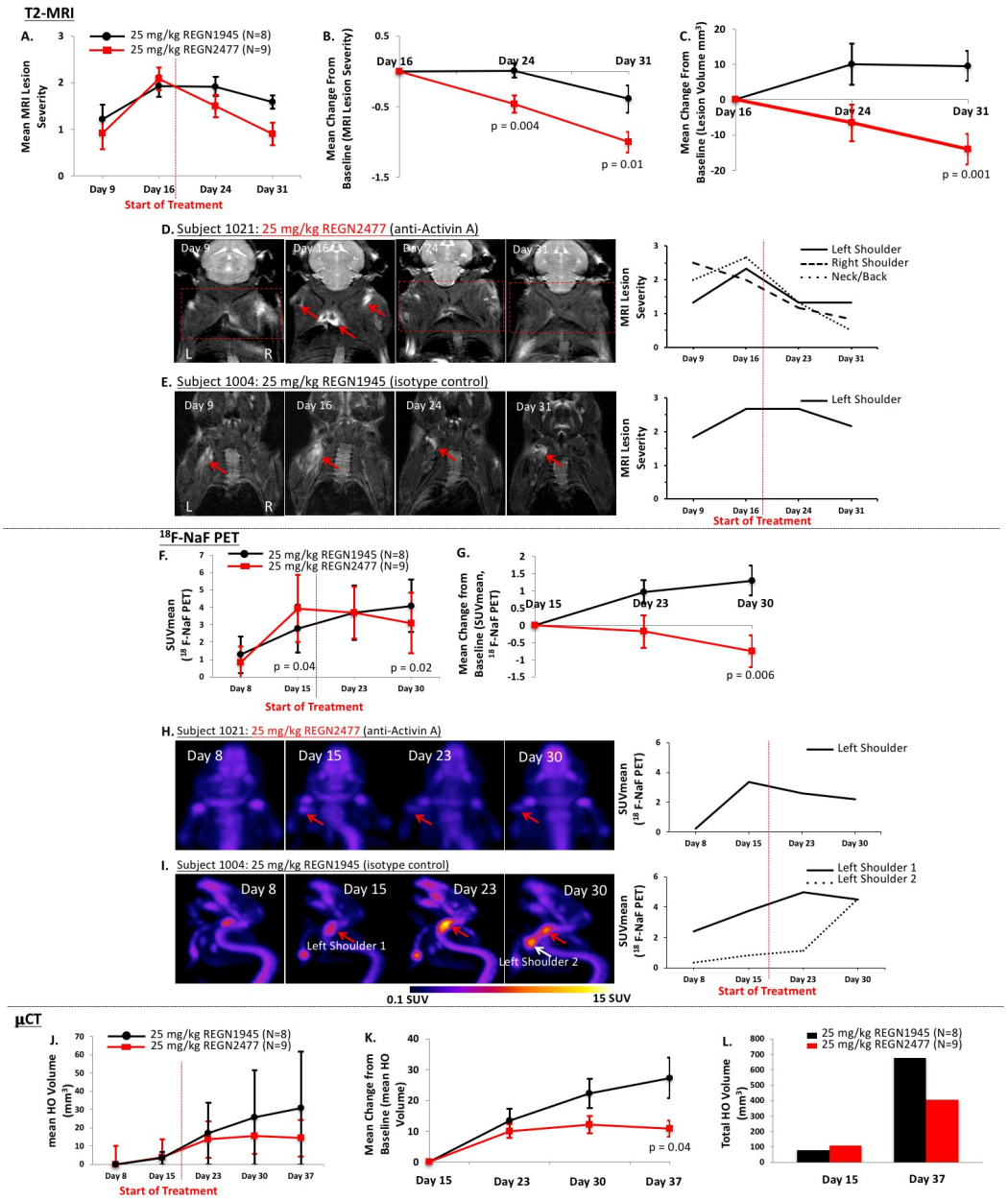

(**A**) Mean T2-MRI lesion severity (averaged over all animals, lesions and 3 readers) time course for each cohort. Mean (± standard error (SE)) change in MRI lesion severity (**B**) and volume (**C**) from the day 16 (baseline) time point. Single-subject MRI data stemming from REGN2477 (**D**) and REGN1945 (**E**) conditions. (**F**) Mean ^{18}F-NaF SUV (averaged over all animals and lesions) time course for each cohort. (**G**) The mean (± SE) change in ^{18}F-NaF SUV from the day 15 time point (baseline). In single-subject data (**H-I**), increases in ^{18}F-NaF uptake (left shoulder 1) from day 15 to 23 and additional post-treatment lesion formation (left shoulder 2) was only observed in the REGN1945 arm. (**J**) The mean HO volume (averaged over all animals and lesions) time course for each treatment arm. (**K**) Mean (± SE) change in HO volume for each treatment. (**L**) The total HO volume for each treatment arm.

IMAGE CAPTION: (**A**) Mean T2-MRI lesion severity (averaged over all animals, lesions and 3 readers) time course for each cohort. Mean (± standard error (SE)) change in MRI lesion severity (**B**) and volume (**C**) from the day 16 (baseline) time point. Single-subject MRI data stemming from REGN2477 (**D**) and REGN1945 (**E**) conditions. (**F**) Mean ^{18}F-NaF SUV (averaged over all animals and lesions) time course for each cohort. (**G**) The mean (± SE) change in ^{18}F-NaF SUV from the day 15 time point (baseline). In single-subject data (**H-I**), increases in ^{18}F-NaF uptake (left shoulder 1) from day 15 to 23 and additional post-treatment lesion formation (left shoulder 2) was only observed in the REGN1945 arm. (**J**) The mean HO volume (averaged over all animals and lesions) time course for each treatment arm. (**K**) Mean (± SE) change in HO volume for each treatment. (**L**) The total HO volume for each treatment arm.

SESSION TITLE: Scientific Session 12: Inflammation

CONTROL ID: 2722048

TITLE: Specificity Evaluation and Disease Monitoring in Arthritis Imaging with Complement Receptor of the Ig superfamily targeting Nanobodies

PRESENTER: Fang Zheng

AUTHORS (FIRST NAME, LAST NAME): Fang Zheng[5, 6], Tony Lahoutte[4], Serge Muyldermans[2], Patrick De Baetselier[2], Steve Schoonooghe[2], Nick Devoogdt[3], Geert Raes[1]

INSTITUTIONS (ALL):

1. VIB - Vrije Universiteit Brussel, Brussels, Belgium.
2. CMIM, Vrije Universiteit Brussel, Brussels, Belgium.
3. ICMI, Vrije Universiteit Brussel, Brussels, Belgium.
4. Nuclear Medicine, Vrije Universiteit Brussel, Jette, Belgium.
5. Biochemisty and molecular biology, Xi'an Jiaotong university, Xi'an, China.
6. Laboratory of Myeloid Cell Immunology, Vrije Universiteit Brussel, Brussels, Belgium.

ABSTRACT BODY:

Abstract Body: Single-photon emission computed tomography combined with micro-CT (SPECT/μCT) imaging using Nanobodies against complement receptor of the Ig superfamily (CRIg), found on tissue macrophages such as synovial macrophages, has promising potential to visualize joint inflammation in experimental arthritis. Here, we further addressed the specificity and assessed the potential for arthritis monitoring. Signals obtained with 99mTc-labelled NbV4m119 Nanobody were compared in joints of wild type (WT) versus CRIg−/− mice with collagen-induced arthritis (CIA) or K/BxN serum transfer-induced arthritis (STIA). In addition, SPECT/μCT imaging was used to investigate arthritis development in STIA and in CIA under dexamethasone treatment. 99mTc-NbV4m119 accumulated in inflamed joints of WT, but not CRIg−/− mice with CIA and STIA. Development and spontaneous recovery of symptoms in STIA was reflected in initially increased and subsequently reduced joint accumulation of 99mTc-NbV4m119. Dexamethasone treatment of CIA mice reduced 99mTc-NbV4m119 accumulation as compared to saline control in most joints except knees. SPECT/μCT imaging with 99mTc-NbV4m119 allows specific assessment of inflammation in different arthritis models and provides complementary information to clinical scoring for quantitatively and non-invasively monitoring the pathological process and the efficacy of arthritis treatment.

(No Image Selected)

SESSION TITLE: Scientific Session 12: Inflammation

CONTROL ID: 2722538

TITLE: Non-invasive imaging of a preclinical model of autoimmune hepatitis with positron emission tomography

PRESENTER: Peter Clark

AUTHORS (FIRST NAME, LAST NAME): Peter M. Clark[1, 2], Jessica Salas[1, 2], Bao Ying Chen[1, 2]

INSTITUTIONS (ALL):

1. UCLA, Los Angeles, CA, United States.
2. Crump Institute, Los Angeles, CA, United States.

ABSTRACT BODY:

Abstract Body: Immune attack on the liver, manifesting as autoimmune hepatitis or hepatic allograft rejection following a liver transplant, is a complex disease that can lead to acute and chronic liver failure[1]. These diseases can be treated with immunosuppressant therapies but the treatments are not without complications. Excessive immunosuppressant therapy can lead to unnecessary side effects, including neurotoxicity and cancer, while inadequate treatments can lead to liver failure[1,2]. Unfortunately, there are few good methods for quantitatively monitoring this process in vivo. New approaches to monitoring hepatic allograft rejection are needed.

Previous studies indicate that hepatic ^{18}F-FDG accumulation is increased in mouse models of autoimmune hepatitis and in rat models of hepatic allograft rejection but that translating this to humans may be challenging due to the higher hepatic ^{18}F-FDG accumulation in humans than in rodents and the relative non-specificity of ^{18}F-FDG for hepatic allograft rejection[3,4]. Additional PET tracers have been developed that can image activated immune cells (^{18}F-FAC) and hepatocyte biology (^{18}F-DFA)[5,6]. We hypothesized that PET imaging with one or more of these tracers could provide a method for monitoring the development and treatment of autoimmune hepatitis. Concanavalin A (Con A) was used to induce an autoimmune hepatitis. For comparison, adenovirus was used to induce a viral hepatitis. Treatments were performed in immunocompetent, and to control for non-immune related effects of the treatments, immunocompromised mice. Each model was imaged with ^{18}F-FDG, ^{18}F-FAC, and ^{18}F-DFA.

Hepatic ^{18}F-FDG accumulation increased and ^{18}F-DFA accumulation decreased in both the autoimmune and viral hepatitis models. Interestingly, hepatic ^{18}F-FAC accumulation only increased in the autoimmune hepatitis model and was unaffected in the viral hepatitis model. Neither the autoimmune nor viral hepatitis treatments affected hepatic accumulation of any tracer in the immunocompromised mice, confirming that the effects of tracer accumulation in the immunocompetent mice required immune activation. Autoradiography suggested that infiltrating lymphocytes in the autoimmune hepatitis model are strongly ^{18}F-FAC avid. Current studies are focused on identifying whether changes in hepatic ^{18}F-FAC accumulation can be used to monitor therapeutic responses to immunosuppressant therapies. Our data suggests that PET imaging with a tracer that measures dCK activity in lymphocytes may provide a method of monitoring the development and treatment of autoimmune hepatitis and hepatic allograft rejection.

1. Eksteen, B. et al. Nat. Clin. Pract. Gastroenterol. Hepatol. 5, 209–219 (2008).
2. Movahedi, Z., et. al. Exp. Clin. Transplant. 8, 83–90 (2010).
3. Tsuji, A. B. et al. J. Nucl. Med. 50, 827–830 (2009).
4. Ishimori, T. et al. J. Nucl. Med. 43, 658–663 (2002).
5. Radu, C. G. et al. Nat. Med. 14, 783–788 (2008).
6. Clark, P. M. et al. Proc. Natl. Acad. Sci. U. S. A. 111, E2866-2874 (2014).

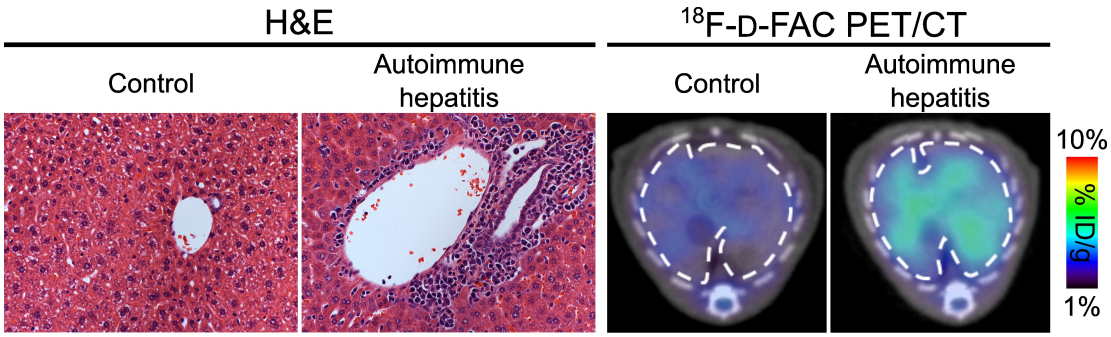

Hepatic ^{18}F-D-FAC accumulation is increased in a mouse model of autoimmune hepatitis

IMAGE CAPTION:

SESSION TITLE: Scientific Session 12: Inflammation

CONTROL ID: 2734385

TITLE: Assessment of Dual Selectins Targeted Liposomes for Rheumatoid Arthritis Optical Imaging

PRESENTER: isabelle Tardy

AUTHORS (FIRST NAME, LAST NAME): isabelle Tardy[1], Patricia Emmel[1], Lucille Valle[1], David Lazarus[1], Charline Alleaume[1], Philippe Bussat[1], Samir Cherkaoui[1], Thierry Bettinger[1]

INSTITUTIONS (ALL):

1. Research, Bracco Suisse SA, Geneva, Switzerland.

ABSTRACT BODY:

Abstract Body: Rheumatoid Arthritis (RA) is a chronic autoimmune inflammatory disease that affects mainly small joints in hands and feet. Synovial membrane hyperplasia and endothelial cell activation are early events in the pathologic process that progresses to uncontrolled inflammation. Emerging therapy in rheumatology enabling control of the progressive process of the disease warrants development of imaging tool for early diagnoses, assessing therapeutic efficiency and prognosis in follow-up examinations. Optical imaging (OI), with the use of Indocyanine Green (ICG) represents an interesting imaging platform for the detection of arthritic joints in humans. However, ICG suffers from a rapid clearance (few minutes) by the liver and has relatively poor fluorescence efficiency. This has prompt us to develop a molecularly-targeted agent specific for P and E selectins, known to play a central role in the early and chronic stages of inflammation, making these biomarkers attractive for the RA diagnosis. In this context, the feasibility of using a recombinant P-selectin glycoprotein ligand-1 fragment (F1) for OI was tested in a clinically relevant RA animal model (Collagen Induced Arthritis or CIA) and compared to ICG, the clinically approved blood pool agent.

Material and Methods: In vitro tests (fluorescence and absorbance spectra) were set up to characterize the F1-liposome formulated with the fluorescent DiR dye (LipoSelectin). RA was induced in animal using the well-established mouse CIA model. The progressive development of RA was daily evaluated at the level of the feet by applying a clinical score (0-4). Animals at different RA staging were then imaged at knees or feet level with FluoBeam™ 700 camera using LipoSelectin (iv, 0.21 mg DIR/kg) and ICG (iv, 2.1 mg/kg). Histopathology analysis and immunohistochemistry (IHC) staining of P and E selectins were performed on inflamed knees to allow correlation with imaging data.

Results: LipoSelectin used as optical targeted contrast agent proved to probe different inflammatory status in the hind paws of the CIA model whereas ICG is more rapidly cleared from the circulation independently of the clinical inflammation scores. Mouse CIA model in the knee is characterized by a chronic active arthritis, with synovial membrane enlargement by fibro-vascular tissue and neutrophils infiltration. P/E-selectin expression was increased in joints with severe inflammation in comparison with joints with discrete inflammatory features or controls. Moreover, optical signal measured in the knee joint increases with the level of P/E selectin expression. The relatively good correlation between OI signal and P-selectin expression (R^2=0.653) suggests this contrast agent is able to specifically probe this biomarker in the inflamed paws of the RA model.

Conclusion: The results showed better performance of LipoSelectin in preclinical arthritis model (CIA) compared to ICG. LipoSelectin appears as a powerful OI targeted agent through its specific detection of E and P selectin markers. This agent might prove to be a powerful diagnostic tool to stage different inflammation status in human rheumatoid arthritis during the therapeutic follow-up.

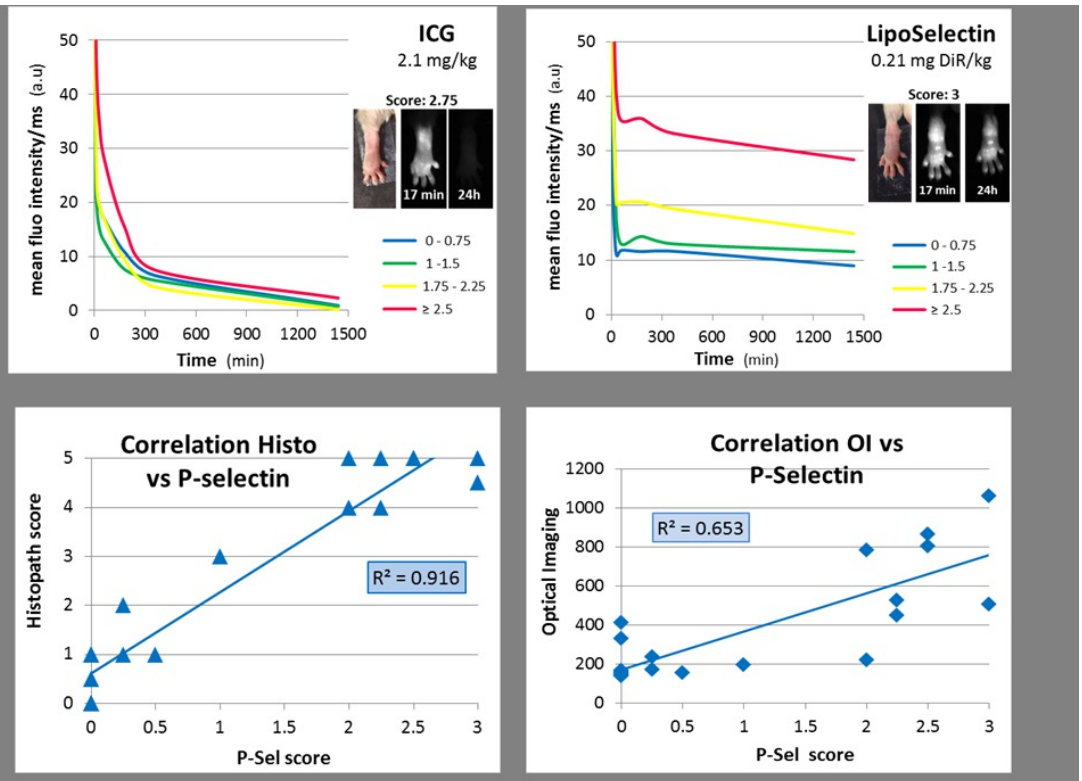

A. Optical signal followed over time after LipoSelectin and ICG in animal foot with different clinical scores. B. Correlation between P selectin expression and optical imaging (OI) values (at 30 min) or histopathology following LipoSelectin injection at knee level.

IMAGE CAPTION:

SESSION TITLE: Scientific Session 12: Inflammation

CONTROL ID: 2734643

TITLE: Monitoring the immune cell infiltration in the LPS-induced neuroinflammation region with simultaneous small animal PET/MR imaging using a TSPO-targeting probe

PRESENTER: Kyungmin Kim

AUTHORS (FIRST NAME, LAST NAME): Kyungmin Kim[12], Juri Na[11], Ha Kim[2], Chul-Hee Lee[5], Min Sun Lee[2], Guen Bae Ko[3], Kyeong Yun Kim[2], Jae Ho Jung[13], Byung Seok Moon[6], Sang Eun Kim[7], Keon Wook Kang[4], June-Key Chung[10], Byung Chul Lee[9], Jae Sung Lee[8], Hyewon Youn[1]

INSTITUTIONS (ALL):

1. Cancer Imaging Center, Seoul National Univ, Seoul, Jongno-Gu, Korea (the Republic of).
2. Seoul National University, Seoul, Korea (the Republic of).
3. Department of Nuclear Medicine, Seoul National University, Seoul, Korea (the Republic of).
4. Nuclear Medicine, Seoul National University, Seoul, Korea (the Republic of).
5. Nuclear medicine, Seoul National University, Seoul, Korea (the Republic of).
6. Department of Nuclear Medicine, Seoul National University Bundang Hospital, Seoul National University College of Medicine, Bundang-gu, Seongnam-si, Korea (the Republic of).
7. Department of Nuclear Medicine , Seoul National University College of Medicine, Seongnam, Korea (the Republic of).
8. Nuclear Medicine, Seoul National University College of Medicine, Seoul, Korea (the Republic of).
9. Nuclear Medicine, Seoul National University College of Medicine, Seoul National University Bundang Hospital, Bundang-gu, Seongnam-si, Korea (the Republic of).
10. Nuclear Medicine, Seoul National University Hospital, Seoul, Korea (the Republic of).
11. Seoul national univ., Seoul, Korea (the Republic of).
12. Seoul national university cancer research institute, Seoul, Korea (the Republic of).
13. Seoul National University Hospital, Seongnam, Korea (the Republic of).

ABSTRACT BODY:

Abstract Body: Objectives: Recently, activated immune cell infiltration has been reported to involve in neuronal damages. Trafficking adoptive-transferred immune cells may provide valuable information to understand of various neuroinflammatory diseases. Here, we asked whether acute brain regional inflammation have any potential to recruit adoptively transferred splenocytes using simultaneous small animal PET/MR.

Methods: Lipopolysaccharide (LPS) was used to induce regional inflammation in the right striatum of a mouse brain (anteroposterior, +1.8; mediolateral, +2.0; dorsoventral,-3.0) using a Hamilton syringe at a rate of 0.25 ul/ min using a robotic stereotacxic device (Stoelting, IL, USA). Saline was used as a control treatment. Splenocytes (2×10^7) were isolated from luciferase expressing transgenic mice ($B6.Luc^{Tg}$), and adoptively transferred to recipient B6 (C57BL/6) mouse by intravenously injection for visualizing immune cell localization with bioluminescence imaging. To assess the degree of inflammatory response, simultaneous PET/MR scans were acquired using simultaneous small animal PET insert combined with 1T MRI (SimPET, Aspect imaging, Israel). ^{18}F-CB251 probe was used to detect the 18-kDa translocator protein (TSPO, a marker for activated immune cells in the inflammatory region) activity at a dose ranging from 9.25 to 11.1 MBq per mouse. CDDO-methyl ester, inflammatory cytokine inhibitor, was treated in acute inflammation mouse model for visualizing therapeutic efficacy (200 nM, 3 times) using ^{18}F-CB251 probe. In vitro uptake assay was also performed for confirming the correlation between TSPO expression level and uptake of ^{18}F-CB251 probe.

Results: Uptake experiments of ^{18}F-CB251 probe were measured in the cells with differential TSPO expression such as TSPO-overexpressed 293FT cells and activated-macrophage Raw 264.7 cells. Higher uptake of ^{18}F-CB251 was found in cells with higher TSPO expression.

PET signals from ^{18}F-CB251 showed 1.86 times (n=7) higher uptake in LPS treated group, 1.5 times (n=5) higher uptake in LPS and inhibitor treated group than saline treated group (n=7). MR scan, which is taken simultaneously, also showed slightly increased T2-weigthed signals in the right striatum of LPS-induced inflammatory region. In addition, luciferase-expressing splenocytes were localized at the LPS-treated site in right striatum of mouse brain. Though BLI signals in LPS-treated region were 4.46 times (n=7) higher and those in LPS and inhibitor treated region were 1.56 times (n=5) higher than that of saline-treated region (n=7) after skin removal, ^{18}F-CB251 PET signals

generate more quantitative and non-invasive images for whole body scan. Immunohistochemistry using anti-luciferase antibody also showed intense staining in right striatum (LPS-injected site).
Conclusion: We successfully visualized adoptively-transferred immune cell recruitment in the inflammatory region of brain using three different imaging modalities. Simultaneous scanning from simultaneous small animal PET/MR provides more accurate spatiotemporal information of immune cell localization in the neuro-inflammation site.
(No Image Selected)